MODELLING AND ANALYSIS OF LEGGED ROBOTS WITH TEMPORARY FLIGHT CAPABILITIES

KISA MESAFE UÇUŞ YETENEĞİNE SAHİP BACAKLI ROBOTLARIN MODELLEMESİ VE KONTROLÜ

OĞUZHAN GÜLTEKİN

ASST. PROF. DR. EMİR KUTLUAY
Supervisor
PROF. DR. YİĞİT YAZICIOĞLU
2nd Supervisor

Submitted to
Graduate School of Science and Engineering of Hacettepe University
as a Partial Fulfillment to the Requirements
for the Award of the Degree of Master of Science
in Mechanical Engineering

December 2022

ABSTRACT

MODELLING AND ANALYSIS OF LEGGED ROBOTS WITH TEMPORARY FLIGHT CAPABILITIES

Oğuzhan Gültekin

Master of Science , Mechanical Engineering

Supervisor: Asst. Prof. Dr. EMİR KUTLUAY

2nd Supervisor: Prof. Dr. YİĞİT YAZICIOĞLU

December 2022, 109 pages

The high obstacle-crossing potential of legged robots has made them a widely studied subject. However, the obstacles that can be overcome are generally proportional to the length of the legs. And any study, that states a legged robot can overcome an obstacle higher than twice the length of the leg has not been encountered in the literature. This situation has made many researchers think about the integration of the capability of flying. Also, this thesis covers the same idea on the RHex robot which is not studied yet. Also, no study has been presented so far in which the orientation of a RHex robot's body is controlled with the help of legs in space. The basis of this thesis is how we humans use our arms and bodies while trying to stay in balance. Similarly, the orientation of the robot's body was controlled by the reactions of the forces applied to the legs in space so that it was possible to control the magnitude and direction of the thrust vector of a thruster fixed to the robot. This means that the movements of the robot could also be controlled. In this study, an existing robot platform RHex was used. The complex geometry and dynamics of the RHex robot were not studied; instead, a 2D simplified model was obtained, and a controller with the desired transient behavior was designed by extracting and linearizing the equations of motion from of the simplified model. Then, with the help of a designed flight simulator, the designed controllers' transient behaviors and actuator efforts were examined, and their performances were evaluated.

Keywords: Flying-Legged Robots, Robot Dynamics and Control, Motion Control, Linearization of Equations of Motion, Modern Control, State Space Controller Design Legged Robots, Flight Control, RHex Robot, Attitude Control, Control System Design

ÖZET

KISA MESAFE UÇUŞ YETENEĞİNE SAHİP BACAKLI ROBOTLARIN MODELLEMESİ VE KONTROLÜ

Oğuzhan Gültekin
Yüksek Lisans, Makina Mühendisliği
Danışman: Asst. Prof. Dr. EMİR KUTLUAY
Eş Danışman: Prof. Dr. YİĞİT YAZICIOĞLU
Eylül 2021, 109 sayfa

Bacaklı robotların yüksek engel aşma potansiyelleri onları üzerine çokça çalışılan bir konu haline getirmiştir. Ancak, bacakların kullanım şekilleri gereği aşılabilecek engeller genelde bacakların boyları ile orantılıdır ve bacak boyunun iki katından daha yüksek bir engeli aşabildikleri bir durum literatürde karşılaşılmamıştır. Bu durum bir çok araştırmacıya uçma yeteneğinin entegrasyonunu düşündürmüştür. Bu tez de aynı fikri şimdiye kadar çalışılmamış olan uçabilen RHex robot üzerinde uygulamak üzerinedir. Ayrıca şu ana dek robotun bedeninin oyantasyonunun uzayda bacaklar yardımı ile kontrol edildiği bir çalışmaya imza atılmamıştır. Bu tezin temelinde biz insanların da dengede durmaya çalışırken kollarımız ve bedenlerimizi kullanışımız yatmaktadır. Benzer şekilde robotun bedeninin oryantasyonunun uzayda bacaklara uygulanan kuvvetlerin reaksiyonları ile kontrol edilmesi sağlanacak ve böylece robota sabitlenmiş bir iticinin itki vektörünün büyüklüğünün ve yönünün kontrolü mümkün olacaktır. Bu, robotun hareketlerinin de kontrol edilebileceği anlamına gelmektedir. Bu çalışmada hali hazırda var olan bir robot platformu RHex kullanılmıştır. RHex robotun complex geometrisi ve dinamiği ile çalışılmamış bunun yerine 2B basitleştirilmiş modeli elde edilmiş ve bu model üzerinden hareket denklemleri çıkarılarak arzu edilen geçici davranışa sahip kontrolcü tasarımı yapılmıştır. Daha sonra tasarlanan bir uçuş simülatörü yardımı ile tasarlanan kontrolcülerin geçici davranışları ile eyleyici eforları incelenmiş ve performansları değerlendirilmiştir.

Keywords: Uçabilen Bacaklı Robotlar, Robot Dinamiği ve Kontrolü, Haraket Kontrolü, Haraket Denklemleri Lineerizasyonu, Modern Kontrol, State Space Kontrolcü Tasarımı

ACKNOWLEDGEMENTS

I would like to express my deep appreciation and sincere gratitude to my esteemed supervisors Asst. Prof. Dr. Emir Kutluay and Prof. Dr. Yiğit Yazıcıoğlu for their continuous support, encouragement, and great leadings. They have been a light to my path and guidance in the dark. I would like to thank the committee members, Asst. Prof. Dr. Selçuk Himmetoğlu, Asst. Prof. Dr. Okan Görtan, Asst. Prof. Dr. Mehmet Nurullah Balcı, and Asst. Prof. Dr. Ali Amini, for their valuable feedback and contributions to the thesis.

I would also like to thank my dear friend Burak Arıkan, Emre Kızıltav, Tolga Özkan, Burhan Çomruk, Yusuf Emek, Buğra Aydın, and Bilal Toprak for their moral support.

Finally but most importantly, this study could not have existed without my great family, my parents Suzan and Hazım, my sisters Gizem and Sinem, and my precious wife Buğçe, who have always stood by me and supported me.

CONTENTS

Page

TABLES

FIGURES

ABBREVIATIONS

EOM	:	**E**quation **O**f **M**otion
COM	:	**C**enter **O**f **M**ass
DOF	:	**D**egree **O**f **F**reedom
LTI	:	**L**inear **T**ime **I**nvariant
$\mathbf{L}$	:	Length of the body (from rear leg joint to front leg joint)
$\mathbf{L_f}$	:	Distance between front leg joint and body center of mass
$\mathbf{L_r}$	:	Distance between rear leg joint and body center of mass
$\mathbf{R_f}$	:	Distance between front leg joint and front leg center of mass
$\mathbf{R_r}$	:	Distance between rear leg joint and rear leg center of mass
$\mathbf{M_b}$	:	Mass of the Body
$\mathbf{M_l}$	:	Mass of a leg
$\mathbf{I_b}$	:	Body inertia around centroidal z-axis
$\mathbf{I_l}$	:	Leg inertia around centroidal z-axis
$\boldsymbol{\theta}$	:	Angle between body fixed ground oriented frame x-axis and body center line.
$\boldsymbol{\theta_f}$	:	Front leg angle according to body center line
$\boldsymbol{\theta_r}$	:	Rear leg angle according to body center line
$\mathbf{r_b}$	:	Body COM position vector
$\mathbf{r_f}$	:	Front leg COM position vector
$\mathbf{r_r}$	:	Rear leg COM position vector
$\mathbf{v_b}$	:	Body COM velocity vector
$\mathbf{v_f}$	:	Front leg COM velocity vector
$\mathbf{v_r}$	:	Rear leg COM velocity vector
$\mathbf{a_b}$	:	Body COM acceleration vector
$\mathbf{a_f}$	:	Front leg COM acceleration vector
$\mathbf{a_r}$	:	Rear leg COM acceleration vector

1. INTRODUCTION

This thesis focused on modeling and control of a legged robot (RHex) in temporary flight conditions. Although a terrestrial robot with the capability of flying is not a novel idea, the use of legs in the air for attitude control and so positioning the thrust vector is one.

Wheeled robots are at the forefront with their high speed on flat surfaces and easily controllable dynamics. However, when it comes to overcoming obstacles, the chances of success of wheeled robots are meager. Since the robot is expected to use its flight capability as a last choice due to the high power requirements of thrusters, the robot developed for uneven terrains is expected to have a high obstacle-overcoming capability. On the other hand, legged robots are the man of the day when comparison comes to overcoming obstacles. Also, legged robots have one advantage in attitude control: limb asymmetry with respect to the limb joint axis. A wheeled robot also can be used for body pitch motion control in the air since the reaction torque of the wheel effect this axis. However, for roll motion, wheels are not usable actuators since they are symmetric around the axis of rotation.

A well-designed terrestrial robot can succeed in rough terrains, but this success always has a proportionality to limb lengths. Although some special-purpose robots can climb flat vertical walls, it is not the case in harsh environments. But for robotics engineers, a robot with perfect obstacle-overcoming capability is always a goal. To achieve this, many scientists have turned to robots with hybrid locomotion: a robot that can walk and fly. The same concept will be examined in this study with a different approach. Only one thruster will be used on the robot, while the legs will be used for attitude control with; as a result, thrust vector positioning.

1.1. Scope Of The Thesis

This thesis is focused on the modeling and the control of a novel robot and also, offers a procedure for a novel robot modeling and control. In the thesis, a 2D simplified model of the robot is obtained, and equations of motions are created and validated. The validated equations of motion are linearized for an LTI controller design. Also designed controller is simulated with a multibody dynamics program, and the controller's performance is discussed.

1.2. Organization

The organization of the thesis is as follows:

- Chapter 1 presents our motivation, contributions, and the scope of this thesis.
- Chapter 2 provides examples of different parts of the thesis. Since leg-controlled flying is a novel idea, literature is mostly used to decide on a robot platform and usable technics for control.
- Chapter 3 gives the theory that will be used later in the thesis to inform the reader. Hence equation of motion determination and linearization are well-known to the expected readers; theory explanations mainly focus on state-space control methodology.
- Chapter 4 introduces the derivation and linearization of system dynamics and a designed controller.
- Chapter 5 demonstrates validations of steps introduced in chapter 4 and discusses the controller performance
- Chapter 6 states the results obtained from this thesis.

2. LITERATURE SURVEY

2.1. Introduction

In this chapter, some studies that inspired this thesis are explained and the current literature on flying-legged robots is shared. In the section 2.2. robots, some robots that are candidates for flying capability integration are investigated. In section 2.3., some studies in legged flying robots are given, and in the 2.4., some studies in attitude control by reaction torques concept is examined.

2.2. Highly Maneuverable Robots

Robots are thriving in many areas, including terrains with obstacles. However, an obstacle a terrestrial robot can overcome often depends on the length of the robot's limbs and the physical nature of the barrier, such as slope and surface shape. While some wheeled robot types suggest different use of wheels to obtain better obstacle-overcoming performance, they lost some of their advantageous properties coming from wheels, such as fastness on flat surfaces. Shiroma et al. proposed a different approach to wheeled robots, such as using wheel assemblies as legs in some cases to preserve the advantages of both platforms [1]. Their robot HANZO comprises three subassemblies: left wheel-arm, right wheel-arm, and body. The HANZO robot can position itself in five modes to overcome obstacles when required. In the first mode, the robot is a wheeled robot that uses differential steering; in the second mode, it can change the body COM position; in the third mode, its left and right wheel-arms are placed oppositely to be longer. Its fourth and fifth modes are vertical modes with higher and lower COM positions.

Jihoon Kim et al., in 2017, worked on a mobile robot with passively articulated driving tracks for high terrainability and maneuverability on unstructured rough terrains [2]. They proposed a Tiltable Quad-Tracked Mobile Robot (TQTMR) and compared it with several existing mechanisms. TQTMR mechanism consists of four driving tracks, two rocker links,

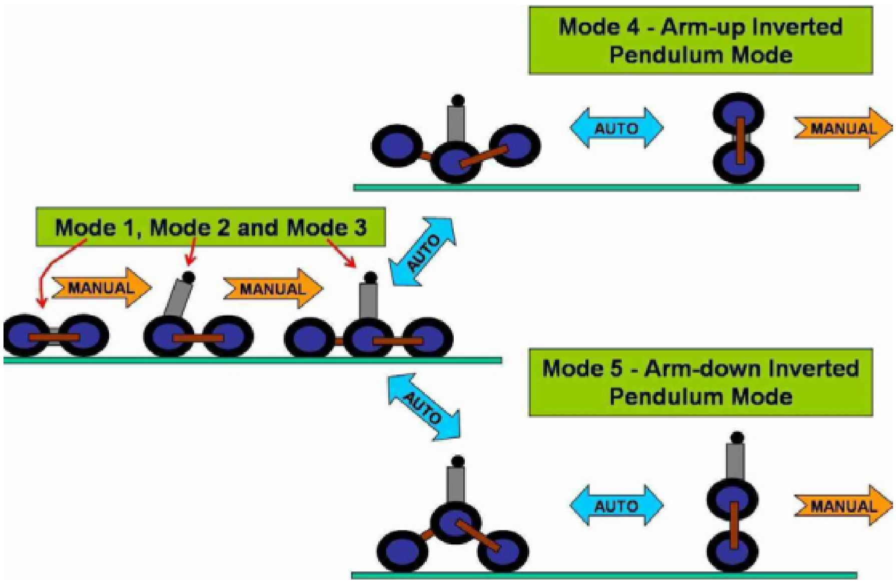

Figure 2.1 Locomotion modes of the HANZO robot [1]

and four 2-DOF pitch-roll passive joints, allowing the track posture to adapt freely to the ground curvature. A photo of this mechanism is given in figure 2.2.

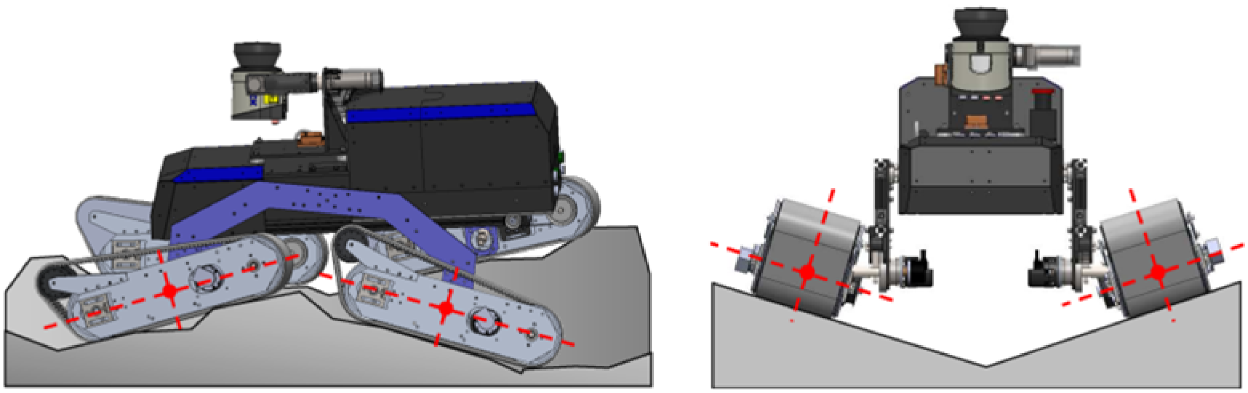

Figure 2.2 TQTMR mechanism on different type of environments [2]

Ozcelik et al. designed a robot with wheels at the end of its six legs, and the robot can extend each using a spiral lift [3]. This robot is designed to adapt surface shapes by adjusting the length of its legs. Ozcelik et al. stated in their study that no 'ideal' system could simultaneously maximize controllability, maneuverability, and stability. Their design solutions are excellent for smoothly changing surface shapes but are hard to use in a harsh environment.

In another study by Kilin et al., Omni-wheel mobile robots are experimentally investigated, and a dynamic model for controlling an Omni-wheel robot is presented [4]. This study also stated that the theoretical model of the motion is based on the condition of no rollers slipping. Still, in practice, the condition of slipping rollers is only sometimes a solvable but always a complicated problem.

Saranli et al. investigated the high mobility of a six-legged RHex robot [5]. The robot has a rigid body and six compliant legs connected to the body via a revolute joint. Saranli et al. stated that this robot also prevents the common problem of toe stubbing in the protraction phase by rotating its legs in a full circle. In addition, the RHex robot use advantage of tripod gait as the two tripods are driven relative antiphase. The retraction phase is conducted slowly, followed by a fast protraction phase. As stated in this study, robot rough-terrain performances and obstacle-crossing capabilities are not carefully documented in the literature. Saranli et al. established new standards such as body lengths per second, specific resistance $\epsilon = P/mgv$ (to compare the endurance of robots), and metric characterization (to reach the success of robots on various terrain features).

Figure 2.3 First generation RHex robot [5]

The authors have created a test setup to test the RHex robot's locomotion performance in maneuverability, obstacle-crossing capability, and payload resistance. The tests have been performed on different terrains such as carpet, linoleum, grass, gravel, rough, and obstacle course. At least ten successful tests have been made on each condition, while payload tests have been made on a flat surface. Experiments show that the fastest speed is achieved on grass and gravel because their irregular surfaces provide improved traction, resulting in more significant variations in rate. Since the friction coefficient is lower on linoleum, the speed is less than other flat surface tests. The test made on the carpet is the most consistent, with a speed of 0.51 m/s and minimum rate variations. The rough surface environment is created using wooden blocks with the same surface shape but different heights. It is stated that the RHex robot has shown unexpectedly good performance in this environment. The obstacle crossing test is designed with two obstacles; one is 15 cm high (this represents 80% of the robot's leg length and exceeds ground clearance), and the other is 22 cm high while they are placed a half robot length apart. According to the authors, the robot has surmounted both obstacles, neither sensing nor changing the controller parameters used in the flat surface forward locomotion [5].

D. Campbell and M. Buehler studied an open loop controller for the RHex robot for stair descending [6]. Their clock-driven controllers require no operator input other than a selection of one of two sets of trajectories depending on the slope of stairs. E.Z. Moore et al. described an open loop controller that enables the RHex robot to reliably climb a wide range of regular, full-size stairs with no operator input during stair climbing [7].

2.3. Flying Legged Robots

Building a ground vehicle with the short-term flying capability to create a robot with excessive obstacle-crossing ability is not a novel idea. A miniature robot that combines wheeled ground locomotion with rotary-wing flight capabilities is studied in [8]. As stated in the article, to reach the full potential of the robot, additional works are presented in another paper [9]. The study found that hybrid-locomotion vehicles utilizing rotary-wing flight are most valuable when the design is optimized for ground mode performance. It is also an important statement for this thesis because the approach to the vehicle concept is quite similar. Another necessary inference from the study is that using mechanisms with multiple functions will help reduce mass. Kevin Peterson and Ronald S. Fearing worked on a bipedal ornithopter; the BOLT robot [10]. The BOLT transitions from the ground running to aerial hovering in as little as one meter of the runway. In terrestrial locomotion, the robot also uses its wings because of the coupling between its legs and wings. A robot that combines a wheel shape swimming float with a quadcopter is studied in [11]. In terrestrial locomotion, it uses its surrounding ring as a robot wheel and the reaction torques of its propellers as actuators. It also steers itself by propeller thrust vectors.

A humanoid robot with four thrusters, each on one end effector (two on hands, two on feet), is controlled in flight [12]. The control objective proposed in the paper is to obtain asymptotic stabilization of the robot's center of mass and body angular momentum in the sense of Lyapunov. The desired trajectory is followed by the robot's center of mass, while the errors between the reference orientation and the robot base frame are kept small. A humanoid robot, seventeen kg in mass and 830mm in height, is mobilized with four thrusters, two on its waist and two on each foot [13]. The robot is controlled in aerial motion by the attitude of its legs and leg-fixed thrusters' thrust vectors. Ducted fans are used as thrusters. The study also states that actuators capable of the necessary joint torque are required when the thrusters are at their total capacity.

On the other side, thrust vector control stabilizes legged locomotion in Harpy and Leonardo robots [14, 15]. HARPY robot controls two ducted fans on its head at the right and left sides, while LEONARDO has four propellers on its head. LEONARDO robot even can skateboard by using its propellers for stabilization.

2.4. Attitude Control With Reaction Torques

While the RHex platform planned to have a body-fixed thruster, its thurst vector should be controlled by body attitude. Its leg actuators will be used in body attitude control and to achieve body positioning; it is beneficial to the profit of its legs' reaction torques. It is pretty studied in spacecraft attitude control. A. Weiss et al. studied a control algorithm that controls

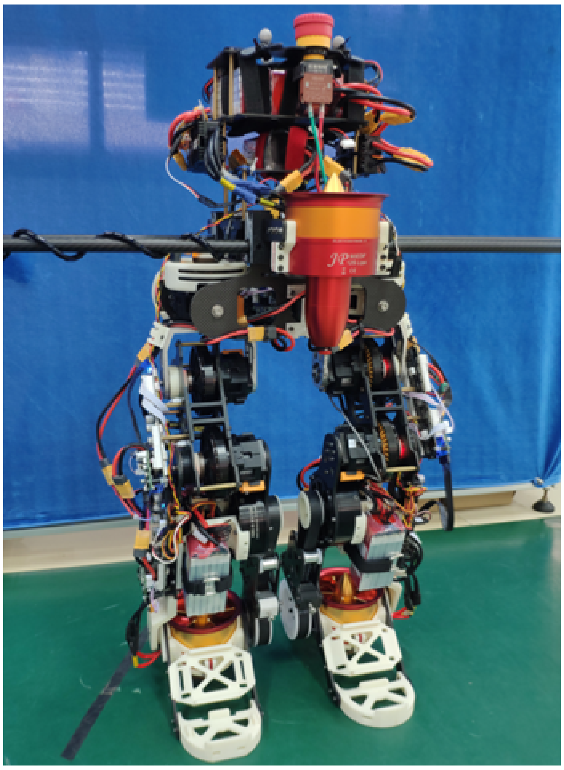

Figure 2.4 Humanoid robot Jet-HR2 with four thrusters [13]

the spacecraft's attitude using applied reaction torques [16], while Narottama Esser studied variable inertia reaction wheels [17].

2.5. Conclusion

In this chapter, the state of the art was presented. This chapter also shows that the RHex robot is very easy-to-use and highly maneuverable, with many maneuvering algorithms studied. Implementation of a fixed thruster is also straightforward on the RHex robot. The section 2.4. also shows the use of reaction torque motion control, which was planned to use in this study.

3. THEORY

3.1. Introduction

In this section, the reader will be informed about the control system analysis and design for a RHex robot.

State space representation, system analysis, and control system design in state space will be covered. These theoretical explanations are also will be used or can be used in the chapter 4.

Some well-known concepts will not be covered in this section because, for an expected reader, some concepts like Newton's method for EOM derivation, Lagrange's method for EOM derivation, linearization of system dynamics, and classical control theory are frequently used. Although they are not explained in this chapter, they will be used in chapter 4.

3.2. Control System Analysis in State Space

Modern control problems mainly deal with complex systems with multiple inputs and outputs and complex interrelations between these inputs and outputs. To reduce this complexity state space model can be used.

3.2.1. State Space Representation

It is possible to create n first-order differential equations to represent an nth-order differential equation. Also, those n first-order differential equations can be expressed in the matrix form. A system represented by n first-order linear differential equation with m-many inputs (each input shown by u and subscript number) and l-many outputs (each output shown by y and a subscript number) can be formed to state space notation as shown in equation 1 and 2.

$$\begin{Bmatrix} \dot{x}_1 \\ \dot{x}_2 \\ \cdot \\ \dot{x}_n \end{Bmatrix} = \begin{bmatrix} A_{11} & A_{12} & \cdot & A_{1,n} \\ A_{21} & A_{22} & \cdot & A_{2,n} \\ \cdot & \cdot & \cdot & \cdot \\ A_{n,1} & A_{n,2} & \cdot & A_{n,n} \end{bmatrix} \begin{Bmatrix} x_1 \\ x_2 \\ \cdot \\ x_n \end{Bmatrix} + \begin{bmatrix} B_{11} & B_{12} & \cdot & B_{1,m} \\ B_{21} & B_{22} & \cdot & B_{2,m} \\ \cdot & \cdot & \cdot & \cdot \\ B_{n,1} & B_{n,2} & \cdot & B_{n,m} \end{bmatrix} \begin{Bmatrix} u_1 \\ u_2 \\ \cdot \\ u_m \end{Bmatrix} \tag{1}$$

$$\begin{Bmatrix} y_1 \\ y_2 \\ \cdot \\ y_l \end{Bmatrix} = \begin{bmatrix} C_{11} & C_{12} & \cdot & C_{1,n} \\ C_{21} & C_{22} & \cdot & C_{2,n} \\ \cdot & \cdot & \cdot & \cdot \\ C_{l,1} & C_{l,2} & \cdot & C_{l,n} \end{bmatrix} \begin{Bmatrix} x_1 \\ x_2 \\ \cdot \\ x_n \end{Bmatrix} + \begin{bmatrix} D_{11} & D_{12} & \cdot & D_{1,m} \\ D_{21} & D_{22} & \cdot & D_{2,m} \\ \cdot & \cdot & \cdot & \cdot \\ D_{l,1} & D_{l,2} & \cdot & D_{l,m} \end{bmatrix} \begin{Bmatrix} u_1 \\ u_2 \\ \cdot \\ u_m \end{Bmatrix} \tag{2}$$

This representation can be abbreviated to the form shown in 3.

$$\begin{aligned} \dot{\mathbf{x}} &= \mathbf{Ax} + \mathbf{Bu} \\ \mathbf{y} &= \mathbf{Cx} + \mathbf{Du} \end{aligned} \tag{3}$$

Eigenvalues of A matrix are roots of the characteristic polynomial and eigenvalues are stated with λ in equation 4.

$$|\lambda \boldsymbol{I} - \mathbf{A}| = 0 \tag{4}$$

The transfer function matrix of a MIMO system can be obtained from its state space representation, as shown in equation set 5. An important note to know about the notation used in this thesis, a bold letter indicates a vector while bold capital letters are for matrices.

$$
\begin{gathered}
\mathcal{L}\{\dot{\boldsymbol{x}}\} = \mathcal{L}\{\boldsymbol{Ax} + \boldsymbol{Bu}\} \\
\mathcal{L}\{\boldsymbol{y}\} = \mathcal{L}\{\boldsymbol{Cx} + \boldsymbol{Du}\} \\
\{s\boldsymbol{X} = \boldsymbol{AX} + \boldsymbol{BU} \\
s\boldsymbol{X} - \boldsymbol{AX} = \boldsymbol{BU} \\
(s\boldsymbol{I} - \boldsymbol{A})\boldsymbol{X} = \boldsymbol{BU} \\
\boldsymbol{X} = (s\boldsymbol{I} - \boldsymbol{A})^{-1}\boldsymbol{BU} \\
\boldsymbol{Y} = \boldsymbol{CX} + \boldsymbol{DU} \\
\boldsymbol{Y} = \boldsymbol{C}(s\boldsymbol{I} - \boldsymbol{A})^{-\mathbf{1}}\boldsymbol{BU} + \boldsymbol{DU} = \big(\boldsymbol{C}(s\boldsymbol{I} - \boldsymbol{A})^{-\mathbf{1}}\boldsymbol{B} + \boldsymbol{D}\big)\,\boldsymbol{U} \\
\frac{\boldsymbol{Y}}{\boldsymbol{U}} = \boldsymbol{C}(s\boldsymbol{I} - \boldsymbol{A})^{-\mathbf{1}}\boldsymbol{B} + \boldsymbol{D}
\end{gathered}
\tag{5}
$$

3.2.2. Solution of Homogeneous State Equations

First, the power series expansion of an exponential function is shown in equation 6.

$$
e^{at} = \sum_{k=0}^{\infty} \frac{(at)^k}{k!} = 1 + at + \frac{a^2t^2}{2} + \frac{a^3t^3}{6} + \frac{a^4t^4}{24} + \cdots \frac{a^nt^n}{n!} + \cdots \tag{6}
$$

This power series expansion also can be applied for matrix exponential functions and it is shown in equation 7.

$$
e^{\mathbf{A}t} = \sum_{k=0}^{\infty} \frac{(\boldsymbol{A}t)^k}{k!} = \boldsymbol{I} + \boldsymbol{A}t + \frac{\boldsymbol{A}^2t^2}{2} + \frac{\boldsymbol{A}^3t^3}{6} + \frac{\boldsymbol{A}^4t^4}{24} + \cdots \frac{\boldsymbol{A}^nt^n}{n!} + \cdots \tag{7}
$$

If the state space model is reduced to a homogeneous form given in equation 8

$$
\dot{\mathbf{x}} - \mathbf{A}\mathbf{x} = \mathbf{0} \tag{8}
$$

Let's assume that x is a function in the form of power series, so its solution is as given in equation 9.

$$\mathbf{x}(t) = \mathbf{b}_0 + \mathbf{b}_1 t + \mathbf{b}_2 t^2 + \cdots + \mathbf{b}_k t^k + \cdots \tag{9}$$

If this assumed solution is substituted into equation 8, it is obtained as given in equation 10.

$$\begin{aligned} &\mathbf{b}_1 + 2\mathbf{b}_2 t + 3\mathbf{b}_3 t^2 + \cdots + k\mathbf{b}_k t^{k-1} + \cdots \\ &= \mathbf{A}\left(\mathbf{b}_0 + \mathbf{b}_1 t + \mathbf{b}_2 t^2 + \cdots + \mathbf{b}_k t^k + \cdots\right) \end{aligned} \tag{10}$$

Thus, equating all coefficients of 't' that appear on both sides of equation set 11 will be created.

$$\begin{aligned} \mathbf{b}_1 &= \mathbf{A}\mathbf{b}_0 \\ \mathbf{b}_2 &= \frac{1}{2}\mathbf{A}\mathbf{b}_1 = \frac{1}{2}\mathbf{A}^2\mathbf{b}_0 \\ \mathbf{b}_3 &= \frac{1}{3}\mathbf{A}\mathbf{b}_2 = \frac{1}{3\times 2}\mathbf{A}^3\mathbf{b}_0 \\ &. \\ &. \\ \mathbf{b}_k &= \frac{1}{k!}\mathbf{A}^k\mathbf{b}_0 \end{aligned} \tag{11}$$

At last, t can be equated to zero to find the states's initial value as expressed in equation 12

$$\mathbf{x}(0) = \mathbf{b}_0 \tag{12}$$

Thus the solution of x(t) can be obtained as given in equation 13.

$$\mathbf{x}(t) = \left(\mathbf{I} + \mathbf{A}t + \frac{1}{2!}\mathbf{A}^2 t^2 + \cdots + \frac{1}{k!}\mathbf{A}^k t^k + \cdots\right)\mathbf{x}(0) \tag{13}$$

In equation 13, the expression in the parentheses is the expansion of the exponential matrix power series given in equation 7. So, it can be rewritten as shown in equation 14.

$$\mathbf{x}(t) = e^{\mathbf{A}t}\mathbf{x}(0) \tag{14}$$

3.2.3. Solution of Nonhomogeneous State Equations

Let's start with representing nonhomogeneous state equations given in equation 15.

$$\dot{\boldsymbol{x}}(t)=\boldsymbol{A}\boldsymbol{x}(t)+\boldsymbol{B}\boldsymbol{u}(t) \tag{15}$$

Rewriting equation 15, one can find equation 16

$$.\dot{\boldsymbol{x}}(t)-\boldsymbol{A}\boldsymbol{x}(t)=\boldsymbol{B}\boldsymbol{u}(t) \tag{16}$$

Pre-multiplying both sides of equation by e^{-At}, equation 17 will be obtained.

$$e^{-\mathbf{A}t}[\dot{\mathbf{x}}(t)-\mathbf{A}\mathbf{x}(t)]=\frac{d}{dt}\left[e^{-\mathbf{A}t}\mathbf{x}(t)\right]=e^{-\mathbf{A}t}\mathbf{B}\mathbf{u}(t) \tag{17}$$

And integrating both sides from zero to t with respect to time, solutions of nonhomogeneous state equations can be found as given in equations 18 and 19.

$$e^{-\mathbf{A}t}\mathbf{x}(t)-\mathbf{x}(0)=\int_0^t e^{-\mathbf{A}\tau}\mathbf{B}\mathbf{u}(\tau)d\tau \tag{18}$$

$$\mathbf{x}(t)=e^{\mathbf{A}t}\mathbf{x}(0)+\int_0^t e^{\mathbf{A}(t-\tau)}\mathbf{B}\mathbf{u}(\tau)d\tau \tag{19}$$

3.2.4. Controllability

Controllability defines the capability of a system, to transfer its states from any initial state to any desired state utilizing an unconstrained control input vector. If all system states are controllable, the system is named as completely state-controllable. The solution of system state equations can be considered to investigate a system in a controllability manner. If the desired final state is accepted as the origin of the space and t_0 is taken as zero, one can write equation 20.

$$\mathbf{x}\left(t_1\right)=\mathbf{0}=e^{\mathbf{A}t_1}\mathbf{x}(0)+\int_0^{t_1} e^{\mathbf{A}(t_1-\tau)}\mathbf{B}u(\tau)d\tau \tag{20}$$

According to equation 20, initial states can be found as given in equation 21.

$$\mathbf{x}(0) = -\int_0^{t_1} e^{-\mathbf{A}\tau}\mathbf{B}u(\tau)d\tau \tag{21}$$

Exponential function expansion is known as equation 22:

$$e^{-\mathbf{A}\tau} = \sum_{k=0}^{n-1} \alpha_k(\tau)\mathbf{A}^k \tag{22}$$

By substitution, equation 23 will be obtained.

$$\mathbf{x}(0) = -\sum_{k=0}^{n-1} \mathbf{A}^k\mathbf{B}\int_0^{t_1} \alpha_k(\tau)u(\tau)d\tau \tag{23}$$

Assume a new variable β as given in equation 24

$$\mathbf{x}(0) = -\sum_{k=0}^{n-1} \mathbf{A}^k\mathbf{B}\int_0^{t_1} \alpha_k(\tau)u(\tau)d\tau \tag{24}$$

With this new variable equation, 23 becomes as in 25.

$$\mathbf{x}(0) = -\sum_{k=0}^{n-1} \mathbf{A}^k\mathbf{B}\beta_k \tag{25}$$

This equation can be written in the matrix form as shown in equation 26.

$$\mathbf{x}(0) = -\begin{bmatrix} \mathbf{B} & \mathbf{AB} & \cdots & \mathbf{A}^{n-1}\mathbf{B} \end{bmatrix} \begin{bmatrix} \beta_0 \\ \hline \beta_1 \\ \hline \cdot \\ \cdot \\ \cdots \\ \hline \beta_{n-1} \end{bmatrix} \tag{26}$$

The controllability matrix is given in equation 27 as the first multiplier of equation 26. The controllability matrix is expected to be the rank of 'n' to satisfy the complete state controllability condition.

$$M_{co} = \begin{bmatrix} \mathbf{B} & \mathbf{AB} & \cdots & \mathbf{A}^{n-1}\mathbf{B} \end{bmatrix} \tag{27}$$

3.3. Control System Design in State Space

3.3.1. State Feedback Control

State feedback control is based on the pole placement approach. The main idea behind the pole placement is to determine dominant pole locations and place all other poles far from these dominant poles to suppress their effects. The poles of the transfer functions are the eigenvalues of the system. If one can place all eigenvalues in desired places, one can determine the system's behavior. So, a control system design can be made for transient behavior or frequency response as well as steady state requirements. To determine the gain matrix, let's say that inputs are proportional to instantaneous values of states as in equation 28

$$\mathbf{u} = -\mathbf{K}\mathbf{x} \tag{28}$$

Substitution of equation 28 to equation 15 results in equation 29

$$\dot{\mathbf{x}}(t) = (\mathbf{A} - \mathbf{BK})\mathbf{x}(t) \tag{29}$$

As it is discussed in subsection 3.2.2., the solution of equation 8 is found as equation 30

$$\mathbf{x}(t) = e^{(\mathbf{A}-\mathbf{BK})t}\mathbf{x}(0) \tag{30}$$

Where $\mathbf{x}(0)$ indicates initial states caused by external disturbances.

To prove the statement for arbitrary pole placement, let's assume that the system is not completely state-controllable. So, the controllability matrix can be written as given in inequality 31.

$$\mathrm{rank}\begin{bmatrix} \mathbf{B} & \mathbf{AB} & \cdots & \mathbf{A}^{n-1}\mathbf{B} \end{bmatrix} = q < n \tag{31}$$

Let's assume that $\mathbf{f_1}$, $\mathbf{f_2}$, and $\mathbf{f_q}$ are independent rows of controllability matrix where $(n-p)$ additional n vectors of v is added to obtain a non-singular matrix as shown in equation 32

$$\mathbf{P} = \begin{bmatrix} \mathbf{f}_1 & \mathbf{f}_2 & \cdots & \mathbf{f}_q & \mathbf{v}_{q+1} & \mathbf{v}_{q+2} & \cdots & \mathbf{v}_n \end{bmatrix} \tag{32}$$

Then it can be shown as in equation 33

$$\hat{\mathbf{A}} = \mathbf{P}^{-1}\mathbf{A}\mathbf{P} = \begin{bmatrix} \mathbf{A}_{11} & \mathbf{A}_{12} \\ \mathbf{0} & \mathbf{A}_{22} \end{bmatrix}, \quad \hat{\mathbf{B}} = \mathbf{P}^{-1}\mathbf{B} = \begin{bmatrix} \mathbf{B}_{11} \\ \mathbf{0} \end{bmatrix} \tag{33}$$

Let's define the gain matrix as the following equation 34:

$$.\hat{\mathbf{K}} = \mathbf{K}\mathbf{P} = \begin{bmatrix} \mathbf{k}_1 & \mathbf{k}_2 \end{bmatrix} \tag{34}$$

Now following equation set 35 shows the eigenvalues of the obtained controlled system.

$$
\begin{aligned}
|s\mathbf{I}-\mathbf{A}+\mathbf{BK}| &= \left|\mathbf{P}^{-1}(s\mathbf{I}-\mathbf{A}+\mathbf{BK})\mathbf{P}\right| \\
&= \left|s\mathbf{I}-\mathbf{P}^{-1}\mathbf{AP}+\mathbf{P}^{-1}\mathbf{BKP}\right| \\
&= |s\mathbf{I}-\hat{\mathbf{A}}+\hat{\mathbf{B}}\hat{\mathbf{K}}| \\
&= \left|s\mathbf{I}-\begin{bmatrix}\mathbf{A}_{11} & \mathbf{A}_{12} \\ \mathbf{0} & \mathbf{A}_{22}\end{bmatrix}+\begin{bmatrix}\mathbf{B}_{11} \\ \mathbf{0}\end{bmatrix}\begin{bmatrix}\mathbf{k}_1 & \mathbf{k}_2\end{bmatrix}\right| \\
&= \begin{vmatrix}\mathbf{I}_q-\mathbf{A}_{11}+\mathbf{B}_{11}\mathbf{k}_1 & -\mathbf{A}_{12}+\mathbf{B}_{11}\mathbf{k}_2 \\ \mathbf{0} & s\mathbf{I}_{n-q}-\mathbf{A}_{22}\end{vmatrix} \\
&= \left|s\mathbf{I}_q-\mathbf{A}_{11}+\mathbf{B}_{11}\mathbf{k}_1\right|\cdot\left|s\mathbf{I}_{n-q}-\mathbf{A}_{22}\right| = 0
\end{aligned} \tag{35}
$$

In the preceding equations, one can find that in the non-existence of complete state controllability, eigenvalues of part A22 will not be arbitrarily placed at desired locations. Then, complete state controllability appears as a necessary condition for arbitrary pole placement. In the next step, let's prove it is also a sufficient condition.

When the system is entirely state-controllable, the controllability matrix will be rank of n. W matrix is given in equation 36, which is defined from coefficients of the characteristic polynomial:

$$
\mathbf{W} = \begin{bmatrix}
a_{n-1} & a_{n-2} & \cdots & a_1 & 1 \\
a_{n-2} & a_{n-3} & \cdots & 1 & 0 \\
. & . & & . & . \\
. & . & & . & . \\
. & . & & . & . \\
a_1 & 1 & \cdots & 0 & 0 \\
1 & 0 & \cdots & 0 & 0
\end{bmatrix} \tag{36}
$$

Where a_i's are obtained from the characteristic equation as shown in equation 37.

$$|s\mathbf{I} - \mathbf{A}| = s^n + a_1 s^{n-1} + \cdots + a_{n-1}s + a_n \tag{37}$$

A transformation matrix that is defined as given in equation38 will be obtained.

$$\mathbf{T} = \mathbf{TW} \tag{38}$$

With this transformation matrix, a new state vector will be created as given in equation 39.

$$\mathbf{x} = \mathbf{T}\hat{\mathbf{x}} \tag{39}$$

With the required arrangements new state equation will be expressed as in equation 40

$$\dot{\hat{\mathbf{x}}} = \mathbf{T}^{-1}\mathbf{AT}\hat{x} + \mathbf{T}^{-1}\mathbf{B}u \tag{40}$$

By the definition of desired eigenvalues, the desired characteristic equation will be formed as in equation 41.

$$(s - \mu_1)(s - \mu_2) \cdots (s - \mu_n) = s^n + \alpha_1 s^{n-1} + \cdots + \alpha_{n-1}s + \alpha_n = 0 \tag{41}$$

Inputs of the system will be linearly dependent on the states as given in the equation 42

$$\mathbf{u} = -\mathbf{KT}\hat{\mathbf{x}} \tag{42}$$

Then, the state equation for the regulator system will be obtained as the following equation (43).

$$\dot{\hat{\mathbf{x}}} = \mathbf{T}^{-1}\mathbf{AT}\hat{\mathbf{x}} - \mathbf{T}^{-1}\mathbf{BKT}\hat{\mathbf{x}} \tag{43}$$

This resulted in a new characteristic equation shown in equation 44.

$$\left|s\mathbf{I} - \mathbf{T}^{-1}\mathbf{A}\mathbf{T} + \mathbf{T}^{-1}\mathbf{B}\mathbf{K}\mathbf{T}\right| = 0 \tag{44}$$

It can be expanded for further inspection as in 45.

$$\begin{aligned}
&= \left| s\boldsymbol{I} - \begin{bmatrix} 0 & 1 & \cdots & 0 \\ . & . & & . \\ . & . & & . \\ . & . & & . \\ 0 & 0 & \cdots & 1 \\ -a_n & -a_{n-1} & \cdots & -a_1 \end{bmatrix} + \begin{bmatrix} 0 \\ . \\ . \\ . \\ 0 \\ 1 \end{bmatrix} [\delta_n \delta_{n-1} \cdots \quad \delta_1] \right| \\
&= \begin{vmatrix} s & -1 & \cdots & 0 \\ 0 & s & \cdots & 0 \\ . & . & & . \\ . & . & & . \\ . & . & . & \\ a_n + \delta_n & a_{n-1} + \delta_{n-1} & \cdots & s + a_1 + \delta_1 \end{vmatrix} \\
&= s^n + (a_1 + \delta_1)\, s^{n-1} + \cdots + (a_{n-1} + \delta_{n-1})\, s + (a_n + \delta_n) = 0
\end{aligned} \tag{45}$$

If equation 41 and equation 45 are equated equation 46 will be obtained.

$$\begin{aligned}
a_1 + \delta_1 &= \alpha_1 \\
a_2 + \delta_2 &= \alpha_2 \\
a_n + \delta_n &= \alpha_n
\end{aligned} \tag{46}$$

Then the gain matrix will be obtained as the following equation (47).

$$\mathbf{K} = \left[\begin{array}{cccc} \delta_n & \delta_{n-1} & \cdots & \delta_1 \end{array} \right] \mathbf{T}^{-1}$$

$$\alpha_n - a_n \quad \alpha_{n-1} - a_{n-1} \quad \cdots \quad \alpha_2 - a_2 \quad \alpha_1 - a_1] \, \mathbf{T}^{-1} \tag{47}$$

3.4. Design of Type-1 Servo Systems when the Plant has Integrator

If the plant involves an integrator, the design of a type 1 servo system is relatively straightforward. It is pervasive to select some state variables as output, so for the scalar case, let's choose the first state as output. All other states can be regulated with the state feedback regulator while the first state is compared with a reference value, and the error is fed to the controller. The current controller configuration will be in the form given in figure 3.1.

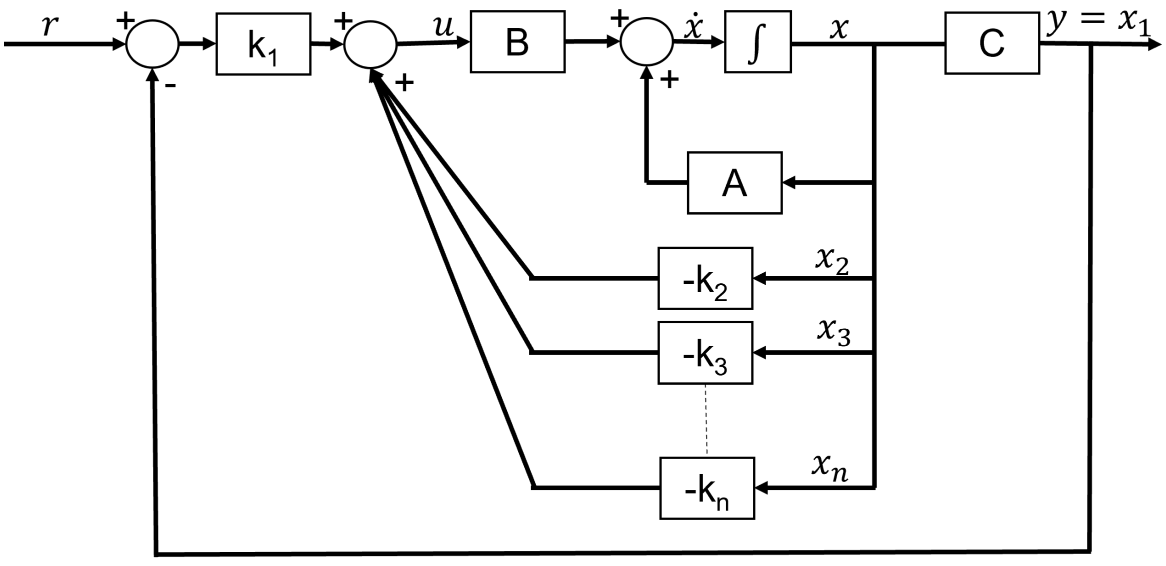

Figure 3.1 Block diagram of a SISO type 1 state feedback servo system when the plant has an integrator. [18]

The input u of the plant now can be written as in equation 48

$$
\begin{aligned}
u &= -\begin{bmatrix} 0 & k_2 & k_3 & \cdots & k_n \end{bmatrix} \begin{bmatrix} x_1 \\ x_2 \\ \cdot \\ \cdot \\ \cdot \\ x_n \end{bmatrix} + k_1\left(r - x_1\right) \\
&= -\mathbf{K}\mathbf{x} + k_1 r
\end{aligned} \tag{48}
$$

Where,

$$
\mathbf{K} = \begin{bmatrix} k_1 & k_2 & k_3 & \cdots & k_n \end{bmatrix} \tag{49}
$$

The system dynamics of the system given in figure 3.1 can be modeled by equation 50.

$$
\dot{\mathbf{x}} = \mathbf{A}\mathbf{x} + \mathbf{B}u = (\mathbf{A} - \mathbf{B}\mathbf{K})\mathbf{x} + \mathbf{B}k_1 r \tag{50}
$$

At steady state, the state equation will be in the form equation 51

$$
\dot{\mathbf{x}}(\infty) = (\mathbf{A} - \mathbf{B}\mathbf{K})\mathbf{x}(\infty) + \mathbf{B}k_1 r(\infty) \tag{51}
$$

Since the $r(t)$ is a step function, the $r(\infty)$ will be equal to $r(t)$ and r. By subtracting equation 50 from equation 51 one can obtain equation 52

$$
\dot{\mathbf{x}}(t) - \dot{\mathbf{x}}(\infty) = (\mathbf{A} - \mathbf{B}\mathbf{K})[\mathbf{x}(t) - \mathbf{x}(\infty)] \tag{52}
$$

With the definition of error, equation 53 will be obtained.

$$
\mathbf{x}(t) - \mathbf{x}(\infty) = \mathbf{e}(t) \tag{53}
$$

The new state space equation will be in the form given in equation 54

$$\dot{\mathrm{e}} = (\mathbf{A} - \mathbf{BK})\mathbf{e} \tag{54}$$

3.5. Design of Type-1 Servo System when the Plant Has No Integrator

When the plant has no integrator, the system is called a type-zero system. With state feedback control, the steady-state error of the type-zero system against step input will be constant. An integrator will be added between the error comparator and the state feedback gain to obtain a type-one system. The Block diagram of the introduced servo control system is shown in figure 3.2

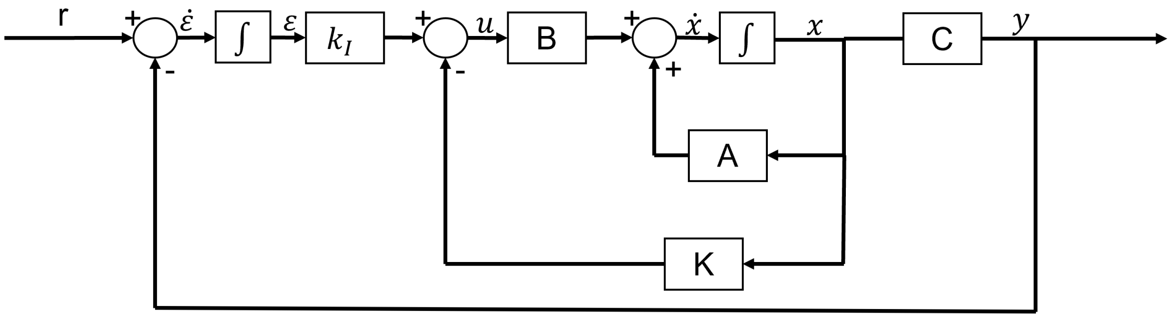

Figure 3.2 Block diagram of a type-1 servo system when the plant has no integrator. [18]

A new state will be introduced if the new state equations are written as in equation 55 according to the figure above.

$$\begin{bmatrix} \dot{\mathbf{x}}(t) \\ \dot{\xi}(t) \end{bmatrix} = \begin{bmatrix} \mathbf{A} & \mathbf{0} \\ -\mathbf{C} & 0 \end{bmatrix} \begin{bmatrix} \mathbf{x}(t) \\ \xi(t) \end{bmatrix} + \begin{bmatrix} \mathbf{B} \\ 0 \end{bmatrix} u(t) + \begin{bmatrix} \mathbf{0} \\ 1 \end{bmatrix} r(t) \tag{55}$$

If the same equation is arranged at a steady state, which means time goes to infinite, equation shown in 56 will be obtained.

$$\begin{bmatrix} \dot{\mathbf{x}}(\infty) \\ \dot{\xi}(\infty) \end{bmatrix} = \begin{bmatrix} \mathbf{A} & \mathbf{0} \\ -\mathbf{C} & 0 \end{bmatrix} \begin{bmatrix} \mathbf{x}(\infty) \\ \xi(\infty) \end{bmatrix} + \begin{bmatrix} \mathbf{B} \\ 0 \end{bmatrix} u(\infty) + \begin{bmatrix} \mathbf{0} \\ 1 \end{bmatrix} r(\infty) \tag{56}$$

If a subtraction operation is applied to equation 55 and equation 56, equation 57 will be obtained with new state variables.

$$\begin{bmatrix} \dot{\mathbf{x}}(t) - \dot{\mathbf{x}}(\infty) \\ \dot{\xi}(t) - \dot{\xi}(\infty) \end{bmatrix} = \begin{bmatrix} \mathbf{A} & \mathbf{0} \\ -\mathbf{C} & 0 \end{bmatrix} \begin{bmatrix} \mathbf{x}(t) - \mathbf{x}(\infty) \\ \xi(t) - \xi(\infty) \end{bmatrix} + \begin{bmatrix} \mathbf{B} \\ 0 \end{bmatrix} [u(t) - u(\infty)] \tag{57}$$

Let’s define these new state variables as follows (58):

$$\begin{aligned} \mathbf{x}(t) - \mathbf{x}(\infty) &= \mathbf{x}_e(t) \\ \xi(t) - \xi(\infty) &= \xi_e(t) \\ u(t) - u(\infty) &= u_e(t) \end{aligned} \tag{58}$$

Thus, a new form of the state equation appears as in equation 59.

$$\begin{bmatrix} \dot{\mathbf{x}}_e(t) \\ \dot{\xi}_e(t) \end{bmatrix} = \begin{bmatrix} \mathbf{A} & \mathbf{0} \\ -\mathbf{C} & 0 \end{bmatrix} \begin{bmatrix} \mathbf{x}_e(t) \\ \xi_e(t) \end{bmatrix} + \begin{bmatrix} \mathbf{B} \\ 0 \end{bmatrix} u_e(t) \tag{59}$$

Where:

$$u_e(t) = -\mathbf{K}\mathbf{x}_e(t) + k_I \xi_e(t) \tag{60}$$

Error vector can be shown as in equation 61.

$$\mathbf{e}(t) = \begin{bmatrix} \mathbf{x}_e(t) \\ \xi_e(t) \end{bmatrix} = (n+1)\text{-vector} \tag{61}$$

Then equation 60 can be expressed in equation 62

$$.u_e = -\hat{\mathbf{K}}\mathbf{e} \tag{62}$$

With a new gain matrix defined as shown in equation 63.

$$.\hat{\mathbf{K}} = \begin{bmatrix} \mathbf{K} & -k_I \end{bmatrix} \tag{63}$$

The error equation will be obtained as equation 64.

$$\dot{\mathbf{e}} = (\hat{\mathbf{A}} - \hat{\mathbf{B}}\hat{\mathbf{K}})\mathbf{e} \tag{64}$$

The above equation will show a new pole placement problem that can be solved, as shown before. Since a new state was introduced, a matrix of rank $n+1$ will be created for the new A matrix, and it should be completely state-controllable for arbitrary pole placement.

3.6. Conclusion

At the end of this section, the control theory used in this thesis was clarified. The necessary and sufficient condition for pole placement was given, the regulator design was explained and the servo system design was shown. The servo system will be designed according to section 3.4. or 3.5. with the determination of the type number.

4. Model

4.1. Introduction

In this chapter, the known and explained theory will be applied to the novel RHex flying-legged robot platform. Firstly the system dynamics will be obtained by Newton's and Lagrange's methods. After the models are investigated and validated in this chapter, accepted models will be linearized, and the most useful model will be used for control system design. The model's usefulness will be decided according to input and state relations. For the linearized system, controller performances will be investigated and tuned. The validation of the model and linearization are shown in the next chapter.

4.2. Kinematics

In the first stage, the robot will be considered in 2D space and modeled by two legs and one body part as shown in figure 4.1.

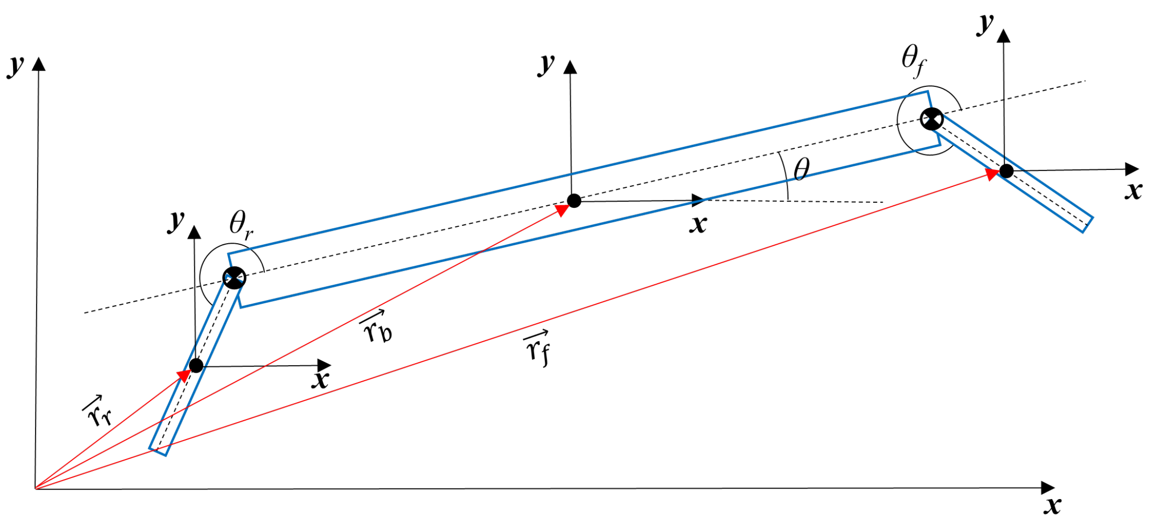

Figure 4.1 Simplified 2D RHex robot and body position vectors

Earth fixed coordinate frame is defined, and three vectors are placed from the origin to each body's center of mass as shown in equations 65, 66, and 67.

$$\overrightarrow{r_b} = x\hat{\boldsymbol{\imath}} + y\hat{\boldsymbol{\jmath}} \tag{65}$$

$$\overrightarrow{r_f} = x\hat{\boldsymbol{\imath}} + y\hat{\boldsymbol{\jmath}} + L_f\cos(\theta)\hat{\boldsymbol{\imath}} + L_f\sin(\theta)\hat{\boldsymbol{\jmath}} + R_f\cos\left(\theta + \theta_{\mathrm{f}}\right)\hat{\boldsymbol{\imath}} + R_f\sin\left(\theta + \theta_{\mathrm{f}}\right)\hat{\boldsymbol{\jmath}} \tag{66}$$

$$\overrightarrow{r_r} = x\hat{\boldsymbol{\imath}} + y\hat{\boldsymbol{\jmath}} + L_r\cos(\theta+\pi)\hat{\boldsymbol{\imath}} + L_f\sin(\theta+\pi)\hat{\boldsymbol{\jmath}} + \mathrm{v}R_r\cos\left(\theta + \theta_{\mathrm{r}}\right)\hat{\boldsymbol{\imath}} + R_r\sin\left(\theta + \theta_{\mathrm{r}}\right)\hat{\boldsymbol{\jmath}} \tag{67}$$

Body angular velocity vectors are defined in equation 68.

$$\begin{aligned}
&\overrightarrow{\omega_{b/e}} = \dot{\theta}\hat{\boldsymbol{k}}\\
&\overrightarrow{\omega_{f/e}} = \overrightarrow{\omega_{b/e}} + \overrightarrow{\omega_{f/b}} = \dot{\theta}\hat{\boldsymbol{k}} + \dot{\theta}_f\hat{\boldsymbol{k}}\\
&\overrightarrow{\omega_{r/e}} = \overrightarrow{\omega_{b/e}} + \overrightarrow{\omega_{r/b}} = \dot{\theta}\hat{\boldsymbol{k}} + \dot{\theta}_r\hat{\boldsymbol{k}}
\end{aligned} \tag{68}$$

Body angular acceleration vectors are defined in equation 69.

$$\begin{aligned}
&\overrightarrow{\alpha_{b/e}} = \ddot{\theta}\hat{\boldsymbol{k}}\\
&\overrightarrow{\alpha_{f/e}} = \overrightarrow{\alpha_{b/e}} + \overrightarrow{\alpha_{f/b}} = \ddot{\theta}\hat{\boldsymbol{k}} + \ddot{\theta}_f\hat{\boldsymbol{k}}\\
&\overrightarrow{\alpha_{r/e}} = \overrightarrow{\alpha_{b/e}} + \overrightarrow{\alpha_{r/b}} = \ddot{\theta}\hat{\boldsymbol{k}} + \ddot{\theta}_r\hat{\boldsymbol{k}}
\end{aligned} \tag{69}$$

Where subscript 'e' symbolizes the earth frame.

Velocity and acceleration vectors will be obtained from time derivatives of the position vectors $\overrightarrow{r_b}$,$\overrightarrow{r_f}$, and $\overrightarrow{r_r}$ as expressed in equations 70 and 71.

$$\overrightarrow{v_b} = \frac{d\overrightarrow{r_b}}{dt}, \quad \overrightarrow{v_f} = \frac{d\overrightarrow{r_f}}{dt}, \quad \overrightarrow{v_r} = \frac{d\overrightarrow{r_r}}{dt} \tag{70}$$

$$\overrightarrow{a_b} = \frac{d\overrightarrow{v_b}}{dt}, \quad \overrightarrow{a_f} = \frac{d\overrightarrow{v_f}}{dt}, \quad \overrightarrow{a_r} = \frac{d\overrightarrow{v_r}}{dt} \tag{71}$$

4.3. Derivation of EOMs With Newton Method

The main body is affected by two constraint forces coming from two legs; one gravitational force exerted at COM, and the thrust force assumed at the COM. The torques applied to each leg create reaction torques on the body. The free-Body diagram of the robot's main body is given in figure 4.2.

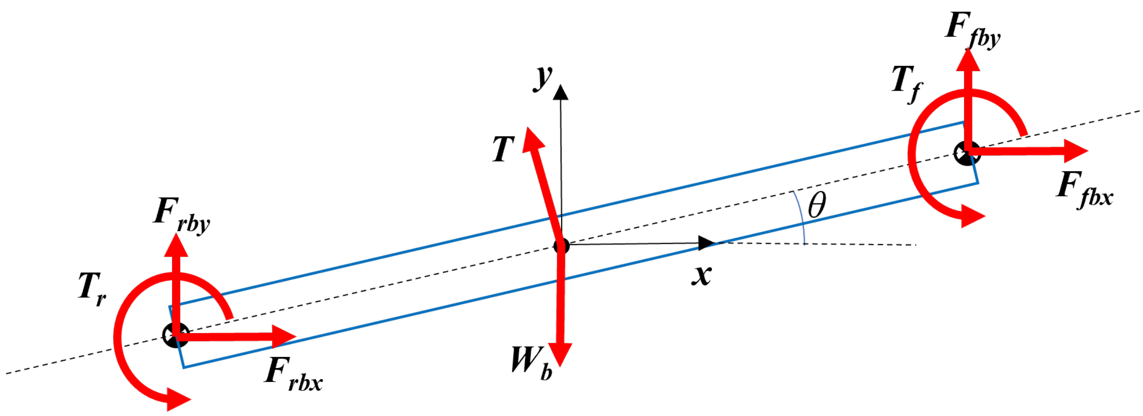

Figure 4.2 Free-Body diagram of the main body

Respective scalar force equations are obtained as given in equations 72, 73, and 74. An important note to know a_{bx} and a_{by} indicate the acceleration of the main body in the x and y axis respectively while α_b stands for angular acceleration of the body.

$$\begin{gathered} \sum F_x = M_b a_{bx} \\ F_{rbx} + F_{fbx} + T\cos\left(\frac{\pi}{2} + \theta\right) = M_b a_{bx} \end{gathered} \tag{72}$$

$$\begin{gathered} \sum F_y = M_b a_y \\ F_{rby} + F_{fby} + T\sin\left(\frac{\pi}{2} + \theta\right) - W = M_b a_{by} \end{gathered} \tag{73}$$

$$\begin{gathered} \sum M_z = I_b \alpha_b \\ T_f + T_r - L_f \sin(\theta) F_{fbx} + L_f \cos(\theta) F_{fby} + L_r \sin(\theta) F_{rbx} - L_r \cos(\theta) F_{rby} = I_b \alpha_b \end{gathered} \tag{74}$$

The applied forces on the front leg are constraint forces and gravitational force. The free-body diagram of the front leg is given in figure 4.3.

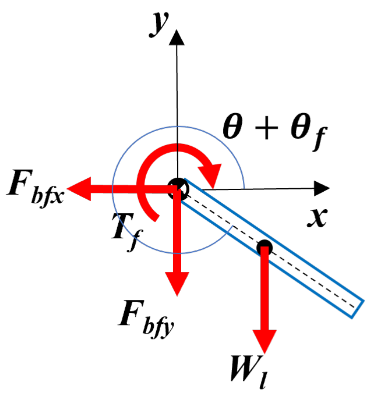

Figure 4.3 Free-Body-Diagram of the front leg

Respective scalar force equations are given in equations 75, 76, and 77. Note that a_{fx}, a_{fy}, and α_f are defined with the same notation used for the body.

$$-F_{bfx} = M_l a_{fx} \tag{75}$$

$$-F_{bfy} - W_l = M_l a_{fy} \tag{76}$$

$$-T_f + R\sin\left(2\pi - \theta - \theta_f\right) F_{bfx} + R\cos\left(2\pi - \theta - \theta_f\right) F_{bfy} = I_l \alpha_f \tag{77}$$

The applied forces on the rear leg are constraint force and gravitational force. The free-body diagram of the rear leg is given in figure 4.4.

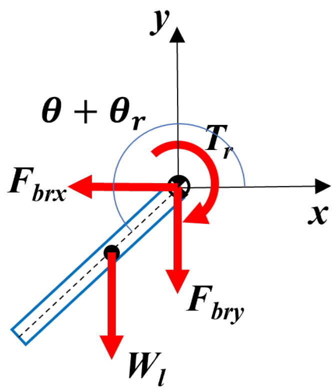

Figure 4.4 Free-Body-Diagram of the rear leg

Respective scalar force equations are given in equations 78, 79, and 80. Note that a_{rx}, a_{ry}, and α_r are defined with the same notation used for the body.

$$-F_{brx} = M_l a_{rx} \tag{78}$$

$$-F_{bry} - W_l = M_l a_{ry} \tag{79}$$

$$-T_r - R\sin(\theta + \theta_r)\, F_{brx} + R\cos(\theta + \theta_r)\, F_{bry} = I_l \alpha_r \tag{80}$$

While constraint forces can be obtained from equations 75, 76, 78, and 79, one can define equations of motion without constraint forces by substitution of constraint forces into the equations 72, 73, 74, 77 and 80. These EOMs are given in the appendix 7.1.

In these five EOMs, there are known variables as position variables (x, y, θ, θ_f and θ_r), velocity variables ($\dot{x}$, $\dot{y}$, $\dot{\theta}$, $\dot{\theta}_f$, and $\dot{\theta}_r$), and input variables (T, T_f and T_r) as well as unknown variables as acceleration variables ($\ddot{x}$, $\ddot{y}$, $\ddot{\theta}$, $\ddot{\theta}_f$ and $\ddot{\theta}_r$). If the equations of motion are rearranged to the form shown in the equation 81:

$$[K(t)]_{5\times5} \times \begin{Bmatrix} \ddot{x}(t) \\ \ddot{y}(t) \\ \ddot{\theta}(t) \\ \ddot{\theta}_f(t) \\ \ddot{\theta}_r(t) \end{Bmatrix} = \{l(t)\}_{5\times1} \tag{81}$$

Solution of this equation for $\ddot{x}$, $\ddot{y}$, $\ddot{\theta}$, $\ddot{\theta}_f$ and $\ddot{\theta}_r$ will be possible by crossing l with the inverse of K, as shown in the equation 82

$$\begin{Bmatrix} \ddot{x}(t) \\ \ddot{y}(t) \\ \ddot{\theta}(t) \\ \ddot{\theta}_f(t) \\ \ddot{\theta}_r(t) \end{Bmatrix} = [K(t)]^{-1}_{5\times5} \times \{l(t)\}_{5\times1} \tag{82}$$

4.4. Derivation of EOMs with Lagrange Method

Due to 2D modeling, all body parts will have two in-plane translational DOFs and one rotational DOF around the plane-normal. Since a revolute joint will be used to connect each leg to the body, each joint will create two reductions in DOF so that the system will have five DOFs, which can also be calculated according to the Chebyshev-Grübler-Kutzbach DOF formula [19]. The calculation of DOF is given in the equation 83.

$$DOF = \lambda(l-1-j) + \sum_{i=0}^{j} f_i = 3(4-1-3) + (3+1+1) = 5 \tag{83}$$

Where λ is the degree of freedom of the working space, l is the number of links or parts, including the ground, j is the number of joints and f_i is the degree of freedom of the i^{th} joint. Due to the five DOFs system described, a total of five EOMs are obtained, according to the free body diagrams, one for each degree of freedom. Also, four force equations appeared as constraint forces at each joint. These EOMs are obtained by hand instead of using various computer programs and are also quite prone to human errors even when carefully inspected. Due to this error-proneness, the equations of motions are also obtained through the Lagrange method using Matlab software to compare with the Newtonian way. Generalized coordinates are defined for the Lagrange's method in equation 84.

$$q = \begin{Bmatrix} x \\ y \\ \theta \\ \theta_f \\ \theta_r \end{Bmatrix} \tag{84}$$

In Matlab software, one can not use vectors in the form given in the equations. The matrix form of vectors should be used to represent vectors. Unit vectors will be described to define vectors with unit vector components as stated in equation set 85

$$u_1 = \begin{Bmatrix} 1 \\ 0 \\ 0 \end{Bmatrix}, \quad u_2 = \begin{Bmatrix} 0 \\ 1 \\ 0 \end{Bmatrix}, \quad u_3 = \begin{Bmatrix} 0 \\ 0 \\ 1 \end{Bmatrix} \tag{85}$$

To obtain the position, velocity, and acceleration vectors in matrix form $\hat{\imath}$ and $\hat{\jmath}$ components should be replaced by u_1 and u_2 terms in their respective equations. The kinetic energy of the system should be calculated for the Lagrange method as shown in the equation 86.

$$\begin{aligned} K = &\frac{1}{2}M_b\left(v_b^T v_b\right) + \frac{1}{2}M_l\left(v_f^T v_f\right) + \frac{1}{2}M_l\left(v_r^T v_r\right) + \frac{1}{2}I_b\dot{\theta}^2 \\ &+ \frac{1}{2}I_l\left(\dot{\theta} + \dot{\theta}_f\right)^2 + \frac{1}{2}I_l\left(\dot{\theta} + \dot{\theta}_r\right)^2 \end{aligned} \tag{86}$$

Where M_b is the main body's mass, M_l is the mass of the leg, I_b is the main body's inertia around its center of mass, and I_l is the inertia of the leg around the leg's center of mass. All inertia definitions are made around the plane-normal vector.

The potential energy of the system is calculated in the equation 87

$$U = M_b\left(\overrightarrow{r_b} \cdot \hat{\jmath}\right) + M_l\left(\overrightarrow{r_f} \cdot \hat{\jmath}\right) + M_l\left(\overrightarrow{r_r} \cdot \hat{\jmath}\right) \tag{87}$$

Energy dissipations are not included in this stage, so as in the equation 88.

$$D = 0 \tag{88}$$

Virtual work equation and respective virtual force equations are written in equation set 89.

$$\begin{gathered}\delta w = T\delta y\cos\theta - T\delta x\sin\theta + T_f\delta\theta - T_f\left(\delta\theta + \delta\theta_f\right) + T_r\delta\theta - T_r\left(\delta\theta + \delta\theta_r\right) \\ Q_x = -T\sin\theta, \quad Q_y = T\cos\theta, \quad Q_\theta = 0, \quad Q_{\theta f} = -T_f, \quad Q_{\theta r} = -T_r\end{gathered} \tag{89}$$

Where, $\delta x, \delta y, \delta\theta, \delta\theta_f$ and $\delta\theta_r$ are displacements in generalized coordinates and $Q_x, Q_y, Q_\theta, Q_{\theta f}$ and $Q_{\theta r}$ are the virtual forces. Now one can implement the Lagrange equation in expanded form to find kth EOM as given in the equation 90.

$$\dot{p}_k - \frac{\partial K}{\partial q_k} - \frac{\partial D}{\partial \dot{q}_k} + \frac{\partial U}{\partial q_k} = Q_k \tag{90}$$

Where:

$$p_k = \frac{\partial K}{\partial \dot{q}_k} \tag{91}$$

These EOMs are given in the appendix 7.2. In these five EOMs, there are known variables as position variables (x, y, θ, θ_f and θ_r), velocity variables ($\dot{x}$, $\dot{y}$, $\dot{\theta}$, $\dot{\theta}_f$, and $\dot{\theta}_r$), and input variables (T, T_f and T_r) as well as unknown variables as acceleration variables ($\ddot{x}$, $\ddot{y}$, $\ddot{\theta}$, $\ddot{\theta}_f$ and $\ddot{\theta}_r$). If the equations of motion are rearranged to the form shown in the equation 92:

$$[K]_{5\times5} \times \begin{Bmatrix} \ddot{x} \\ \ddot{y} \\ \ddot{\theta} \\ \ddot{\theta}_f \\ \ddot{\theta}_r \end{Bmatrix} = \{l\}_{5\times1} \tag{92}$$

Solution of this equation for $\ddot{x}$, $\ddot{y}$, $\ddot{\theta}$, $\ddot{\theta}_f$ and $\ddot{\theta}_r$ will be possible by crossing l with the inverse of K, as shown in the equation 93

$$\begin{Bmatrix} \ddot{x} \\ \ddot{y} \\ \ddot{\theta} \\ \ddot{\theta}_f \\ \ddot{\theta}_r \end{Bmatrix} = [K]^{-1}_{5\times5} \times \{l\}_{5\times1} \tag{93}$$

4.5. Linearization

Linearization must be applied to design a linear controller to control a 2D simplified RHex robot. General state space form is given in equation 94

$$\dot{\boldsymbol{x}} = \boldsymbol{f}(\boldsymbol{x}, \boldsymbol{u}) \tag{94}$$

On the other hand, equations of motion obtained from both Newton and Lagrange methods can be adjusted in the form given in the equation 95, while p states for position variables, v states for velocity variables, and u states for input variables.

$$\boldsymbol{a} = \boldsymbol{f}(\boldsymbol{p}, \boldsymbol{v}, \boldsymbol{u}) \tag{95}$$

It means that acceleration variables are functions of position, velocity, and inputs. If the states of the system are chosen as position and velocity variables, and inputs of the system are chosen as thrust force, front leg torque, and rear leg torque as given in the equation 96, the equations of motion perfectly fit the general state space model.

$$\boldsymbol{p} = \begin{Bmatrix} x \\ y \\ \theta \\ \theta_f \\ \theta_r \end{Bmatrix}, \quad \boldsymbol{v} = \begin{Bmatrix} \dot{x} \\ \dot{y} \\ \dot{\theta} \\ \dot{\theta}_f \\ \dot{\theta}_r \end{Bmatrix}, \quad \boldsymbol{u} = \begin{Bmatrix} T \\ T_f \\ T_r \end{Bmatrix} \tag{96}$$

First-order Taylor series expansion should be applied to linearize the equations of motion and obtain a linear state space model. An important note to know about notation, bold characters are related to respective matrices. Applied first-order Taylor series expansion is shown in equation 97.

$$\begin{aligned} \boldsymbol{a} = \dot{\boldsymbol{v}} = \boldsymbol{f}(\boldsymbol{p}, \boldsymbol{v}, \boldsymbol{u}) \approx \dot{\boldsymbol{v}}_{\mathbf{0}} + \left.\frac{\partial \boldsymbol{f}}{\partial \boldsymbol{p}}\right|_{p_0, v_0, u_0} (\boldsymbol{p} - \boldsymbol{p}_{\mathbf{0}}) + \left.\frac{\partial \boldsymbol{f}}{\partial \boldsymbol{v}}\right|_{p_0, v_0, u_0} (\boldsymbol{v} - \boldsymbol{v}_{\mathbf{0}}) \\ + \left.\frac{\partial \boldsymbol{f}}{\partial \boldsymbol{u}}\right|_{p_0, v_0, u_0} (\boldsymbol{u} - \boldsymbol{u}_{\mathbf{0}}) \end{aligned} \tag{97}$$

Linearization will be done around these initial states and inputs. Since all product terms include differences from the initial state, the definitions given in the equation set 98 will simplify the form given above:

$$\boldsymbol{\delta p} = \boldsymbol{p} - \boldsymbol{p}_{\mathbf{0}}, \quad \boldsymbol{\delta v} = \boldsymbol{v} - \boldsymbol{v}_{\mathbf{0}}, \quad \boldsymbol{\delta \dot{v}} = \dot{\boldsymbol{v}} - \dot{\boldsymbol{v}}_{\mathbf{0}}, \quad \boldsymbol{\delta u} = \boldsymbol{u} - \boldsymbol{u}_{\mathbf{0}} \tag{98}$$

The used $\boldsymbol{\delta}$ states for deviations from linearization point and should not be confused with $\boldsymbol{\delta}$ used in the Lagrange method.
The acceleration term also can be rewritten by using the above simplification.

$$
\begin{aligned}
\dot{\boldsymbol{v}} \approx \dot{\boldsymbol{v}}_{\boldsymbol{0}} + \left.\frac{\partial \boldsymbol{f}}{\partial \boldsymbol{p}}\right|_{p_0,v_0,u_0} \boldsymbol{\delta p} + \left.\frac{\partial \boldsymbol{f}}{\partial \boldsymbol{v}}\right|_{p_0,v_0,u_0} \boldsymbol{\delta v} + \left.\frac{\partial \boldsymbol{f}}{\partial \boldsymbol{u}}\right|_{p_0,v_0,u_0} \boldsymbol{\delta u} \\
[htb]\dot{\boldsymbol{v}} - \dot{\boldsymbol{v}}_{\boldsymbol{0}} \approx \left.\frac{\partial \boldsymbol{f}}{\partial \boldsymbol{p}}\right|_{p_0,v_0,u_0} \boldsymbol{\delta p} + \left.\frac{\partial \boldsymbol{f}}{\partial \boldsymbol{v}}\right|_{p_0,v_0,u_0} \boldsymbol{\delta v} + \left.\frac{\partial \boldsymbol{f}}{\partial \boldsymbol{u}}\right|_{p_0,v_0,u_0} \boldsymbol{\delta u} \\
\boldsymbol{\delta \dot{v}} \approx \left.\frac{\partial \boldsymbol{f}}{\partial \boldsymbol{p}}\right|_{p_0,v_0,u_0} \boldsymbol{\delta p} + \left.\frac{\partial \boldsymbol{f}}{\partial \boldsymbol{v}}\right|_{p_0,v_0,u_0} \boldsymbol{\delta v} + \left.\frac{\partial \boldsymbol{f}}{\partial \boldsymbol{u}}\right|_{p_0,v_0,u_0} \boldsymbol{\delta_u}
\end{aligned}
\tag{99}
$$

If the higher-order terms are neglected in the Taylor series expansion, the resultant form can be shown below to clarify expectations.

$$
\begin{aligned}
\begin{Bmatrix} \delta\ddot{x} \\ \delta\ddot{y} \\ \delta\ddot{\theta} \\ \delta\ddot{\theta}_f \\ \delta\ddot{\theta}_r \end{Bmatrix}
= & \left.\begin{bmatrix}
\frac{\partial f_{\ddot{x}}}{\partial x} & \frac{\partial f_{\ddot{x}}}{\partial y} & \frac{\partial f_{\ddot{x}}}{\partial \theta} & \frac{\partial f_{\ddot{x}}}{\partial \theta_f} & \frac{\partial f_{\ddot{x}}}{\partial \theta_r} \\
\frac{\partial f_{\ddot{y}}}{\partial x} & \frac{\partial f_{\ddot{y}}}{\partial y} & \frac{\partial f_{\ddot{y}}}{\partial \theta} & \frac{\partial f_{\ddot{y}}}{\partial \theta_f} & \frac{\partial f_{\ddot{y}}}{\partial \theta_r} \\
\frac{\partial f_{\ddot{\theta}}}{\partial x} & \frac{\partial f_{\ddot{\theta}}}{\partial y} & \frac{\partial f_{\ddot{\theta}}}{\partial \theta} & \frac{\partial f_{\ddot{\theta}}}{\partial \theta_f} & \frac{\partial f_{\ddot{\theta}}}{\partial \theta_r} \\
\frac{\partial f_{\ddot{\theta}_f}}{\partial x} & \frac{\partial f_{\ddot{\theta}_f}}{\partial y} & \frac{\partial f_{\ddot{\theta}_f}}{\partial \theta} & \frac{\partial f_{\ddot{\theta}_f}}{\partial \theta_f} & \frac{\partial f_{\ddot{\theta}_f}}{\partial \theta_r} \\
\frac{\partial f_{\ddot{\theta}_r}}{\partial x} & \frac{\partial f_{\ddot{\theta}_r}}{\partial y} & \frac{\partial f_{\ddot{\theta}_r}}{\partial \theta} & \frac{\partial f_{\ddot{\theta}_r}}{\partial \theta_f} & \frac{\partial f_{\ddot{\theta}_r}}{\partial \theta_r}
\end{bmatrix}\right|_{p_0,v_0,u_0}
\begin{Bmatrix} \delta x \\ \delta y \\ \delta\theta \\ \delta\theta_f \\ \delta\theta_r \end{Bmatrix} \\
& + \left.\begin{bmatrix}
\frac{\partial f_{\ddot{x}}}{\partial \dot{x}} & \frac{\partial f_{\ddot{x}}}{\partial \dot{y}} & \frac{\partial f_{\ddot{x}}}{\partial \dot{\theta}} & \frac{\partial f_{\ddot{x}}}{\partial \dot{\theta}_f} & \frac{\partial f_{\ddot{x}}}{\partial \dot{\theta}_r} \\
\frac{\partial f_{\ddot{y}}}{\partial \dot{x}} & \frac{\partial f_{\ddot{y}}}{\partial \dot{y}} & \frac{\partial f_{\ddot{y}}}{\partial \dot{\theta}} & \frac{\partial f_{\ddot{y}}}{\partial \dot{\theta}_f} & \frac{\partial f_{\ddot{y}}}{\partial \dot{\theta}_r} \\
\frac{\partial f_{\ddot{\theta}}}{\partial \dot{x}} & \frac{\partial f_{\ddot{\theta}}}{\partial \dot{y}} & \frac{\partial f_{\ddot{\theta}}}{\partial \dot{\theta}} & \frac{\partial f_{\ddot{\theta}}}{\partial \dot{\theta}_f} & \frac{\partial f_{\ddot{\theta}}}{\partial \dot{\theta}_r} \\
\frac{\partial f_{\ddot{\theta}_f}}{\partial \dot{x}} & \frac{\partial f_{\ddot{\theta}_f}}{\partial \dot{y}} & \frac{\partial f_{\ddot{\theta}_f}}{\partial \dot{\theta}} & \frac{\partial f_{\ddot{\theta}_f}}{\partial \dot{\theta}_f} & \frac{\partial f_{\ddot{\theta}_f}}{\partial \dot{\theta}_r} \\
\frac{\partial f_{\ddot{\theta}_r}}{\partial \dot{x}} & \frac{\partial f_{\ddot{\theta}_r}}{\partial \dot{y}} & \frac{\partial f_{\ddot{\theta}_r}}{\partial \dot{\theta}} & \frac{\partial f_{\ddot{\theta}_r}}{\partial \dot{\theta}_f} & \frac{\partial f_{\ddot{\theta}_r}}{\partial \dot{\theta}_r}
\end{bmatrix}\right|_{p_0,v_0,u_0}
\begin{Bmatrix} \delta\dot{\theta} \\ \delta\dot{\theta}_f \\ \delta\dot{\theta}_r \end{Bmatrix} \\
& + \left.\begin{bmatrix}
\frac{\partial f_{\ddot{x}}}{\partial T} & \frac{\partial f_{\ddot{x}}}{\partial T_f} & \frac{\partial f_{\ddot{x}}}{\partial T_r} \\
\frac{\partial f_{\ddot{y}}}{\partial T} & \frac{\partial f_{\ddot{y}}}{\partial T_f} & \frac{\partial f_{\ddot{y}}}{\partial T_r} \\
\frac{\partial f_{\ddot{\theta}}}{\partial T} & \frac{\partial f_{\ddot{\theta}}}{\partial T_f} & \frac{\partial f_{\ddot{\theta}}}{\partial T_r} \\
\frac{\partial f_{\ddot{\theta}_f}}{\partial T} & \frac{\partial f_{\ddot{\theta}_f}}{\partial T_f} & \frac{\partial f_{\ddot{\theta}_f}}{\partial T_r} \\
\frac{\partial f_{\ddot{\theta}_r}}{\partial T} & \frac{\partial f_{\ddot{\theta}_r}}{\partial T_f} & \frac{\partial f_{\ddot{\theta}_r}}{\partial T_r}
\end{bmatrix}\right|_{p_0,v_0,u_0}
\begin{Bmatrix} T \\ T_f \\ T_r \end{Bmatrix}
\end{aligned}
\tag{100}
$$

Obtaining this function f is a bit more complicated due to the existence of the inverse of a symbolic matrix in equations 101 and 102.

$$\begin{Bmatrix} \ddot{x} \\ \ddot{y} \\ \ddot{\theta} \\ \ddot{\theta}_f \\ \ddot{\theta}_r \end{Bmatrix} = [\boldsymbol{K}(\boldsymbol{p})]^{-1}{}_{5x5} \times \{\boldsymbol{l}(\boldsymbol{p}, \boldsymbol{v}, \boldsymbol{u})\}_{5x1} \tag{101}$$

$$\{\boldsymbol{\delta\dot{v}}\} = [\boldsymbol{K}]^{-1} \times \{\boldsymbol{l}\} \tag{102}$$

Due to the uninvertable symbolic form of the set of equations of motion, some matrix manipulations are necessary. Substitution cannot be made at this stage because the 'K' matrix will also be differentiated. The 'K' matrix found from Lagrange and Newton methods depends on position variables; it is called the mass matrix, while the 'l' vector depends on position variables, velocity variables, and inputs as stated in equation 101.

Application of first-order Taylor series expansion forms the equation given in 102 to equation 103.

$$\begin{aligned} \boldsymbol{\delta\dot{v}} = & \left(-\boldsymbol{K}^{-1}\left(\frac{\partial \boldsymbol{K}}{\partial \boldsymbol{p}}\right)\boldsymbol{K}^{-1}\boldsymbol{l} + \boldsymbol{K}^{-1}\left(\frac{\partial \boldsymbol{l}}{\partial \boldsymbol{p}}\right)\right)\Bigg|_{p_0,v_0,u_0} \boldsymbol{\delta p} \\ & + \left(-\boldsymbol{K}^{-1}\left(\frac{\partial \boldsymbol{K}}{\partial \boldsymbol{v}}\right)\boldsymbol{K}^{-1}\boldsymbol{l} + \boldsymbol{K}^{-1}\left(\frac{\partial \boldsymbol{l}}{\partial \boldsymbol{v}}\right)\right)\Bigg|_{p_0,v_0,u_0} \boldsymbol{\delta} v \\ & + \left(\boldsymbol{K}^{-1}\left(\frac{\partial \boldsymbol{l}}{\partial \boldsymbol{u}}\right)\right)\Bigg|_{p_0,v_0,u_0} \boldsymbol{\delta u} \end{aligned} \tag{103}$$

Now, substitution can be performed in equation 103 by using linearization point parameters since differentiation is completed. With substitution of A_1, A_2, and B_1 terms in to the equation 103:

$$\boldsymbol{\delta\dot{v}} = \boldsymbol{A}_1\boldsymbol{\delta p} + \boldsymbol{A}_2\boldsymbol{\delta v} + \boldsymbol{B_1\delta u} \tag{104}$$

Where:

$$\boldsymbol{A_1} = \left[-\boldsymbol{K}^{-1} \left(\frac{\partial \boldsymbol{K}}{\partial \boldsymbol{p}} \right) \boldsymbol{K}^{-1}\boldsymbol{l} + \boldsymbol{K}^{-1} \left(\frac{\partial \boldsymbol{l}}{\partial \boldsymbol{p}} \right) \right] \Bigg|_{p_0, v_0, u_0} \tag{105}$$

$$\boldsymbol{A_2} = \left[-\boldsymbol{K}^{-1} \left(\frac{\partial \boldsymbol{K}}{\partial \boldsymbol{v}} \right) \boldsymbol{K}^{-1}\boldsymbol{l} + \boldsymbol{K}^{-1} \left(\frac{\partial \boldsymbol{l}}{\partial \boldsymbol{v}} \right) \right] \Bigg|_{p_0, v_0, u_0} \tag{106}$$

And:

$$\boldsymbol{B_1} = \left[\boldsymbol{K}^{-1} \left(\frac{\partial \boldsymbol{l}}{\partial \boldsymbol{u}} \right) \right] \Bigg|_{p_0, v_0, u_0} \tag{107}$$

If the initial velocities are zero, it is known as given in the equation 108

$$\boldsymbol{\delta\dot{p}} = \boldsymbol{\delta v} \tag{108}$$

If the state vector is defined as:

$$\{\boldsymbol{x}\} = \begin{Bmatrix} \boldsymbol{\delta p} \\ \boldsymbol{\delta v} \end{Bmatrix} \tag{109}$$

An important note, x written boldly is a state vector different from x, which is the projection of the robot's center of mass position vector on the x-axis. Then:

$$\{\dot{\boldsymbol{x}}\} = \begin{pmatrix} \boldsymbol{0} & \boldsymbol{1} \\ \boldsymbol{A}_1 & \boldsymbol{A}_2 \end{pmatrix} \{\boldsymbol{x}\} + \begin{pmatrix} \boldsymbol{0} \\ \boldsymbol{B}_1 \end{pmatrix} \{\boldsymbol{u}\} \tag{110}$$

The above-given form is the same as the linear state space model given in the equation 111.

$$\{\dot{\boldsymbol{x}}\} = [\boldsymbol{A}]\{\boldsymbol{x}\} + [\boldsymbol{B}]\{\boldsymbol{u}\} \tag{111}$$

Where:

$$\boldsymbol{A} = \begin{pmatrix} \boldsymbol{0} & \boldsymbol{1} \\ \boldsymbol{A}_1 & \boldsymbol{A}_2 \end{pmatrix}, \quad \boldsymbol{B} = \begin{pmatrix} \boldsymbol{0} \\ \boldsymbol{B}_1 \end{pmatrix} \tag{112}$$

4.6. Model Parameters

As explained in section 1. 2D simplified model of the RHex robot is created. This robot's center of mass can be translated along the x-axis and y-axis and rotated around the z-axis. So, the model parameters should be determined considering this simplified model. For example, the width of the robot will be unnecessary. Determined parameters can be examined in table 4.1.

Parameter	**Value**
Body Mass	$3.15\ kg$
Leg Mass	$0.05184\ kg$
Distance from Body CoM to Front Leg Rotation Center	$0.125\ m$
Distance from Body CoM to Rear Leg Rotation Center	$0.125\ m$
The Distance from Front Leg Rotation Center to Leg CoM	$0.06\ m$
The Distance from Rear Leg Rotation Center to Leg CoM	$0.06\ m$
Body Inertia around CoM around Z Axis	$0.0176925\ kg \times m^4$
Leg Inertia around CoM around Z Axis	$6.24845e - 5\ kg \times m^4$

Table 4.1 RHex robot 2D simplified robot parameters

The equations are linearized around the hover position. So the hover position parameters are determined as the initial positions as shown in the table 4.2.

Parameter	**Value**
Initial x position of the body	$0\ m$
Initial y position of the body	$0\ m$
Initial body angle from horizontal (θ)	$0\ rad$
Initial front leg angle from body fixed x-axis	$-\pi\ rads$
Initial rear leg position from body fixed x-axis	$-\pi\ rads$
Initial x velocity of the body	$0\ \frac{m}{s}$
Initial y velocity of the body	$0\ \frac{m}{s}$
Initial body angular velocity (θ)	$0\ \frac{rad}{s}$
Initial front leg angular velocity	$0\ \frac{rad}{s}$
Initial rear leg angular velocity	$0\ \frac{rad}{s}$

Table 4.2 RHex robot initial position of states around linearization point

Initial values of the inputs should also be determined and they are given in the table 4.3.

Parameter	**Value**
Thrust force $((M_b + 2M_l) \times g)$	$31.92\ N$
Front leg torque	$0\ Nm$
Rear leg torque	$0\ Nm$

Table 4.3 RHex robot initial position of inputs around linearization point

The section 4.5. shows how to determine state space matrices. According to the parameters given in the table 4.1, state space matrices will be obtained as given in the equation 113 and 114.

$$
\mathbf{A} = \begin{pmatrix}
0 & 0 & 0 & 0 & 0 & 1.0 & 0 & 0 & 0 & 0 \\
0 & 0 & 0 & 0 & 0 & 0 & 1.0 & 0 & 0 & 0 \\
0 & 0 & 0 & 0 & 0 & 0 & 0 & 1.0 & 0 & 0 \\
0 & 0 & 0 & 0 & 0 & 0 & 0 & 0 & 1.0 & 0 \\
0 & 0 & 0 & 0 & 0 & 0 & 0 & 0 & 0 & 1.0 \\
0 & 0 & -9.81 & 0.12 & 0.12 & 0 & 0 & 0 & 0 & 0 \\
0 & 0 & 0 & 0 & 0 & 0 & 0 & 0 & 0 & 0 \\
0 & 0 & 0 & 0 & 0 & 0 & 0 & 0 & 0 & 0 \\
0 & 0 & 0 & -124.0 & -1.498 & 0 & 0 & 0 & 0 & 0 \\
0 & 0 & 0 & -1.498 & -124.0 & 0 & 0 & 0 & 0 & 0
\end{pmatrix} \tag{113}
$$

$$
\mathbf{B} = \begin{pmatrix}
0 & 0 & 0 \\
0 & 0 & 0 \\
0 & 0 & 0 \\
0 & 0 & 0 \\
0 & 0 & 0 \\
0 & 3.931 & 3.931 \\
0.3073 & 0 & 0 \\
0 & 51.78 & 51.78 \\
0 & -4115.0 & -100.9 \\
0 & -100.9 & -4115.0
\end{pmatrix} \tag{114}
$$

Although determining A and B matrices is vital for calculating states, it is not enough to determine the state space equation. C and D matrices should also be defined. While the D matrix is pervasive to appear as a null matrix, like in our case, the C matrix shows the relation between states and outputs. For flying robots, it makes sense to control the robot's speed in flight status so that the outputs can be accepted as those. Since the control buttons of the user's command tool control the robot's speed, there is no means to define other states as outputs. But due to the inspection of all states in this MSc thesis, let's define the outputs as all of the states. In light of this knowledge, C and D matrices can be built as an identity matrix of $[10 \times 10]$ and a null matrix of $[10 \times 3]$ respectively.

4.7. State Feedback Control

As explained in the section 3.3.1., state-feedback control is based on the pole placement approach. To place all poles at arbitrary locations, a necessary and sufficient condition is also shown in section 3.3.1. as complete state controllability.

4.7.1. Controllability

As expressed in the section 3.3.1., the controllability matrix can be obtained as in equation 115.

$$M_{co} = \begin{bmatrix} \mathbf{B} & \mathbf{AB} & \cdots & \mathbf{A}^{n-1}\mathbf{B} \end{bmatrix} \tag{115}$$

Thus, the controllability matrix for the 2D simplified RHex robot system will be formed as given in the matrices 135, 136, 137, 138, 139, and 140 in the appendix 7.3.. It is represented in six parts due to its very long size.

The rank of the controllability matrix should be equal to the rank of the A matrix to provide the complete state controllability condition. So the rank of the controllability matrix can be calculated by using Matlab's rank command and be found as equal to the rank of the A matrix.

4.7.2. Definition of Desired Pole Locations

The desired pole locations can be defined for transient or frequency requirements. In this case, it is pretty logical to define transient requirements. Since the robot's actual locomotion type is not flying and temporary flight capability is enough for this design. Let's accept that it should reach the desired speed in 3 seconds. The transient requirements will be fully determined if a maximum overshoot of 20% is also acceptable for the design. From the maximum overshoot equation, ζ can be calculated as stated in the equation 116.

$$\begin{aligned} M_p &= e^{-\pi\frac{\zeta}{\sqrt{1-\zeta^2}}} \\ \ln 0.2 &= -\pi\frac{\zeta}{\sqrt{1-\zeta^2}} \\ 0.5123 &= \frac{\zeta}{\sqrt{1-\zeta^2}} \\ \zeta^2 = 0.2079 \quad &\Rightarrow \quad \zeta = 0.4560 \end{aligned} \tag{116}$$

From the settling time equation, w_n can be calculated as expressed in the equation 117.

$$\begin{aligned} t_s(\%5) &= \frac{3}{\zeta w_n} \\ 3 &= \frac{3}{\zeta w_n} \\ w_n &= \frac{3}{3 \cdot 0.4560} \\ w_n &= 2.193 \end{aligned} \tag{117}$$

According to equations 116 and 117, desired pole locations can be obtained as given in the equation 118.

$$\begin{aligned} s_{1,2} &= -\zeta w_n \pm \hat{\imath} w_n\sqrt{1-\zeta^2} \\ s_{1,2} &= -1 \pm \hat{\imath}1.9518 \end{aligned} \tag{118}$$

4.7.3. Pole Placement

When the dominant pole locations are defined, all other poles should be placed far from the dominant poles to suppress their effects. The most common way is placing non-dominant poles five times further than the dominant poles from the origin. Thus, the desired pole locations are determined as shown in row vectors 119 and 120. They are given separately due to their long size.

$$s_{1-5} = \;[-1.0 - 1.95\,\mathrm{i} \quad -1.0 + 1.95\,\mathrm{i} \quad -5.0 \quad -5.0 \quad -10.0] \tag{119}$$

$$s_{6-10} = \;[-10.0 \quad -15.0 \quad -20.0 \quad -15.0 \quad -20.0] \tag{120}$$

Since the desired pole locations are determined, one can obtain the gain matrix K to have eigenvalues of $(\mathbf{A} - \mathbf{BK})$ at desired pole locations. $\mathbf{K}$ is given in equations 121 and 122 in the sub-matrix form to be able to use in the thesis format and $\mathbf{K}$ is the combination of those two matrices $\mathbf{K_1}$ and $\mathbf{K_2}$ as stated in equation 123.

$$\mathbf{K_1} = \begin{pmatrix} 1.14\text{e-}7 & 418.0 & -4.32\text{e-}7 & -144.0 & 144.0 \\ -0.566 & 0.0108 & 2.39 & -0.0754 & -0.0694 \\ -0.566 & -0.0108 & 2.39 & -0.0694 & -0.0754 \end{pmatrix} \tag{121}$$

$$\mathbf{K_2} = \begin{pmatrix} 8.82\text{e-}8 & 79.0 & -9.49\text{e-}8 & -11.5 & 11.5 \\ -0.471 & 8.64\text{e-}4 & 0.596 & -0.00248 & 0.00392 \\ -0.471 & -8.64\text{e-}4 & 0.596 & 0.00392 & -0.00248 \end{pmatrix} \tag{122}$$

$$\mathbf{K} = \begin{bmatrix} \mathbf{K_1} & \mathbf{K_2} \end{bmatrix} \tag{123}$$

4.7.4. State Feeback Regulator

Since the gain matrix is also obtained in the previous section, one can investigate the controller in the linear model. The Block diagram of the state feedback regulator is given in figure 4.5.

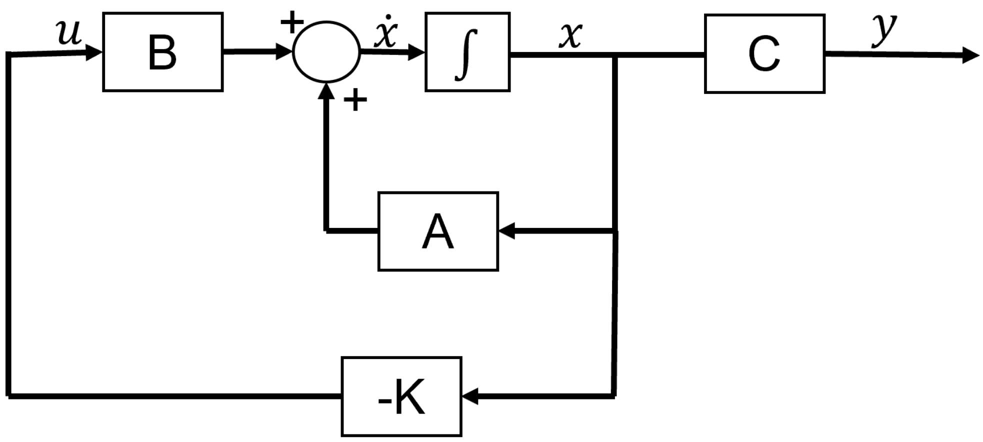

Figure 4.5 State feedback regulator block diagram

This block diagram should be obtained in Matlab/Simulink to investigate the linear model and the Simulink block diagram is given in the figure 4.6

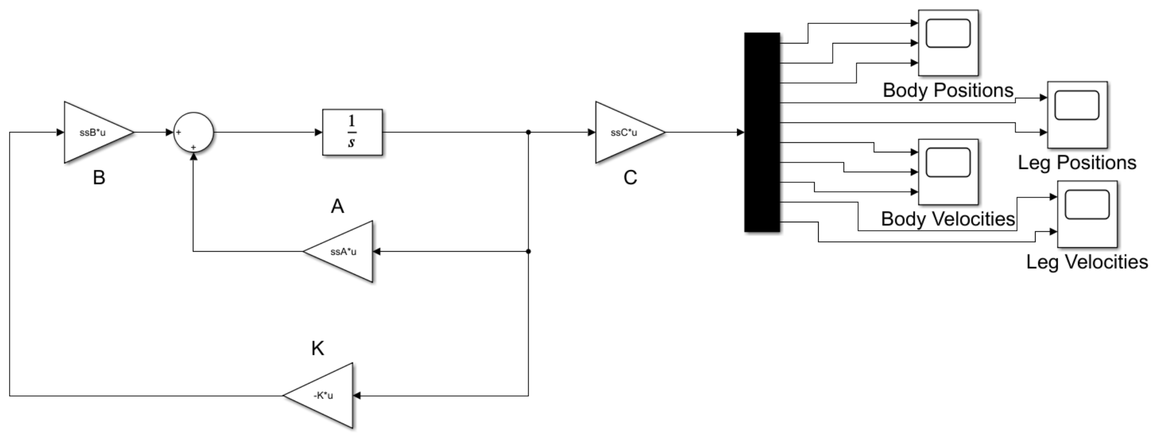

Figure 4.6 State feedback regulator Simulink block diagram

When the Simulink model is created, regulator characteristics due to initial velocities and disturbances can be examined.

4.7.4.1. Non-zero initial states: When the initial values of states are non-zero, the regulator will try to bring the values to zero with desired transient behavior.

When the x initial position is non-zero, responses can be investigated in figure 4.7.

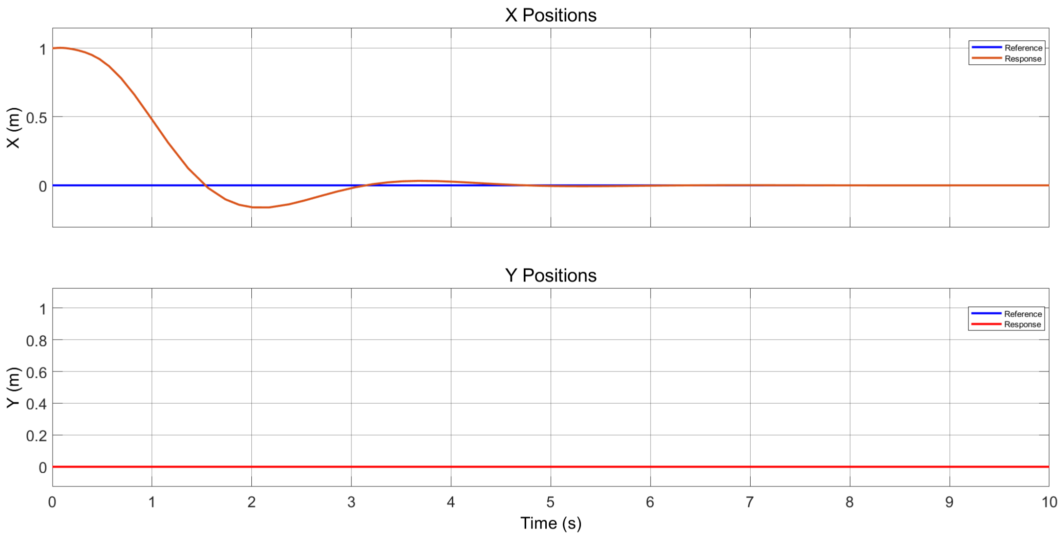

Figure 4.7 Non-zero initial x position case.

As a reminder, θ is the body angle around the plane normal. When the initial position in y is non-zero, responses can be investigated in figure 4.8.

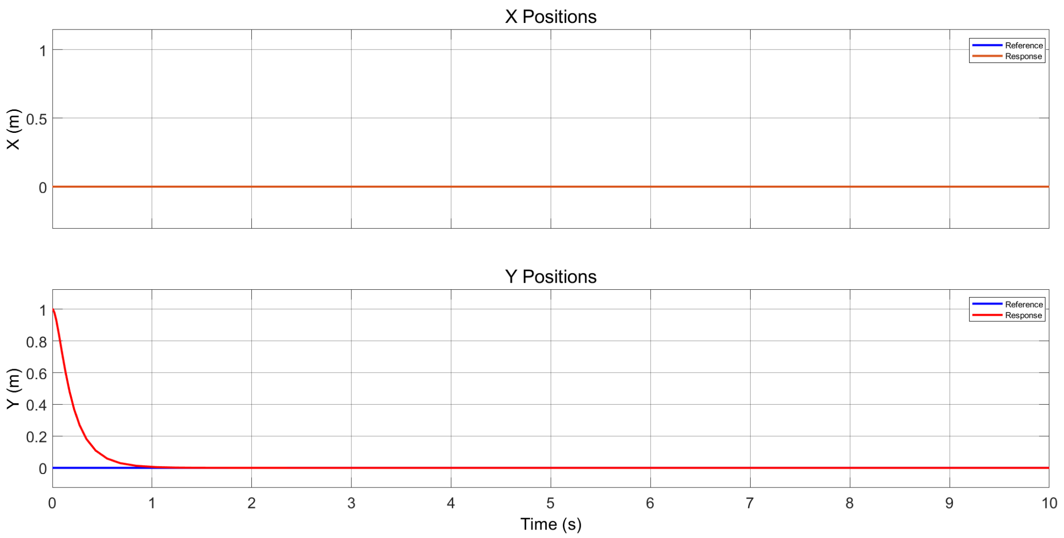

Figure 4.8 Non-zero initial y position case.

The robot's reaction to the non-zero y initial position is faster than the non-zero x initial position case. It settles in nearly 1.6 seconds. When the initial velocity in the x direction is non-zero, responses can be investigated in figure 4.9.

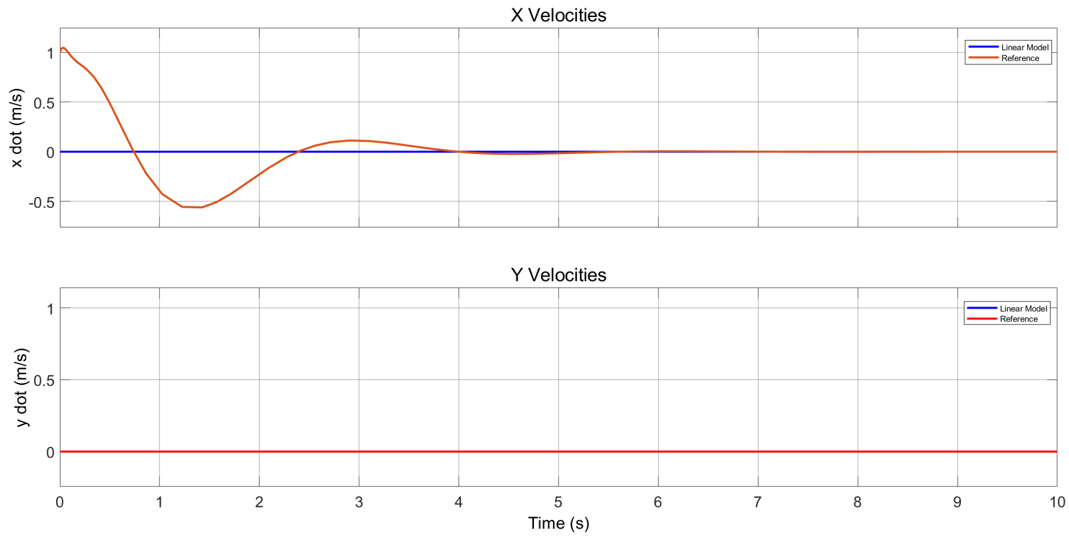

Figure 4.9 Non-zero initial x velocity case.

The settling time for the non-zero x velocity case is 1.1 seconds higher than that for the non-zero x position case. When the initial velocity in the y direction is non-zero, responses can be investigated in figure 4.10.

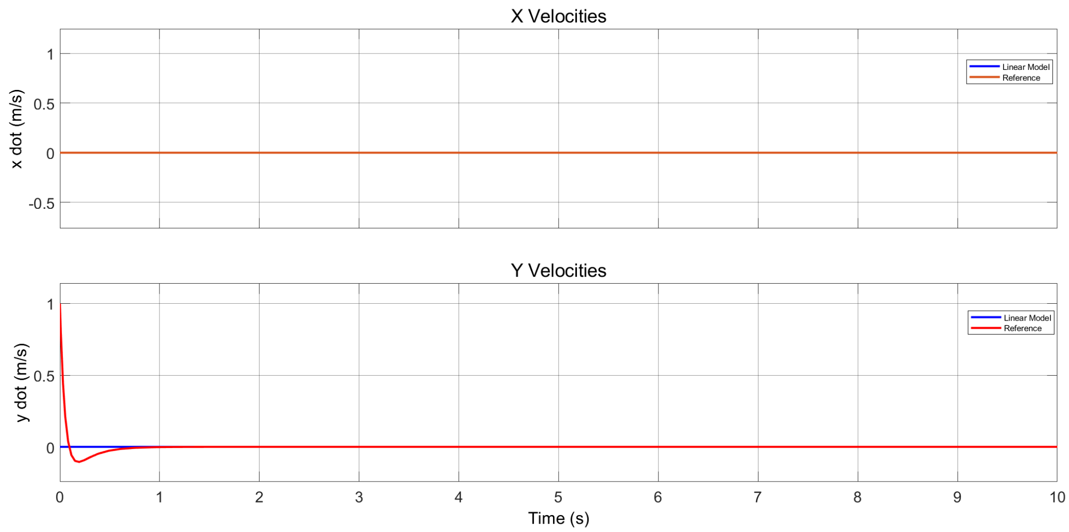

Figure 4.10 Non-zero initial y velocity case.

4.7.4.2. Existence of disturbance: It is not to be forgotten that the expected disturbances that will be applied to the robot are mainly in velocities such as wind speed change.

Disturbance in position has no meaning since the control objective is controlling the velocity. The robot's reaction to the step disturbance will also be expected to be quite similar to that of to initial position. It is shown in the figures 4.11 and 4.12.

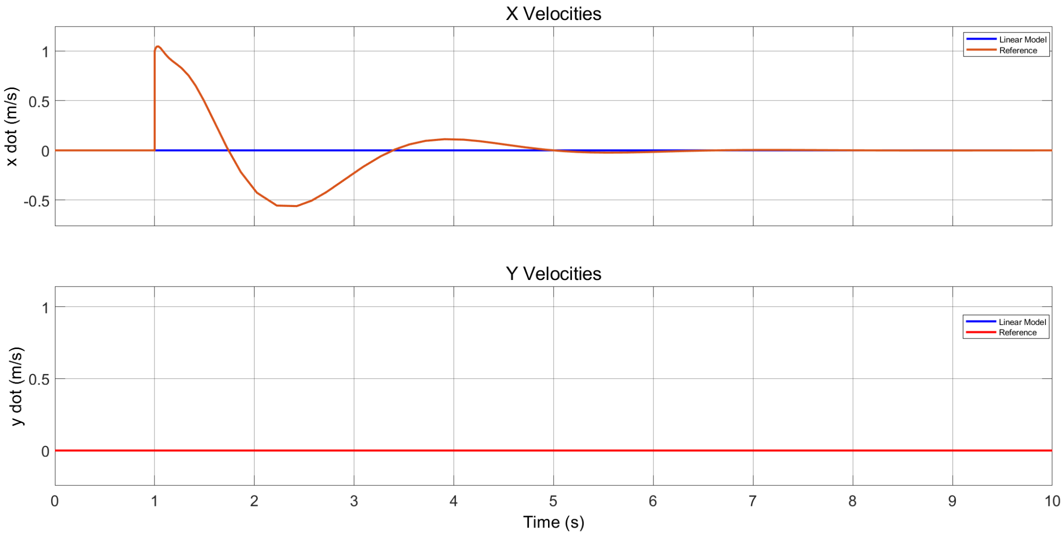

Figure 4.11 Step disturbance in x velocity case.

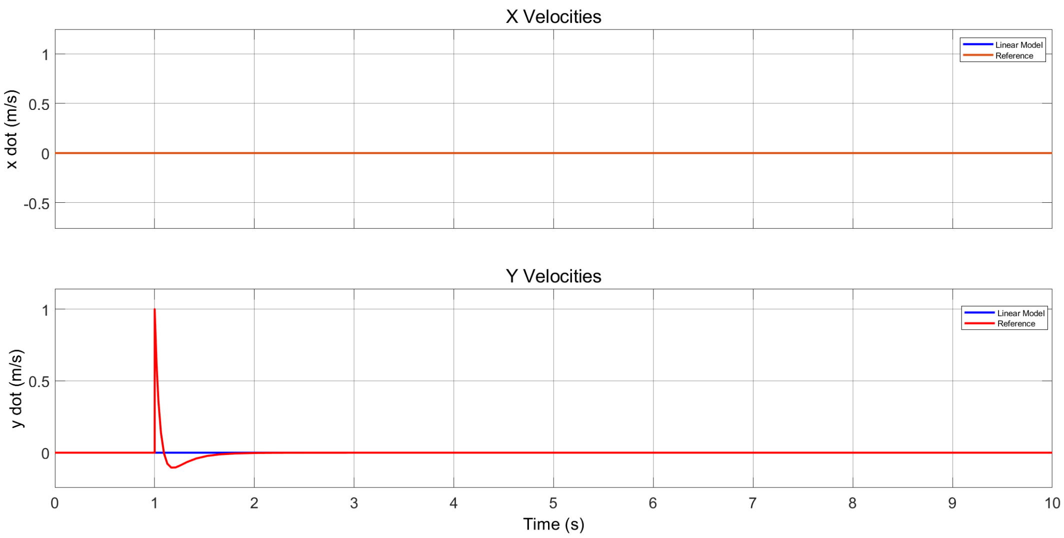

Figure 4.12 Step disturbance in y velocity case.

Although disturbance in positions means nothing, the controller is also examined in this case too. Figure 4.13 and 4.14 show the performance of the robot with respect to unit step disturbance applied in positions.

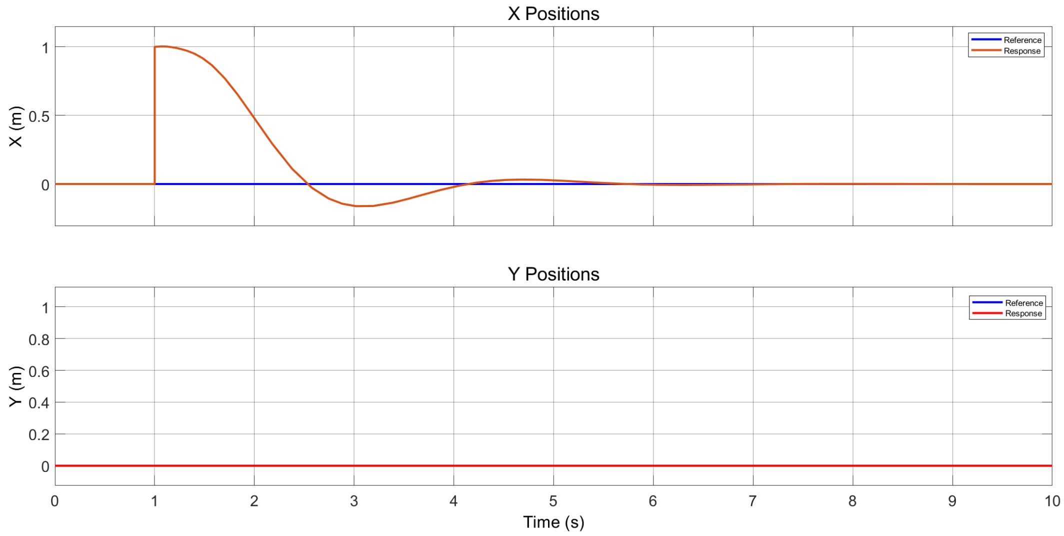

Figure 4.13 Step disturbance in x velocity case.

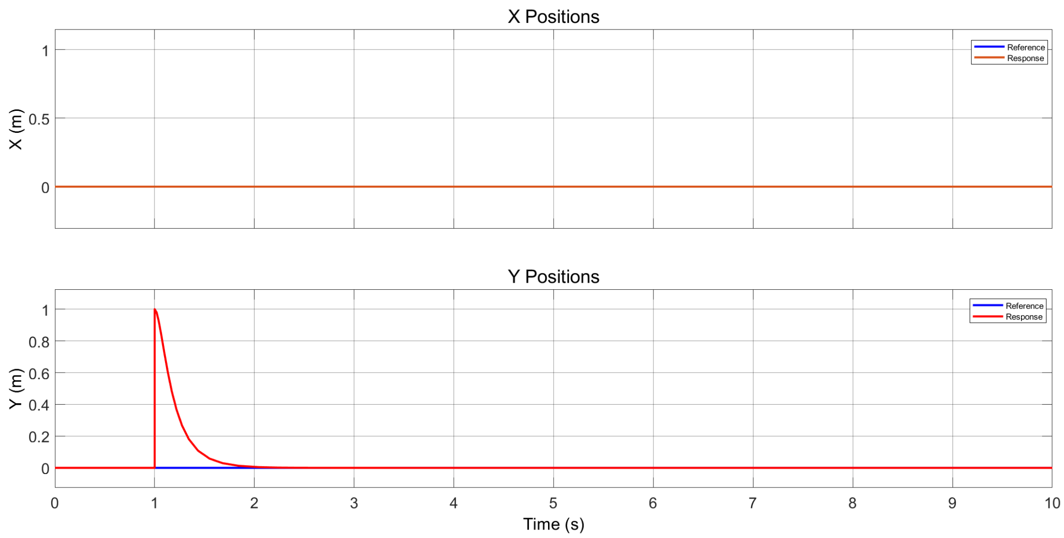

Figure 4.14 Step disturbance in y velocity case.

4.8. Type Number Check

As is discussed in sections 3.4. and 3.5., the servo system design configuration differs according to the type number of the system. Suppose the plant has an integrator; a type-1 servo system can be designed without any integrators. Nevertheless, an integrator should also be added to obtain a type-1 servo system if the system does not have an integrator. The presence or absence of an integrator can be determined by examining the plant's transfer function. As explained in the section 3.2.1., the plant transfer function can be obtained by equation 5. If one needs to determine the transfer function from each reference input to each plant output, the equation 5 will be in the form of 124.

$$\mathbf{G}(s)\mathbf{K} = \mathbf{C}(s\boldsymbol{I} - \mathbf{A})^{-1}\mathbf{B}\mathbf{K} \tag{124}$$

According to the given equation, the transfer function matrix is obtained and can be examined in the appendix 7.4.. Examining the transfer functions shows that the plant has an integrator, and a type-1 servo system can be designed without any additional integrator.

4.8.1. State Feedback Servo Controller

The state feedback serco system design is quite similar to the regulator design [18]. The block diagram of the SISO system with n-many states is given in figure 3.1.

This method is also straightforward to apply in a MIMO system. One can obtain the block diagram of a system with a C matrix as a unit matrix, as shown in figure 4.15.

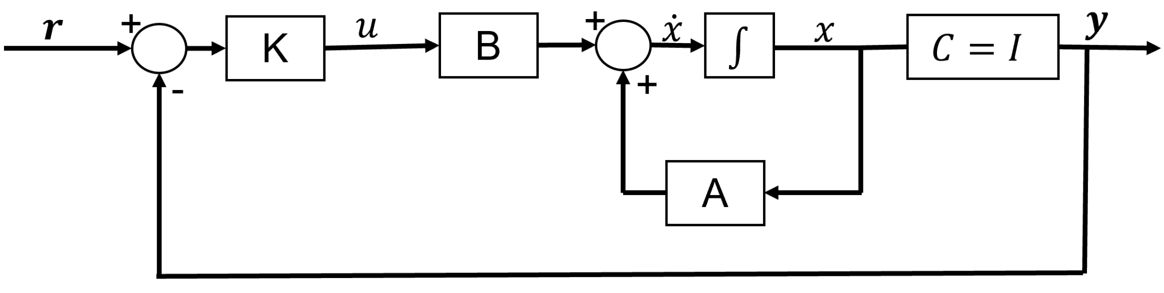

Figure 4.15 Block diagram of a MIMO state feedback servo system.

Given block diagram can be constructed in the Simulink as shown in figure 4.16.

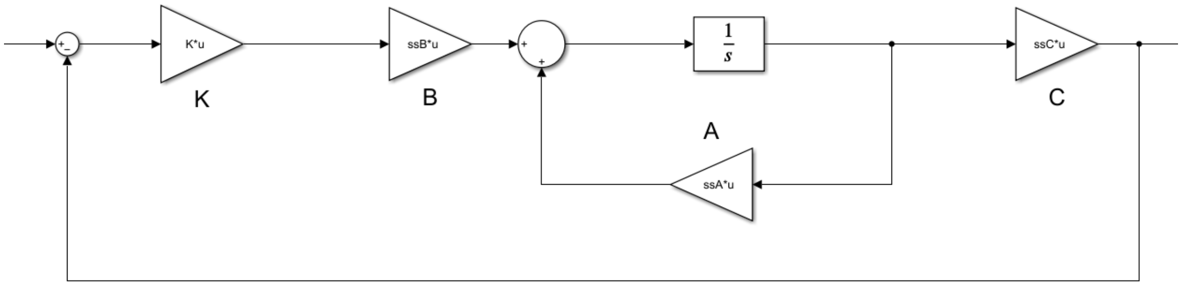

Figure 4.16 Simulink block diagram of a MIMO state feedback servo system.

According to this Simulink block diagram controller performance is also investigated. Figure 4.17 shows the response of the controlled robot to unit step input applied at $t_0 = 0$.

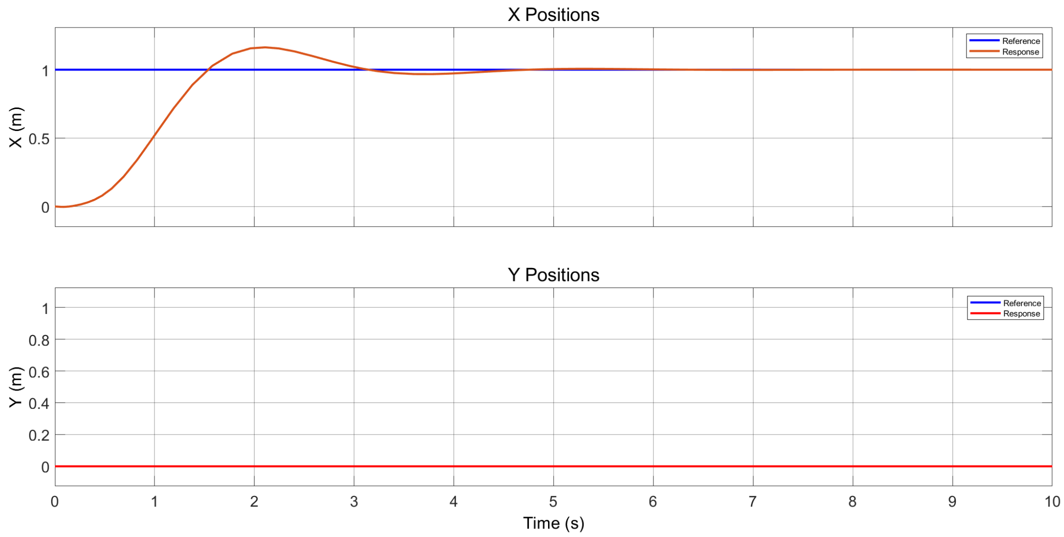

Figure 4.17 Servo system output for step x position input.

In figure 4.17 one can see that the settling time requirements are quite met. The maximum overshoot is also less than 20% which is also as desired. Figure 4.18 shows the response of the controlled robot to unit step y position input applied at $t_0 = 0$. The control system response is found to be faster in the y direction. It has no oscillation and the settling time is less than one second.

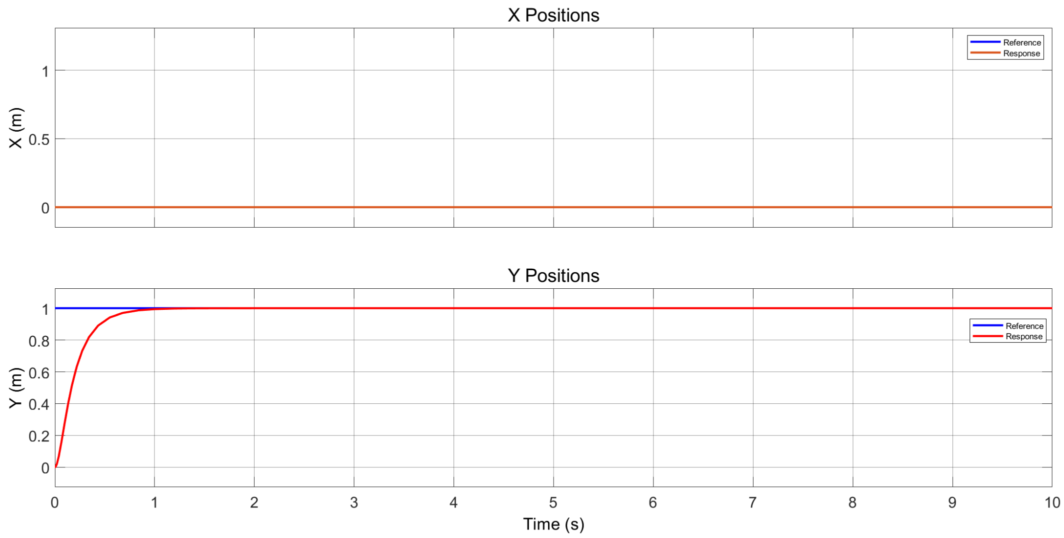

Figure 4.18 Servo system output for step y position input.

Figure 4.19 shows the response of the controlled robot to unit step x velocity input applied at $t_0 = 0$. The transient specs of the control system are as desired for the x-velocity input.

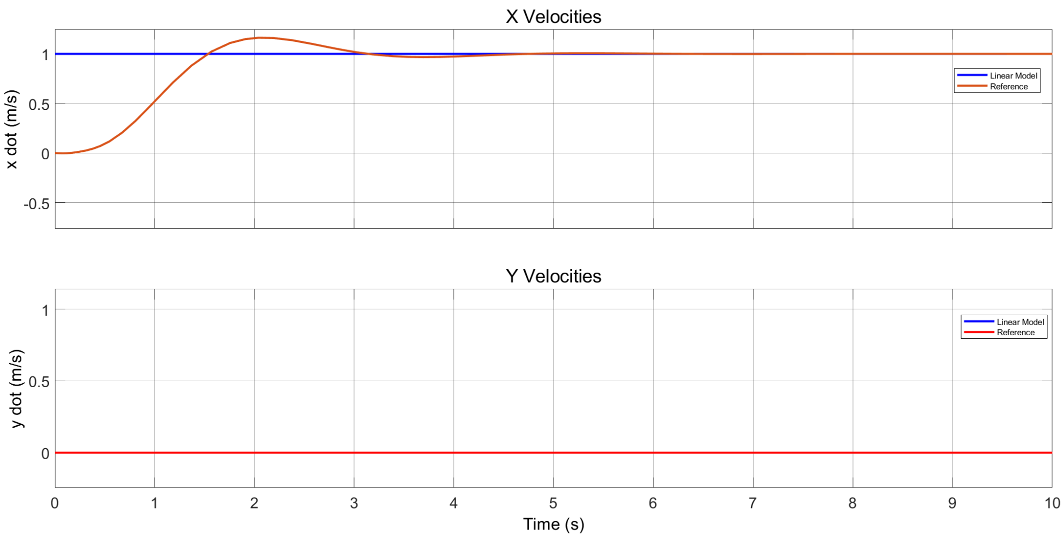

Figure 4.19 Servo system output for step x velocity input.

Figure 4.20 shows the response of the controlled robot to unit step y velocity input applied at $t_0 = 0$. The response of the robot is faster than desired but it has no harm to the user if actuator efforts are in the acceptable range. Actuator efforts will also be investigated in the next chapter with the flight simulator.

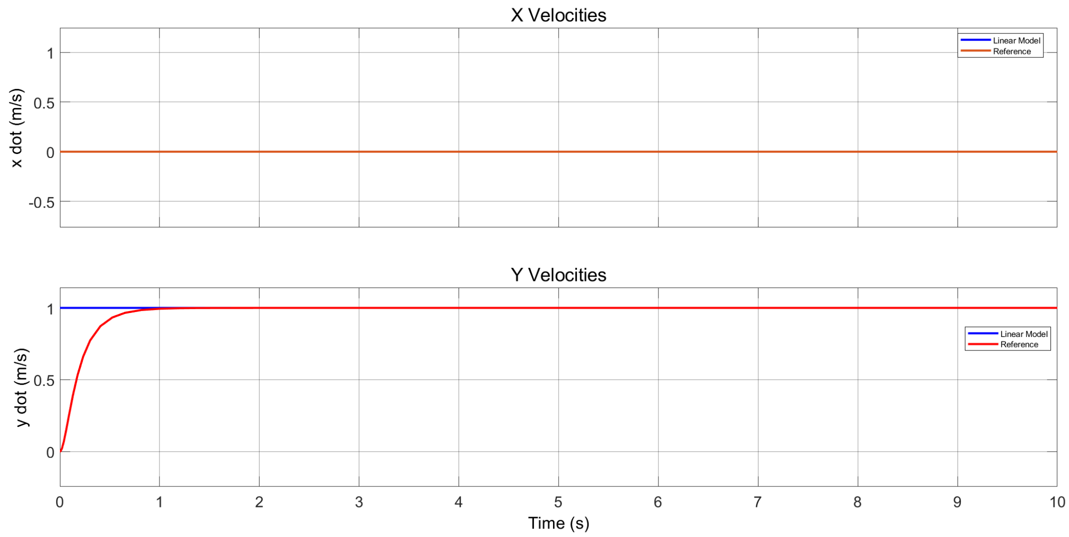

Figure 4.20 Servo system output for step y velocity input.

4.9. Conclusion

The EOMs are obtained by both Newton's and Lagrange's methods. After that, linearization is applied to obtain LTI state space model. Next, the desired pole locations are determined by determining dominant and non-dominant poles according to the desired transient behavior. The State feedback regulator is designed with the pole placement approach, and controller performance is investigated with the linear model. A servo design is obtained from the regulator, and servo controller performance is also analyzed with the linear model.

5. SIMULATION RESULTS

5.1. Introduction

The robot's equations of motion are obtained by Newton's and Lagrange's methods as shown in section 4.3. and 4.4., respectively. These equations of motion can be simulated by using a differential equation solver. Also, as can be examined in the appendix 7.1. and 7.2., these EOMs consist of very long expressions. Hence, defining these expressions without any error is very hard to achieve. On the other hand, they can be cross-checked, validated with basic inputs, and compared with a multibody dynamics software.

Multibody dynamics software Simscape is used to create a flight simulator for the simplified model of flying RHex robots, and EOMs are validated with the flight simulator. The controllers obtained in the previous section are also implemented in the flight simulator to test controller performances.

This chapter starts with validating Newtonian and Lagrangian EOMs with three basic inputs and is followed by validation with the flight simulator. After that, the controller structure and controller performance metrics are presented to the reader.

5.2. Simulations of Newtonian EOMs

As also stated in the section 4.5., position and velocity parameters are accepted as known by used sensors. Acceleration values are calculated in the Matlab Function Block using the equation refAibExNew. The solution diagram is shown in figure 5.1

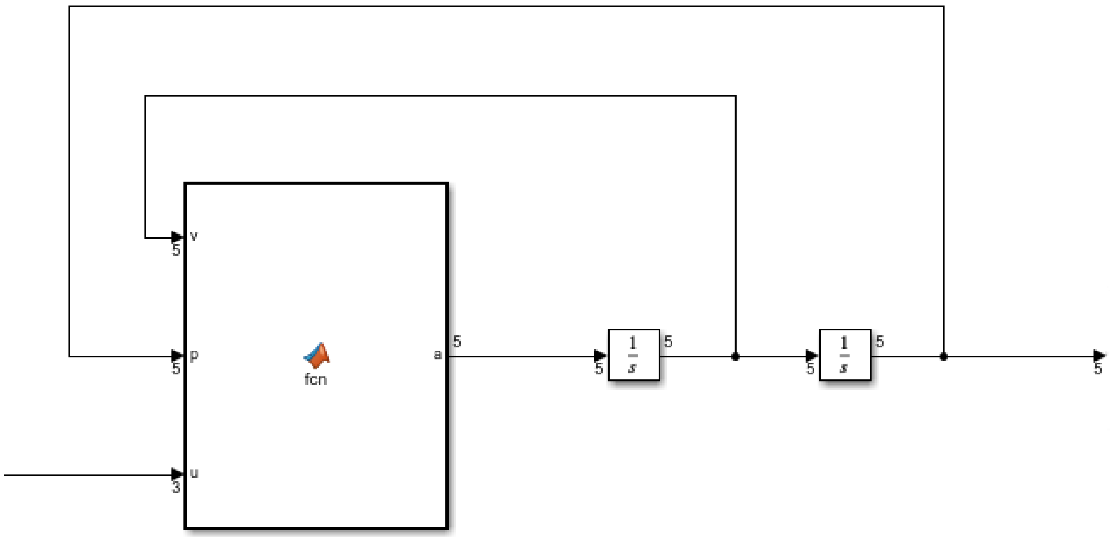

Figure 5.1 Simulink block diagram to solve nonlinear differential equations coming from Newtonian EOMs.

The created function block is simulated using basic inputs to see whether it gives the expected results. To examine the model, three basic input types are defined. At first, a thrust force is applied to be just a bit more than gravitational force where the leg torques are zero. The expected result is the rising of all bodies without oscillations. Figure 5.2 shows the input applied, while figure 5.3 and 5.4 show the motion of the body and legs respectively.

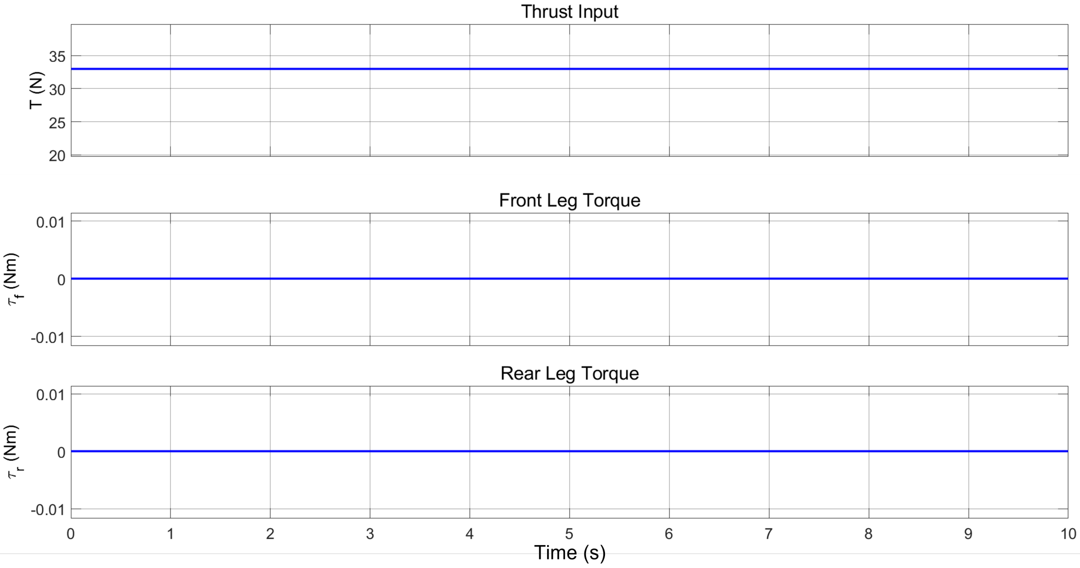

Figure 5.2 First basic input for examination.

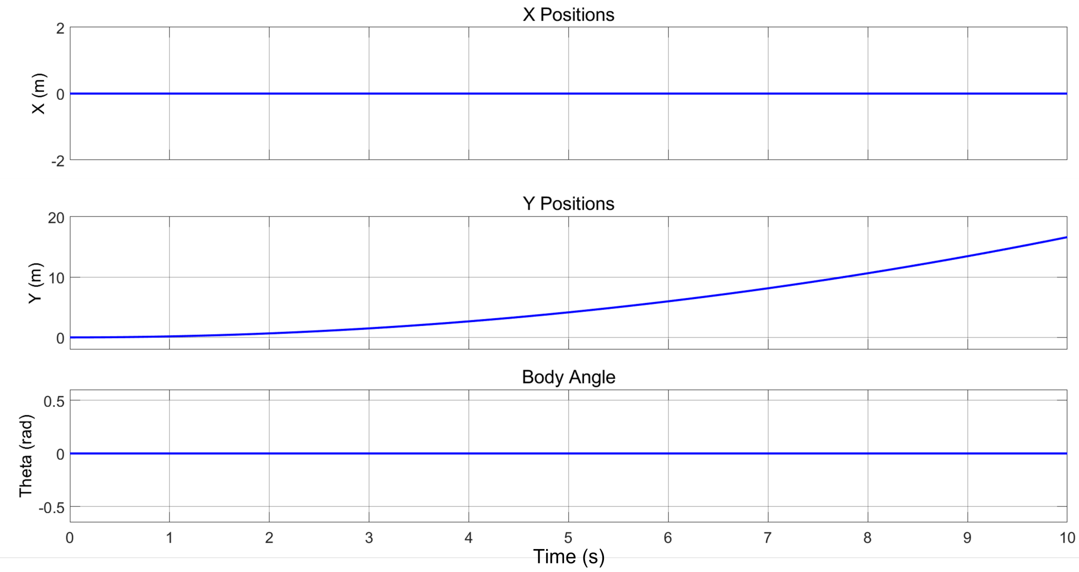

Figure 5.3 Body motions obtained from the model, due to the first basic input.

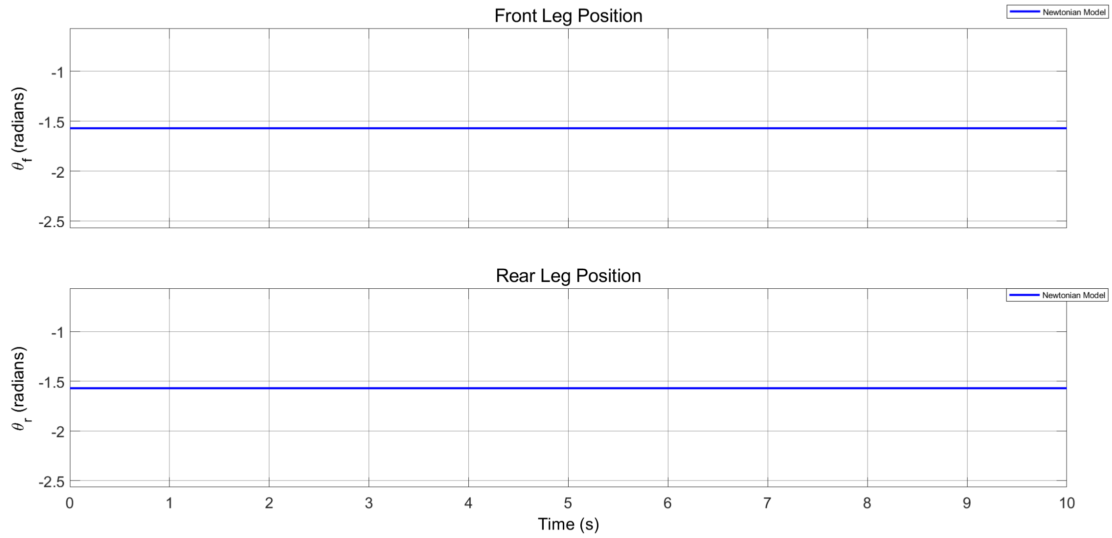

Figure 5.4 Leg motions obtained from the model, due to the first basic input.

The second input is a thrust force equal to the weight while the leg torques are applied in the same direction. The expected result is to see the body lowering in the y direction due to the direction change on the thrust vector. In contrast, the body turns opposite to the legs, and the body's x position will change due to the thrust vector in the x direction. Figure 5.5 shows the input used, and in figure 5.6 with 5.7, one can examine the respective action. Since the simulations are inspected in ten seconds, the torque is kept very low to prevent more than one tumble motion.

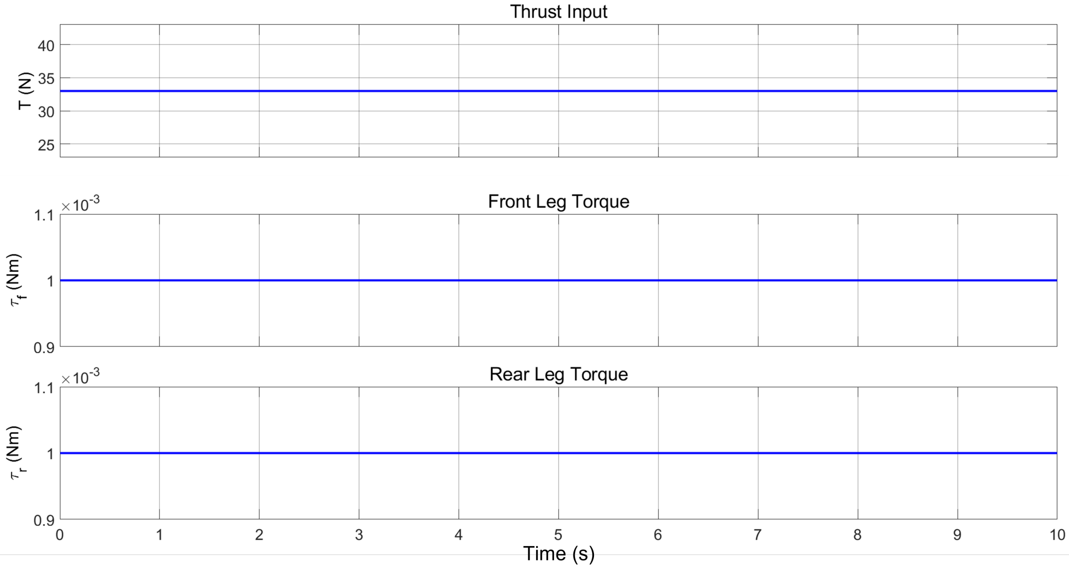

Figure 5.5 Second basic input for examination.

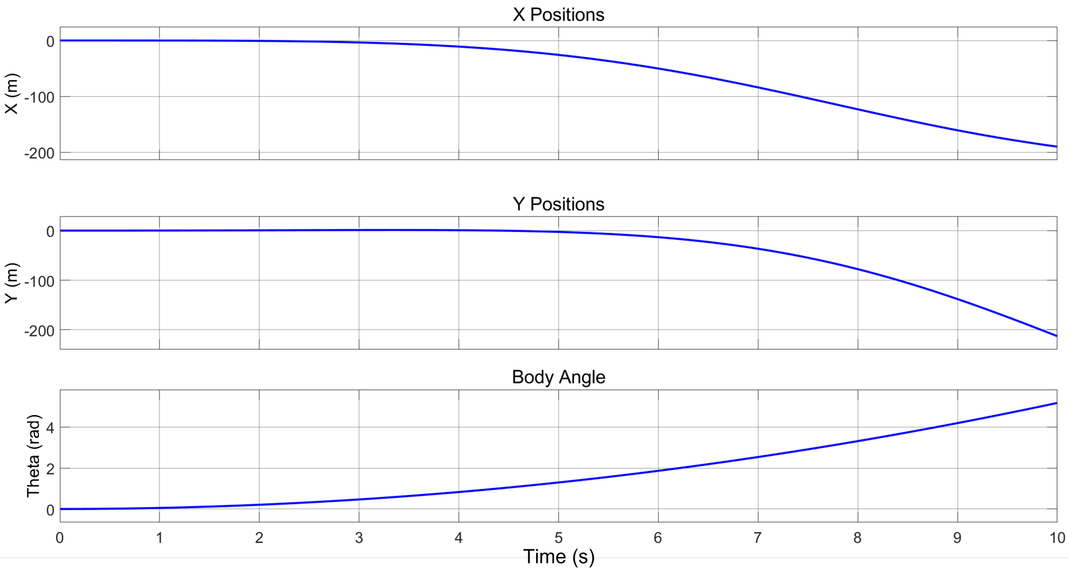

Figure 5.6 Body motions obtained from the model, due to the second basic input.

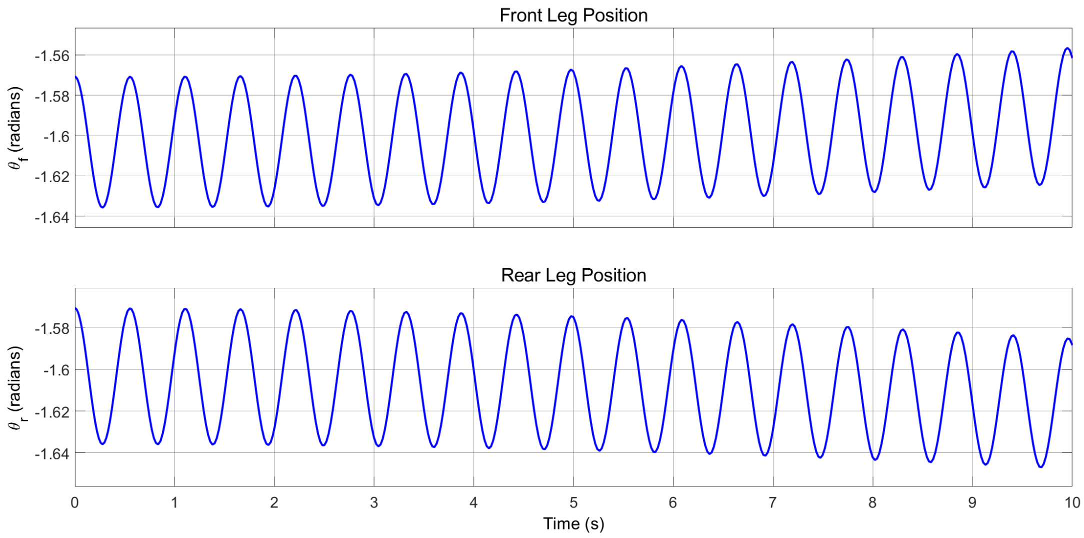

Figure 5.7 Leg motions obtained from the model, due to the second basic input.

As the last input, the thrust force will be equal to the weight while the leg torques are applied in the opposite direction to cancel each other. The expected result is constant x, y, and θ position while the legs turn oppositely. Figure 5.8, figure 5.9, and figure 5.10 show the input and responses, respectively.

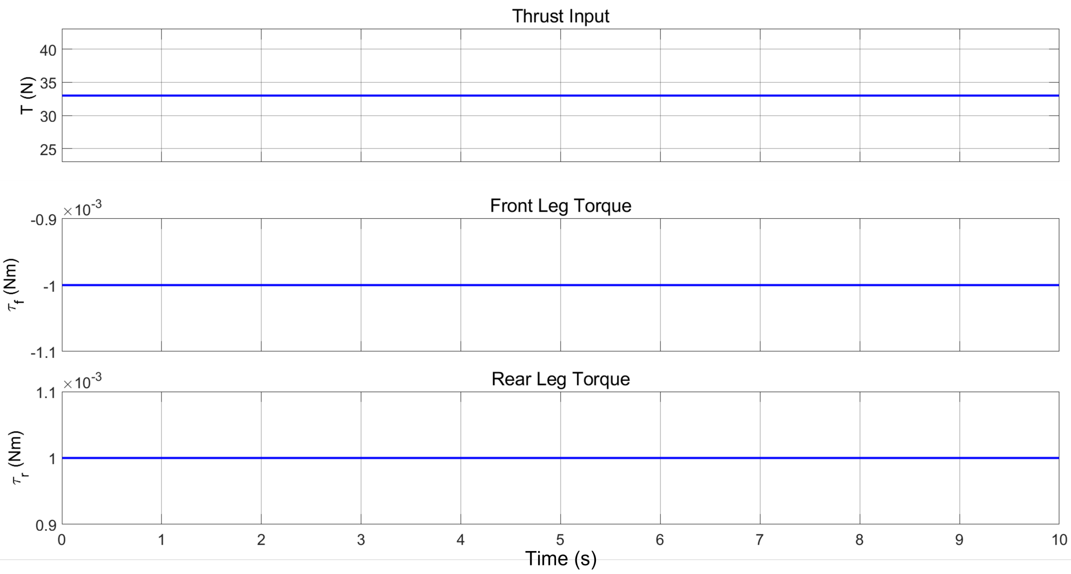

Figure 5.8 Third basic input for examination.

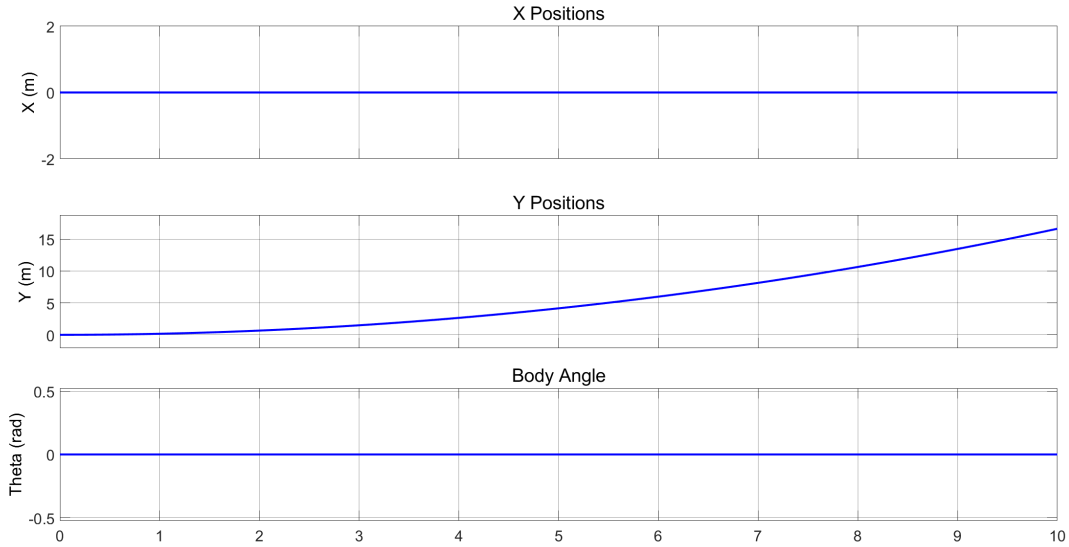

Figure 5.9 Motion obtained from the model, due to the third basic input.

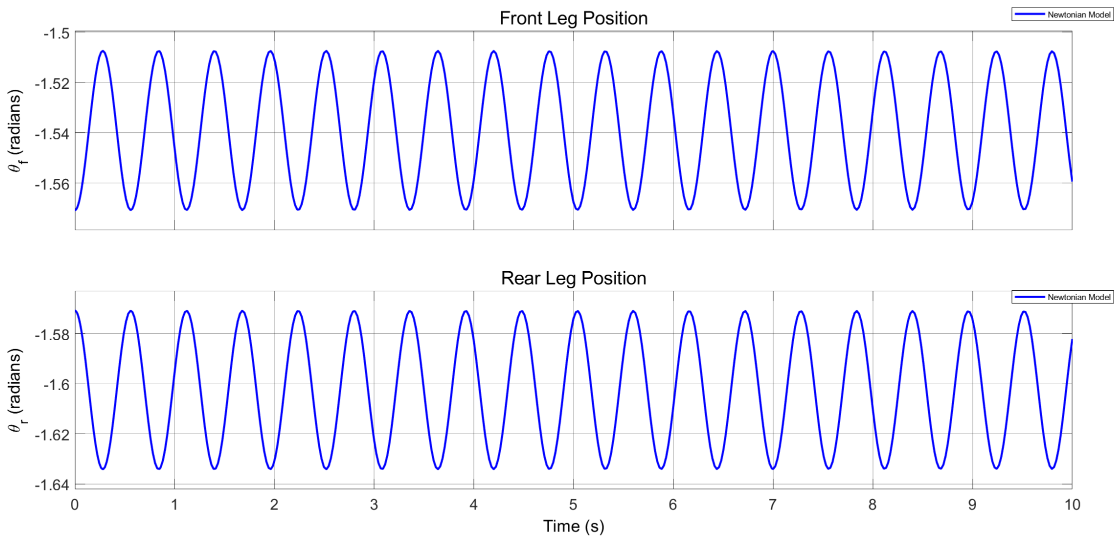

Figure 5.10 Motion obtained from the model, due to the third basic input.

5.3. Simulations of Lagrangian EOMs

In section 4.4., equations of motion are obtained in the matrix form. As validation of the Lagrangian EOMs, the same method is applied as in Newtonian. Three basic inputs are used, and the results are compared with the expected motion profile and this case, with

Newtonian EOMs results. Since a more detailed comparison will already be examined in the next section, they will not be shared in this section.

5.4. Flight Simulator and Validation of EOMs

Newton's and Lagrange's methods are used to create equations of motion of the model. Those equations are examined to be sure they are well-defined and contain no errors. Although the equations are carefully inspected, there is no way to be sure to create error-free equations since the equations are very long. Nevertheless, simulations of those equations can be compared with a multibody dynamics solver, and the existence of any error can be detected. As a multibody dynamics software, Simscape is a very easy-to-use program, and compatibility with Simulink makes it the best choice for EOMs validation. The created Simscape model is given in figure 5.11.

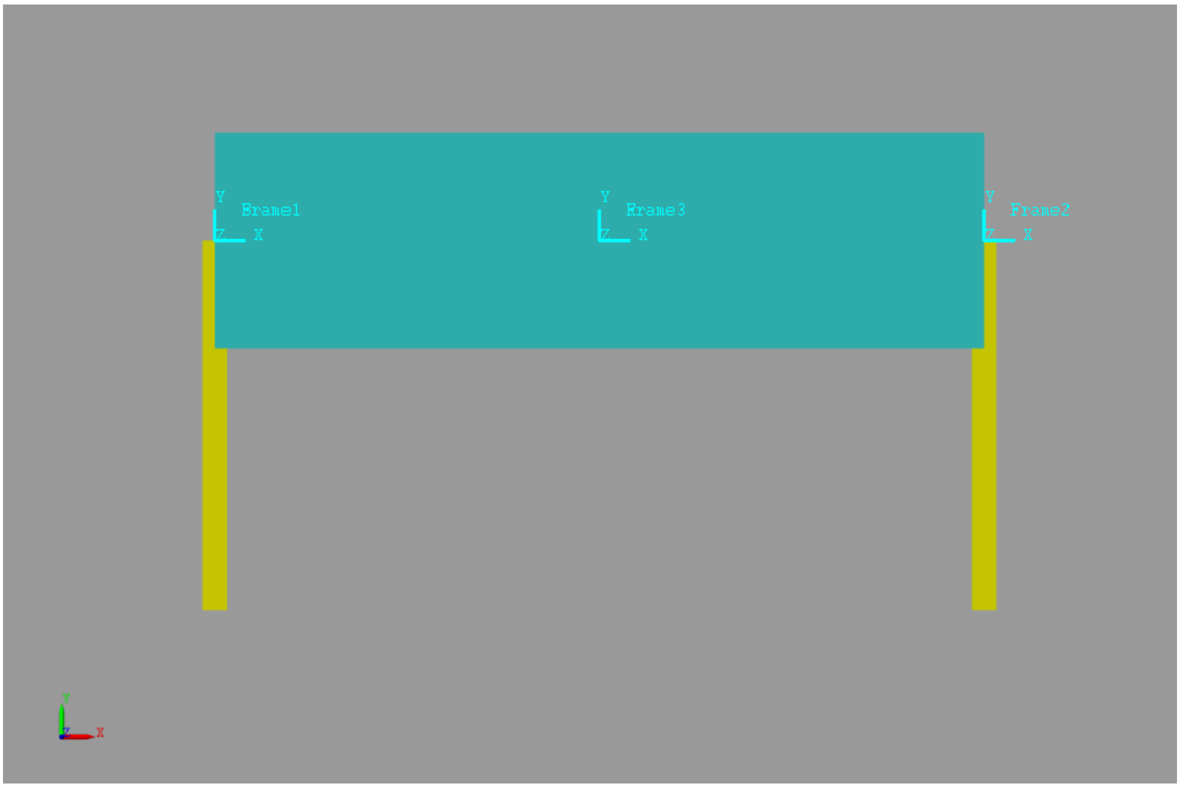

Figure 5.11 Created Simscape multibody dynamics model.

To compare Newtonian and Lagrangian EOMs with the Simscape mode, using a step signal might be a primitive approach, while complex input signals may also be created. An arbitrary input signal is formed as shown in figure 5.12 to detect any error if it exists.

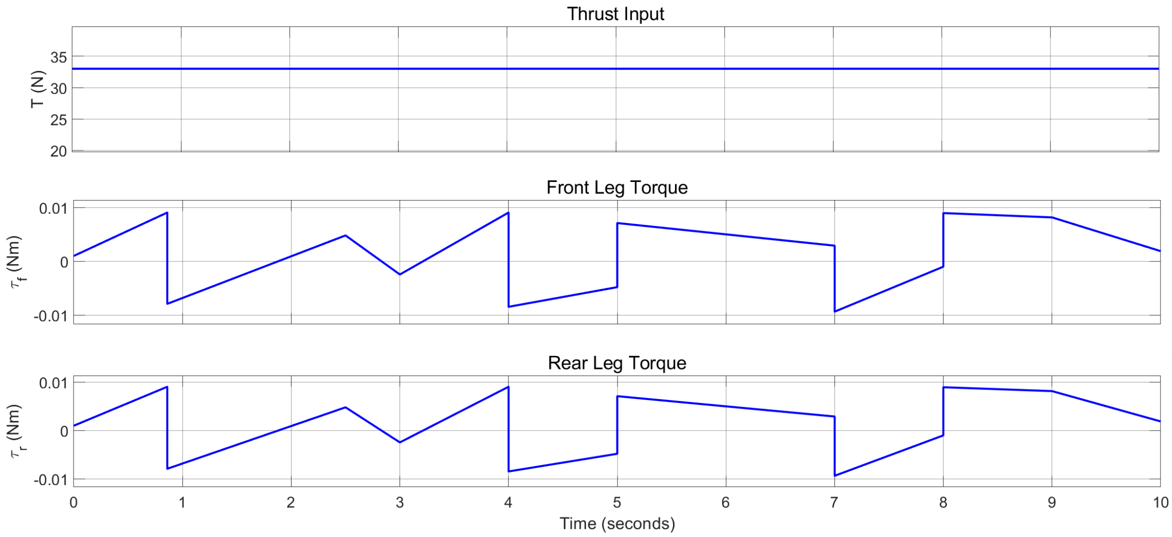

Figure 5.12 An arbitrary input signal to compare outputs of Newtonian, Lagrangian and Simscape models.

The responses are considered, and the errors are eliminated to obtain a perfect fit of reactions. The final outputs of the three models are plotted superimposed in figure 5.13 and 5.14.

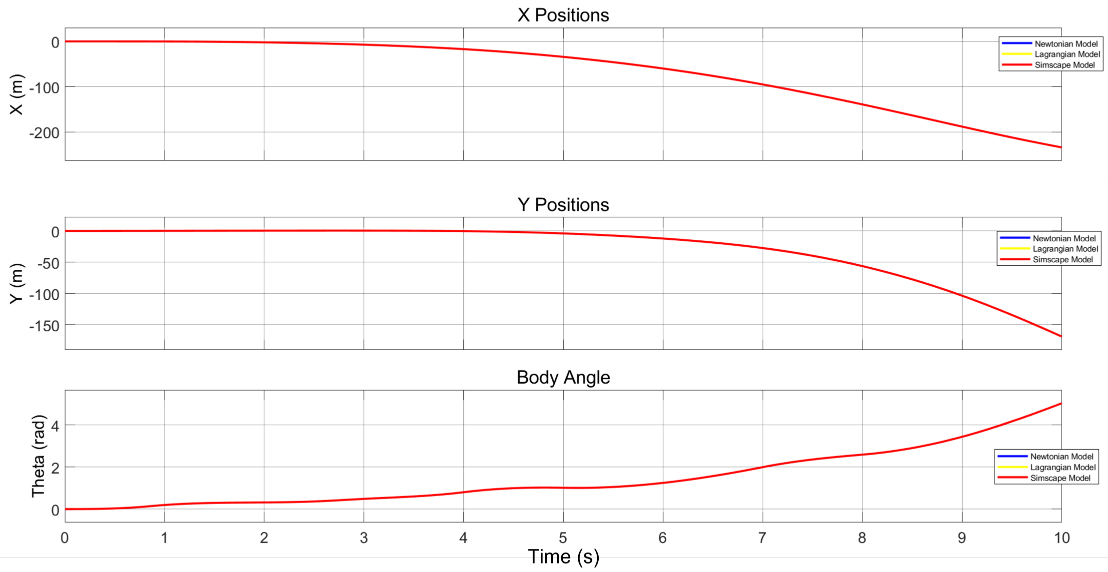

Figure 5.13 Superimposed responses of bodies, against the arbitrary input given in figure 5.12. The responses match perfectly.

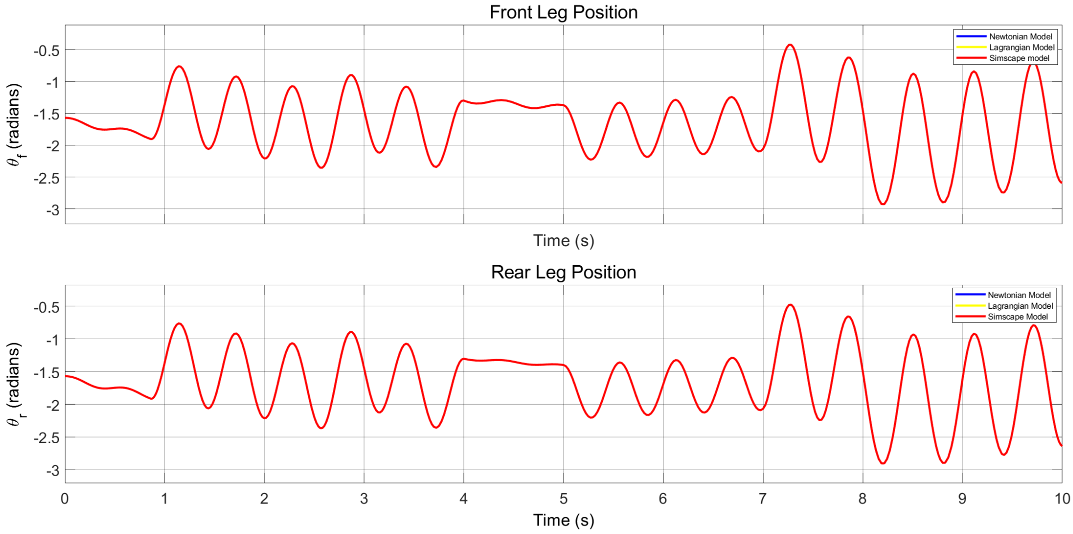

Figure 5.14 Superimposed responses of legs, against the arbitrary input given in figure 5.12. The responses match perfectly.

Although Newtonian, Lagrangian, and Simscape models are seen as they are matched perfectly there are very few differences between their responses due to round of errors. The differences are found to be 10^{-8} in order of magnitude.

5.5. Validation of Linearization

A linearization process is essential to design a linear controller. The linearization procedure is clearly explained in the section 4.5.. Although it is not expected to obtain the same responses from both linear and non-linear models, they are expected to be quite similar in form and very close in response amplitudes. To clarify the statement given in the previous sentence, one can exemplify it as, if the form of the response obtained from the non-linear EOMs are sinusoidal, those of the linear ones should be too. To be sure that the linearized equations are usable in controller design both the linear and non-linear EOMs will be supplied by the same basic inputs and their responses will be investigated.

In figure 5.15 and figure 5.16 one can investigate the body and leg responses against the first basic input respectively.

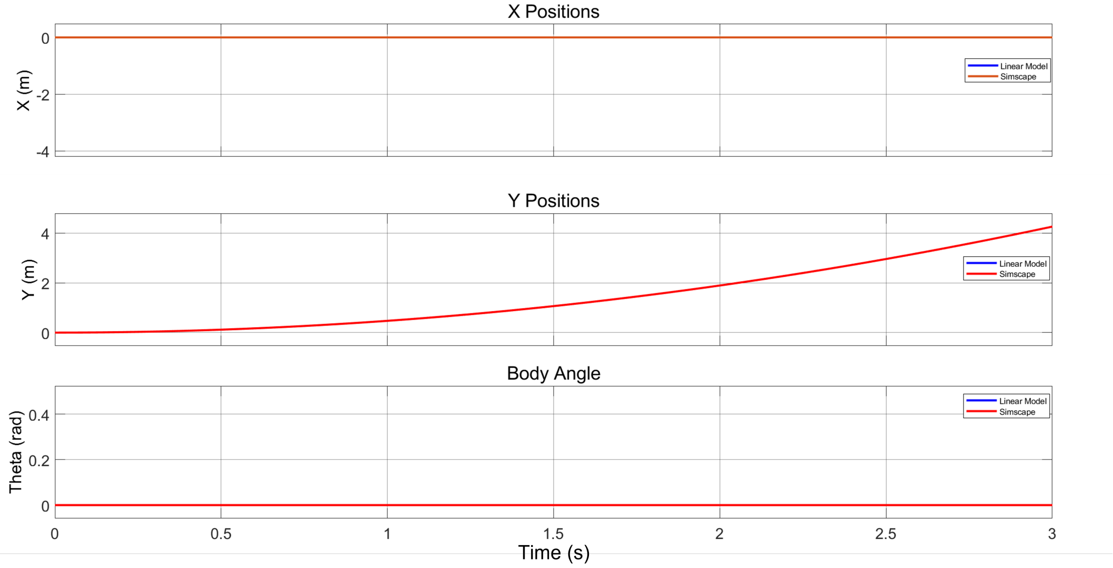

Figure 5.15 Body motions obtained from the linear and multibody model due to the first basic input.

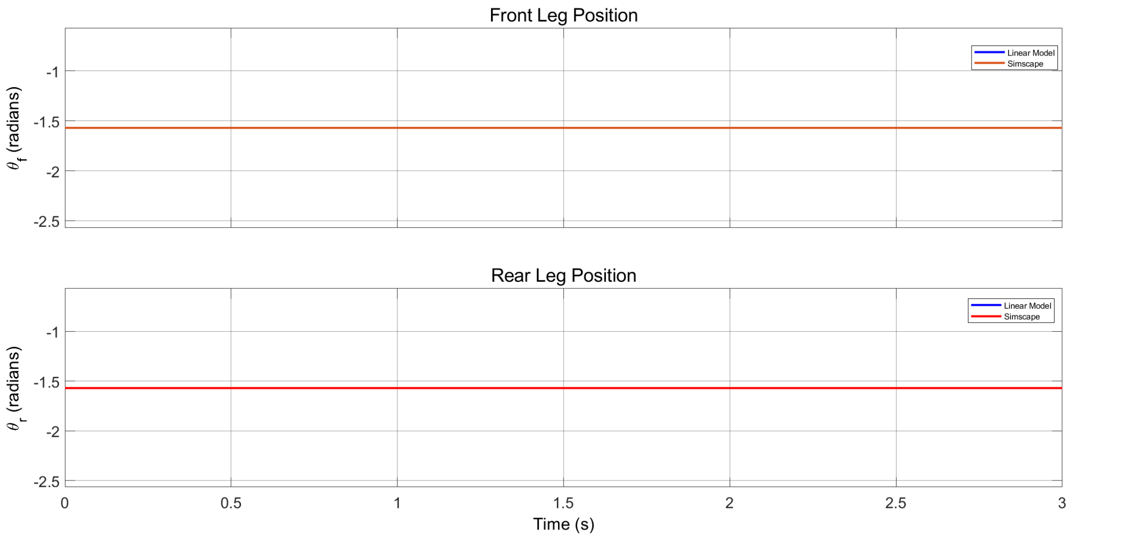

Figure 5.16 Leg motions obtained from the linear and multibody model due to the first basic input.

In figure 5.17 and figure 5.18 one can investigate the body and leg responses against the second basic input respectively.

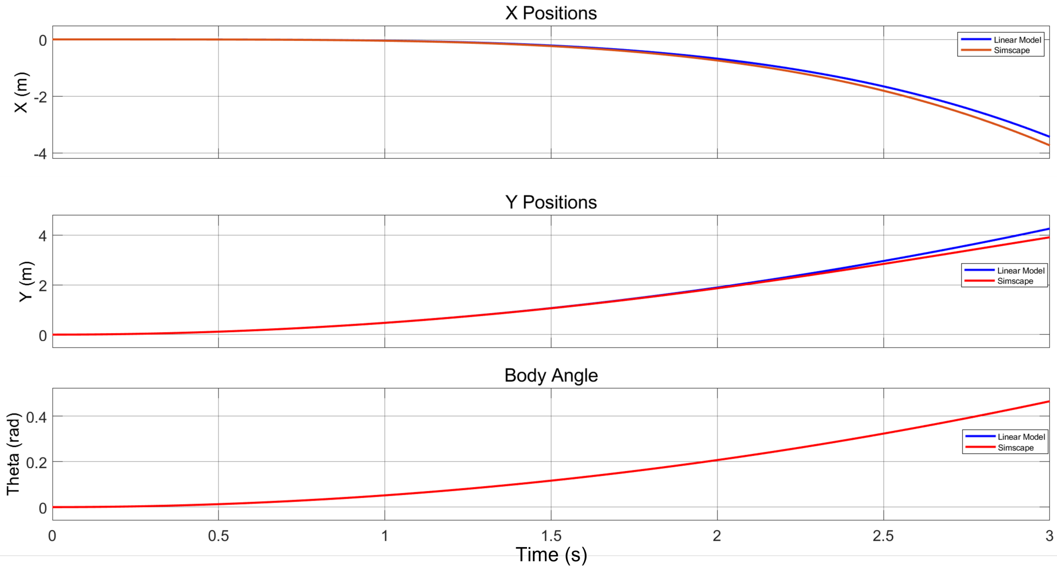

Figure 5.17 Body motions obtained from the linear and multibody model due to the second basic input.

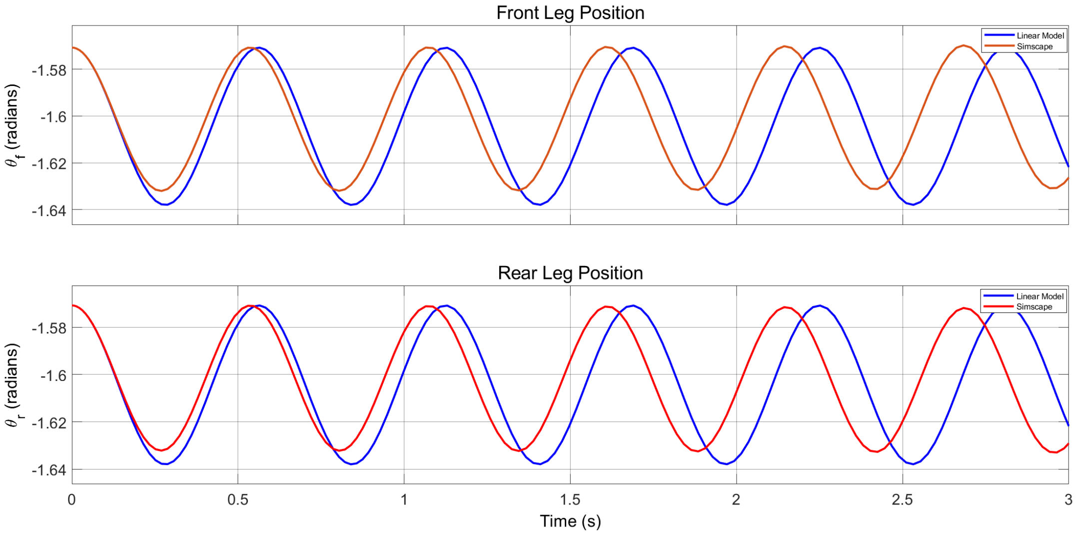

Figure 5.18 Leg motions obtained from the linear and multibody model due to the second basic input.

In figure 5.19 and figure 5.20 one can investigate the body and leg responses against the third basic input respectively.

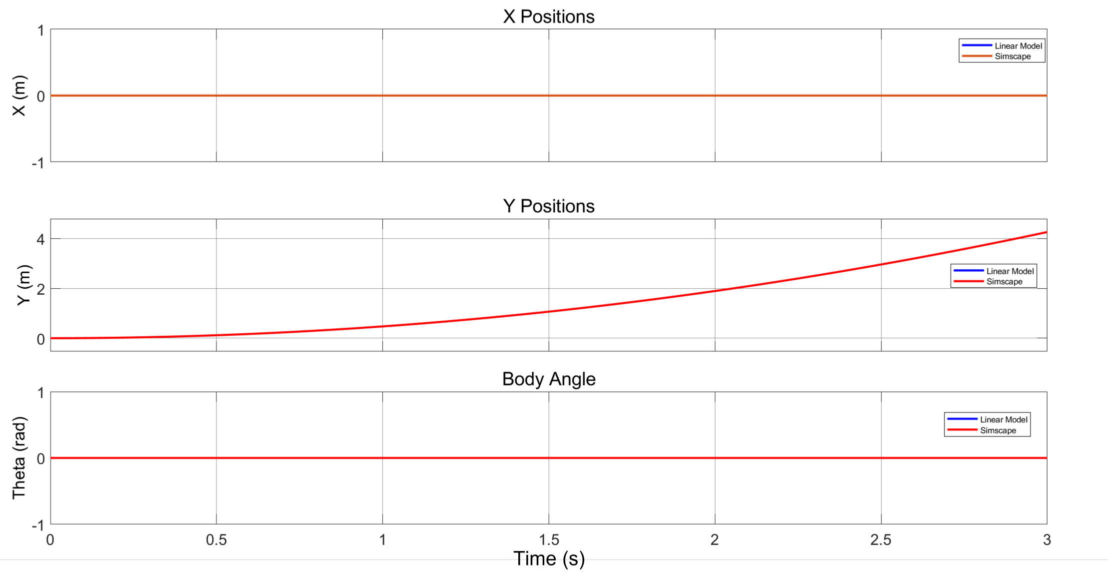

Figure 5.19 Body motions obtained from the linear and multibody model due to the third basic input.

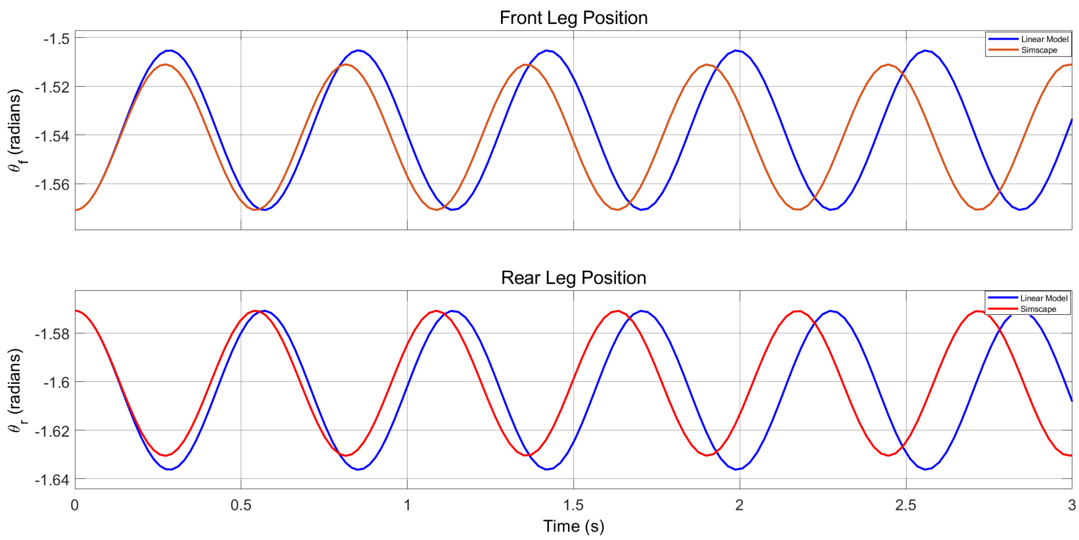

Figure 5.20 Leg motions obtained from the linear and multibody model due to the third basic input.

In figure 5.18 and 5.18, differences in natural frequencies are observed between linear and nonlinear models. These differences are due to nonlinear increments in the torque coming from the moment of gravitational forces. The moment of the gravitational force increases with an increasing trend while the leg rises until its horizontal position. But this increment is linearly proportional to the angle θ in the linear model, so the increment is lower concerning the nonlinear model. Thus, the linear model allows a higher amplitude of motion with the same torque input and it ends up with a longer period.

5.6. Validation of State Feedback Controller

The controller has been designed, and the controller's performance for the linear model is discussed in section 4.7.4.. The discussion of the controller performance on the non-linear model obtained from the multibody dynamics software will take place in the current section. Also, additional discussions for actuator efforts and the satisfaction of the motion from the user's point of view will be made.

The controller implementation can be investigated in figure 5.21.

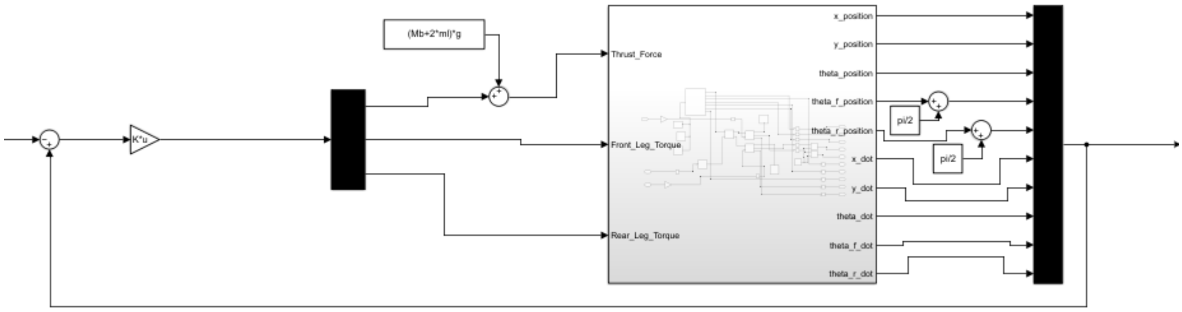

Figure 5.21 Implementation of the controller to the Simscape model.

Six reference step inputs and six respective outputs will be examined to inspect controller performance. The first and second reference inputs will be the step inputs to position on the x-axis and y-axis, respectively. Both inputs will be fed into the controller simultaneously as the third input. The same process will be applied to the velocity inputs.

In figure 5.22, the applied x position reference step input and the system output are given superimposed.

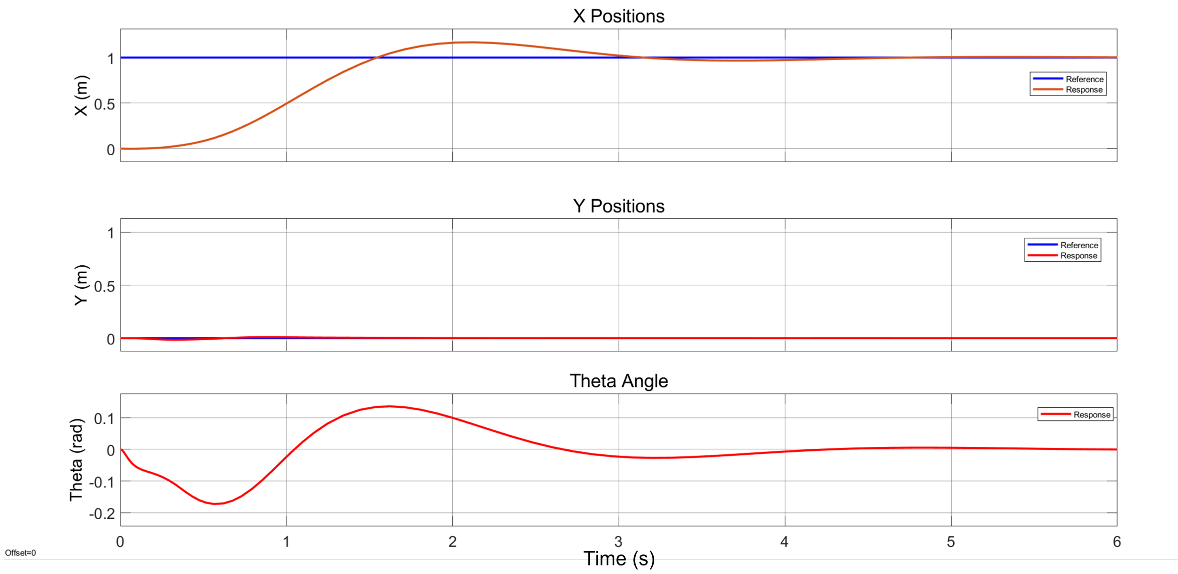

Figure 5.22 X position step input and response.

In figure 5.23, the applied step y position reference input and the system output are given superimposed.

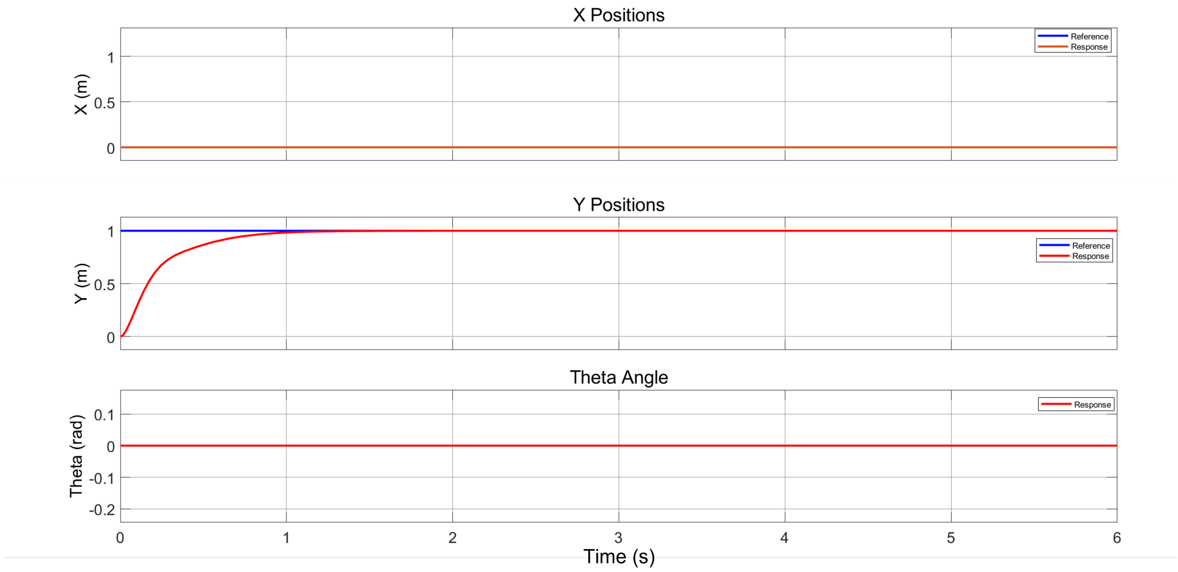

Figure 5.23 Y position step input and response.

In figure 5.24, the applied x and y position step inputs and the system outputs are given superimposed.

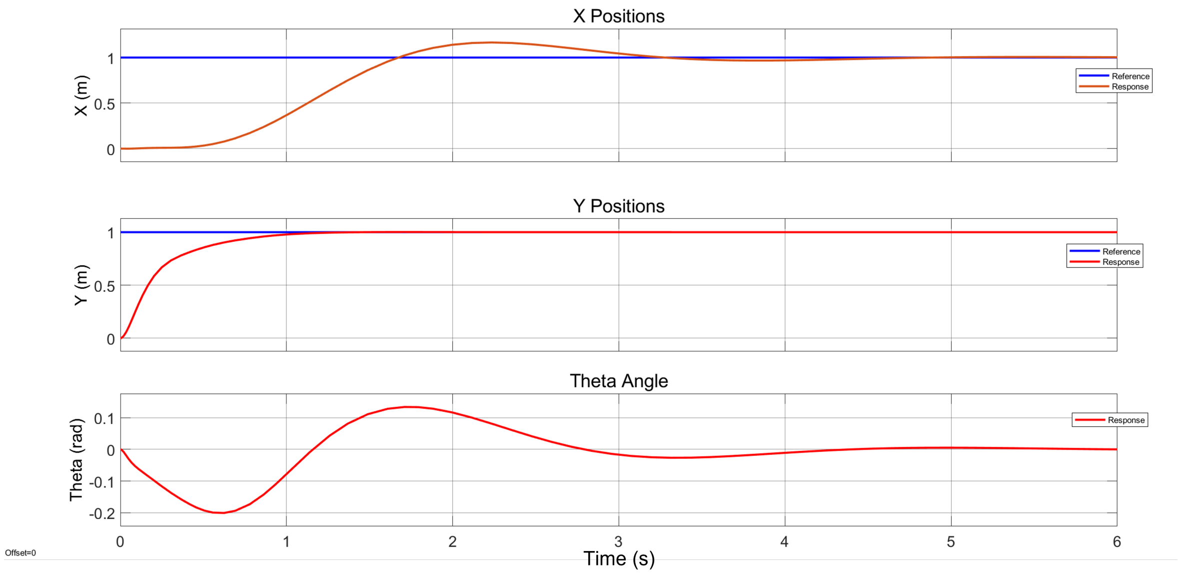

Figure 5.24 Simultaneously applied x and y position step inputs and responses.

The actuator effort should also be examined for the velocity inputs and responses. Since the velocity inputs are the expected user commands for the robot, as stated in section 4.6., the velocity reference tracking performance and actuator efforts are pretty important. On the other hand, position reference tracking capabilities are just mentioned to investigate controller performance. One can examine the step input for x velocity and the response of the robot in figure 5.25 and the respective actuator efforts in figure 5.26.

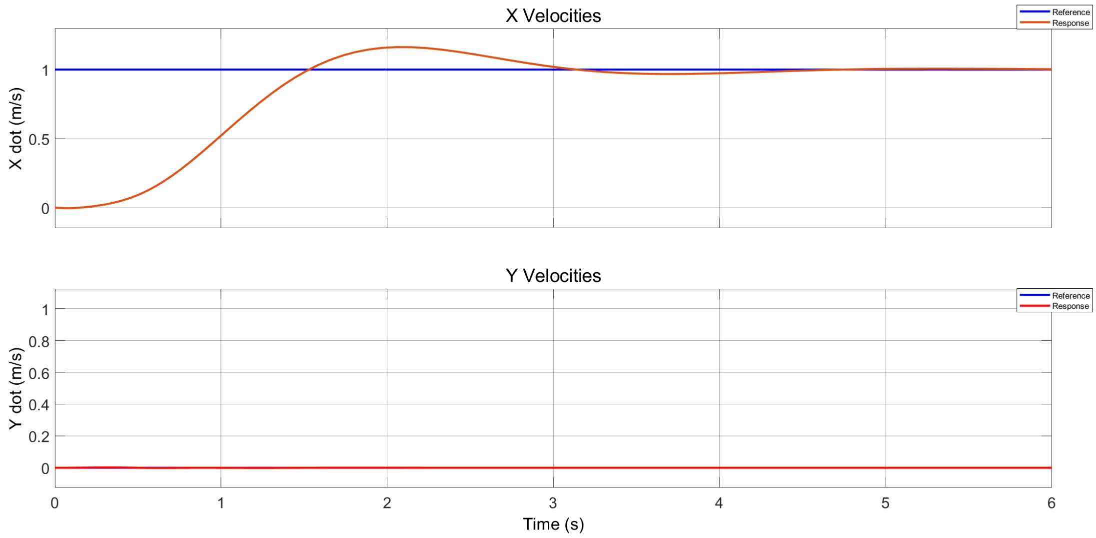

Figure 5.25 X velocity step input and responses.

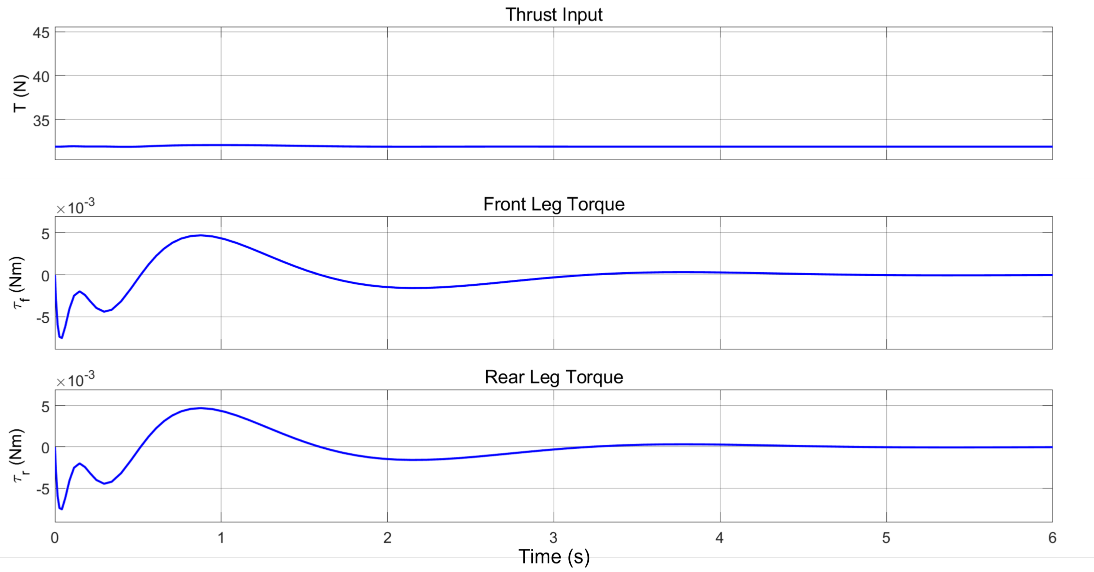

Figure 5.26 Actuator effort for x velocity step input.

The y velocity reference input and the response of the non-linear model are given in figure 5.27 with respective actuator effort in figure 5.28.

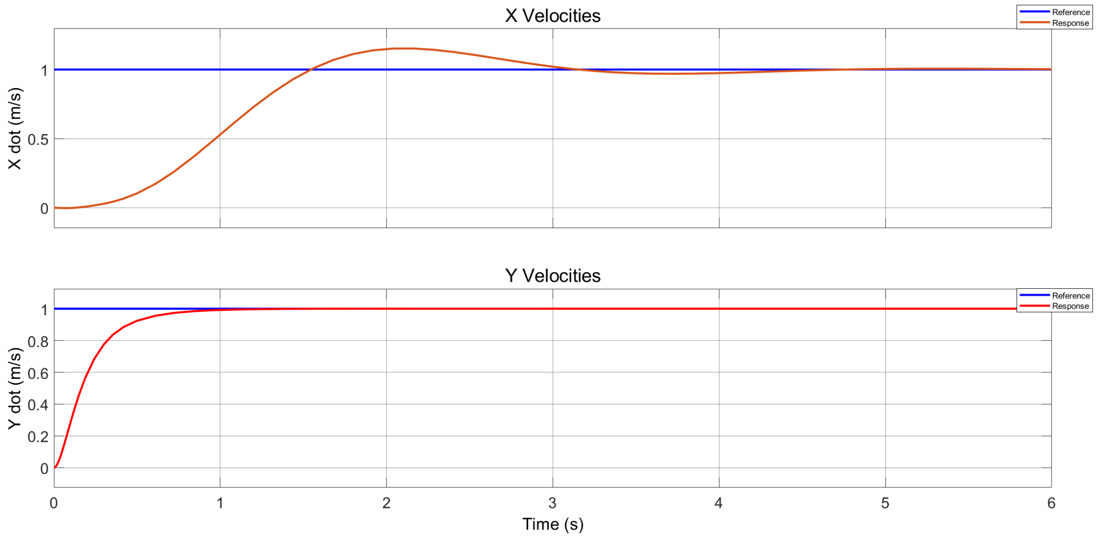

Figure 5.27 Y velocity step input and responses.

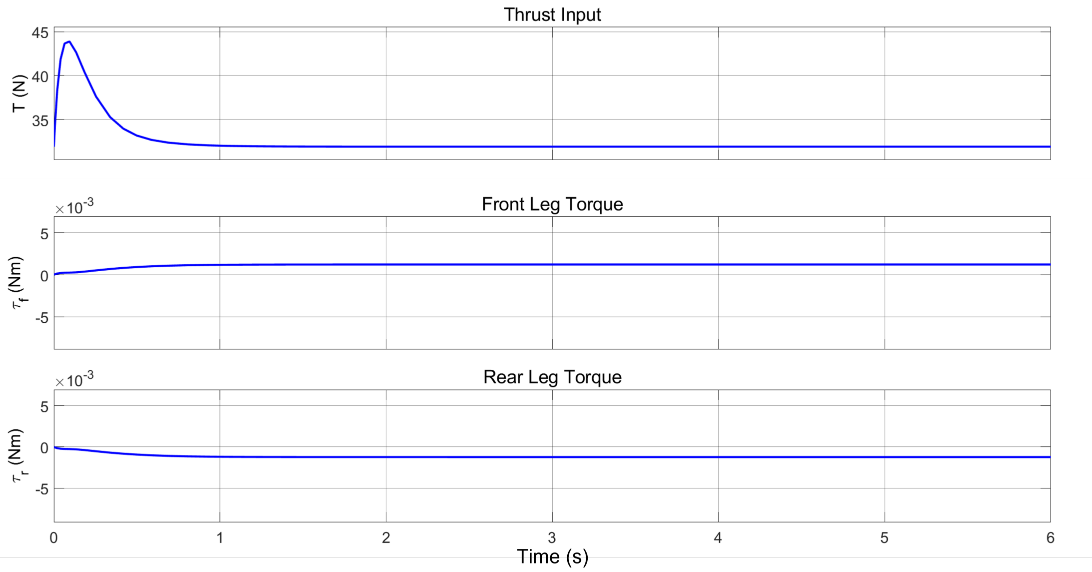

Figure 5.28 Actuator effort for y velocity step input.

At last, both velocity inputs are applied simultaneously as the third input, and the results are in the figure 5.29 with their respective actuator efforts in figure 5.30.

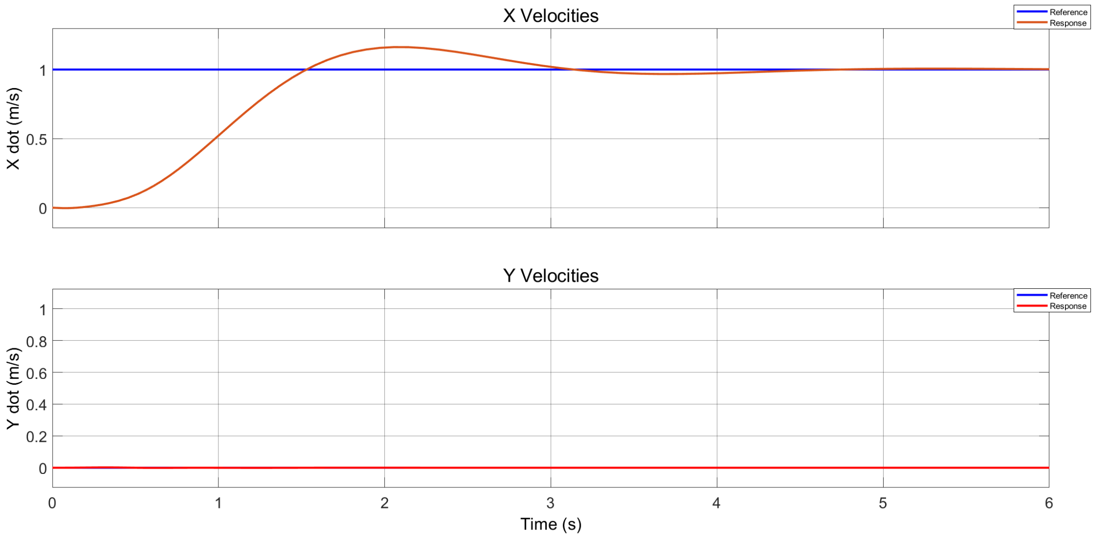

Figure 5.29 Simultaneously applied x and y velocity step inputs and the responses.

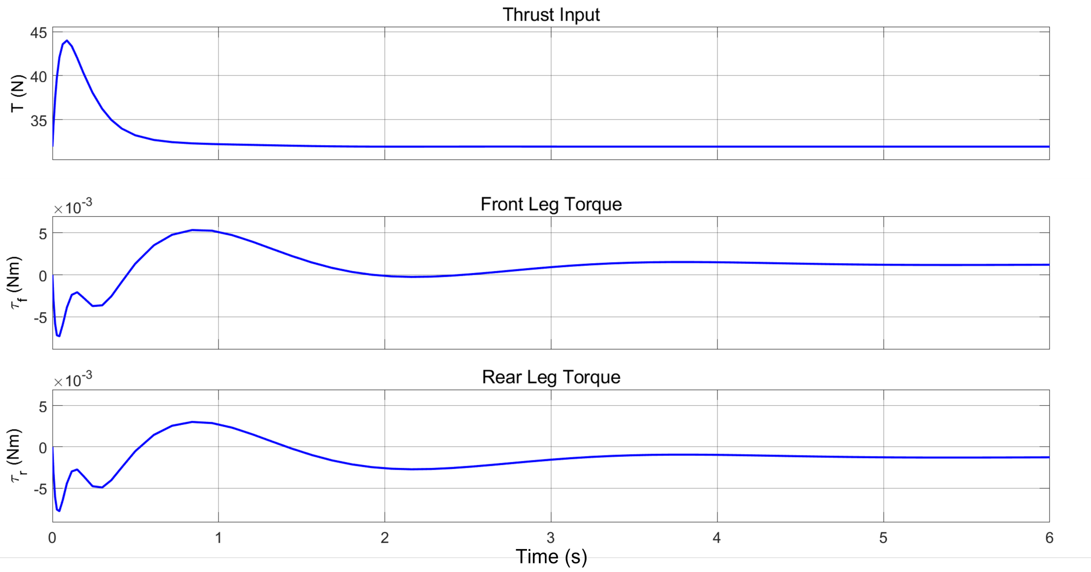

Figure 5.30 Actuator efforts for simultaneously applied x and y velocity step inputs.

Actuator efforts are typical for such a model. To be in detail, [20] shows that the thrust-to-weight ratios of 2-5 are acceptable for drone models while [21] considers much higher thrust-to-weight ratios. Although our robot model is not a drone, drones are good references for such a flying robot. Even for a design with a thrust-to-weight ratio of 1.5, the robot actuator efforts are satisfactory.

The robot motion for step reference position tracking is given in figure 5.31.

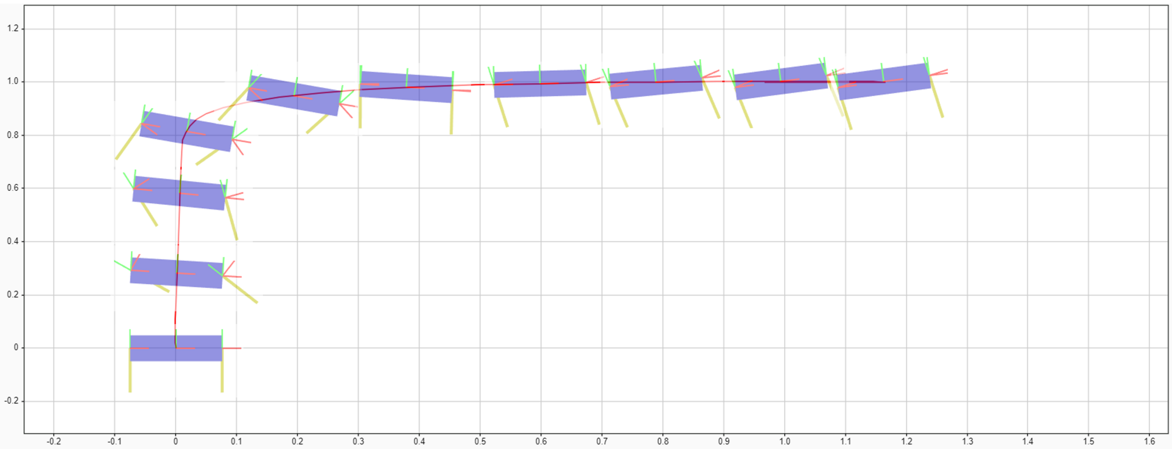

Figure 5.31 Robot motion in the x-y plane with respect to unit step inputs for positions.

The robot response in the y direction is much faster than that in the x direction. So in figure 5.31, the robot can be seen as starting to move in the y direction first and a while later a motion in the x direction follows. Response to the velocity inputs applied at $t = 0$ in both x and y directions are given in figure 5.32. The robot again starts to move in the y direction first but the velocities are got equal in close.

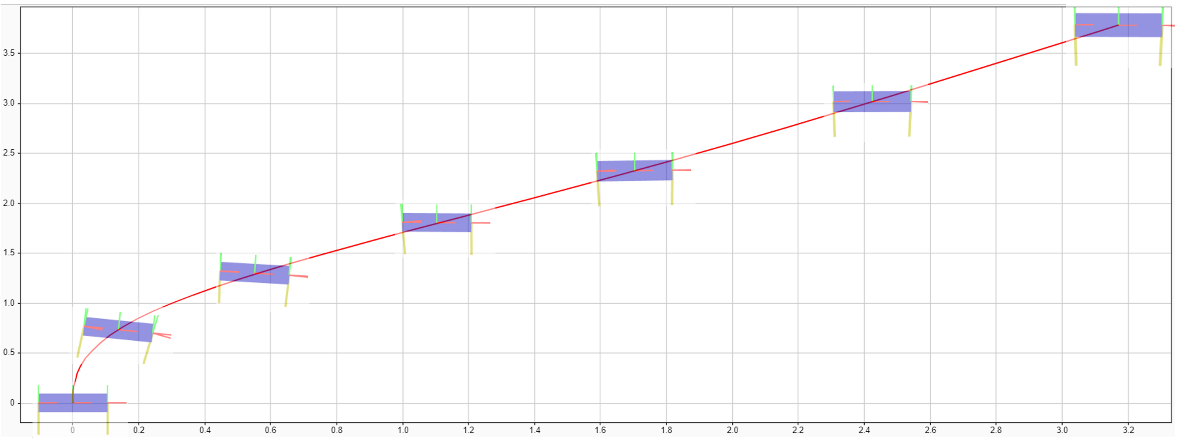

Figure 5.32 Robot motion in the x-y plane with respect to a unit step input for velocities.

Since the temporary flight is expected for the robot, the motions are acceptable and the controller is found to be satisfactory.

5.7. Conclusion

In this section, EOMs obtained by different methods are validated with basic inputs, and the flight simulator is created with the multibody dynamics software Simscape. The controller obtained in the section 4.8.1. is implemented to the flight controller, and performance metrics are discussed. The results are given in the plots, and transient behavior requirements are satisfied. Actuator efforts are compared with thrust-to-weight ratios for similar flying vehicles and found as quite providable for velocity commands which are expected user commands in real scenarios.

6. CONCLUSION

6.1. Conclusion

In this thesis, a novel control method for flying-legged robots is introduced, and A RHex robot with a fixed thruster is modeled in 2D flight and is controlled by the reaction torques of the leg motors.

A RHex robot that typically uses its legs for terrestrial locomotion was chosen as a hybrid platform candidate for temporary aerial movement by utilizing a thruster and reaction torques of its legs. The 2D dynamic model was obtained, and a flight simulator was created with a multibody dynamics software. The flight simulator was used to validate the dynamic model. The model is linearized, and the linear model is compared with the nonlinear model. A linear state feedback regulator was designed and discussed its disturbance rejection capability and initial state regulating capability. The regulator was also used to develop a servo controller, and reference tracking capability was investigated. The designed controller was also implemented in the flight simulator, and controller performance was examined. A settling time of 3 s and a maximum overshoot of 0.2 was satisfied as desired.

The main contribution of this thesis is the motion control of the legged robot RHex in flight by the reaction torques and forces created by the torques applied to the legs in the leg joints. Although there are many studies conducting flight control of legged robots, the flight control of the RHex robot is a novel subject.

6.2. Future Works

In this thesis, a novel control method for flying-legged robots was presented. A 2D simplified model of the robot was used, and a linear controller was implemented to control the robot's motion in 2D.

- First of all future plans is to create a 3D model and control the robot in 3D flight. A nonlinear controller design and implementation are also in consideration.
- In the thesis, a continuous control methodology was applied. However effect of the calculation delays can cause many problems. Thus, discrete control will also be investigated in the 3D model control.
- All states were assumed as measurable, and the controller was designed on this assumption, while it may not be the case, so a state estimator will also be added and implied to the 3D model.
- Some of the measured states will not be sensed quite accurately; a sensor fusion algorithm should also be applied before the prototype. And at last, a prototype is also planned to construct.

REFERENCES

[1] Naoji Shiroma, Yu-huan Chiu, Zi Min, Ichiro Kawabuchi, and Fumitoshi Matsuno. Development and control of a high maneuverability wheeled robot with variable-structure functionality. In *2006 IEEE/RSJ International Conference on Intelligent Robots and Systems*, pages 4000–4005. IEEE, **2006**.

[2] Jihoon Kim, Jongwon Kim, and Donghun Lee. Mobile robot with passively articulated driving tracks for high terrainability and maneuverability on unstructured rough terrain: Design, analysis, and performance evaluation. *Journal of Mechanical Science and Technology*, 32(11):5389–5400, **2018**.

[3] Rahul Shah, Selahattin Ozcelik, and Rajab Challoo. Design of a highly maneuverable mobile robot. *Procedia Computer Science*, 12:170–175, **2012**.

[4] A Kilin, P Bozek, Yury Karavaev, A Klekovkin, and V Shestakov. Experimental investigations of a highly maneuverable mobile omniwheel robot. *International Journal of Advanced Robotic Systems*, 14(6):1729881417744570, **2017**.

[5] Uluc Saranli, Martin Buehler, and Daniel E Koditschek. Rhex: A simple and highly mobile hexapod robot. *The International Journal of Robotics Research*, 20(7):616–631, **2001**.

[6] D Campbell and Martin Buehler. Stair descent in the simple hexapod'rhex'. In *2003 IEEE International Conference on Robotics and Automation (Cat. No. 03CH37422)*, volume 1, pages 1380–1385. IEEE, **2003**.

[7] EZ Moore, D Campbell, Felix Grimminger, and Martin Buehler. Reliable stair climbing in the simple hexapod'rhex'. In *Proceedings 2002 IEEE International Conference on Robotics and Automation (Cat. No. 02CH37292)*, volume 3, pages 2222–2227. IEEE, **2002**.

[8] Alex Kossett, Jesse Purvey, and Nikolaos Papanikolopoulos. More than meets the eye: A hybrid-locomotion robot with rotary flight and wheel modes. In *2009*

IEEE/RSJ International Conference on Intelligent Robots and Systems, pages 5653–5658. IEEE, **2009**.

[9] Alex Kossett, Ruben D'Sa, Jesse Purvey, and Nikolaos Papanikolopoulos. Design of an improved land/air miniature robot. In *2010 IEEE International Conference on Robotics and Automation*, pages 632–637. IEEE, **2010**.

[10] Kevin Peterson and Ronald S Fearing. Experimental dynamics of wing assisted running for a bipedal ornithopter. In *2011 IEEE/RSJ International Conference on Intelligent Robots and Systems*, pages 5080–5086. IEEE, **2011**.

[11] Koji Kawasaki, Moju Zhao, Kei Okada, and Masayuki Inaba. Muwa: Multi-field universal wheel for air-land vehicle with quad variable-pitch propellers. In *2013 IEEE/RSJ International Conference on Intelligent Robots and Systems*, pages 1880–1885. IEEE, **2013**.

[12] Daniele Pucci, Silvio Traversaro, and Francesco Nori. Momentum control of an underactuated flying humanoid robot. *IEEE Robotics and Automation Letters*, 3(1):195–202, **2017**.

[13] Yuhang Li, Yuhao Zhou, Junbin Huang, Zijun Wang, Shunjie Zhu, Kairong Wu, Li Zheng, Jiajin Luo, Rui Cao, Yun Zhang, et al. Design of a flying humanoid robot based on thrust vector control. *arXiv preprint arXiv:2108.11557*, **2021**.

[14] Pravin Dangol, Eric Sihite, and Alireza Ramezani. Control of thruster-assisted, bipedal legged locomotion of the harpy robot. *Frontiers in Robotics and AI*, 8, **2021**.

[15] Kyunam Kim, Patrick Spieler, Elena-Sorina Lupu, Alireza Ramezani, and Soon-Jo Chung. A bipedal walking robot that can fly, slackline, and skateboard. *Science Robotics*, 6(59):eabf8136, **2021**.

[16] Avishai Weiss, Ilya Kolmanovsky, Dennis S Bernstein, and Amit Sanyal. Inertia-free spacecraft attitude control using reaction wheels. *Journal of Guidance, Control, and Dynamics*, 36(5):1425–1439, **2013**.

[17] Narottama Esser. Spacecraft attitude control using variable inertia reaction wheels. **2021**.

[18] Katsuhiko Ogata et al. *Modern control engineering*, volume 5. Prentice hall Upper Saddle River, NJ, **2010**.

[19] Jorge Angeles. *Rational kinematics*, volume 34. Springer Science & Business Media, **2013**.

[20] VM Arellano-Quintana, EA Portilla-Flores, EA Merchan-Cruz, and PA Nino-Suarez. Multirotor design optimization using a genetic algorithm. In *2016 International Conference on Unmanned Aircraft Systems (ICUAS)*, pages 1313–1318. IEEE, **2016**.

[21] Tony Oliver Mogorosi, Rodrigo S Jamisola, N Subaschandar, and Lucky Odirile Mohutsiwa. Thrust-to-weight ratio optimization for multi-rotor drones using neural network with six input parameters. In *2021 International Conference on Unmanned Aircraft Systems (ICUAS)*, pages 1194–1199. IEEE, **2021**.

7. Appendix

7.1. Appendix A

$$\begin{aligned}
0 =\ & \mathrm{L_f}\,\mathrm{M_l}\,\ddot{\theta}\,\sin(\theta) - 2\,\mathrm{M_l}\,\ddot{x} - T\,\sin(\theta) - \mathrm{M_b}\,\ddot{x} - \mathrm{L_r}\,\mathrm{M_l}\,\ddot{\theta}\,\sin(\theta)\\
& + \mathrm{L_f}\,\mathrm{M_l}\,\dot{\theta}^2\,\cos(\theta) - \mathrm{L_r}\,\mathrm{M_l}\,\dot{\theta}^2\,\cos(\theta) + \mathrm{M_l}\,R\,\ddot{\theta}\,\cos(\theta)\,\sin(\theta_f)\\
& + \mathrm{M_l}\,R\,\ddot{\theta}\,\cos(\theta_f)\,\sin(\theta) + \mathrm{M_l}\,R\,\ddot{\theta}\,\cos(\theta)\,\sin(\theta_r) + \mathrm{M_l}\,R\,\ddot{\theta}\,\cos(\theta_r)\,\sin(\theta)\\
& + \mathrm{M_l}\,R\,\ddot{\theta}_f\,\cos(\theta)\,\sin(\theta_f) + \mathrm{M_l}\,R\,\ddot{\theta}_f\,\cos(\theta_f)\,\sin(\theta) + \mathrm{M_l}\,R\,\ddot{\theta}_r\,\cos(\theta)\,\sin(\theta_r)\\
& + \mathrm{M_l}\,R\,\ddot{\theta}_r\,\cos(\theta_r)\,\sin(\theta) + \mathrm{M_l}\,R\,\dot{\theta}^2\,\cos(\theta)\,\cos(\theta_f) + \mathrm{M_l}\,R\,\dot{\theta}^2\,\cos(\theta)\,\cos(\theta_r)\\
& + \mathrm{M_l}\,R\,\dot{\theta}_f^2\,\cos(\theta)\,\cos(\theta_f) + \mathrm{M_l}\,R\,\dot{\theta}_r^2\,\cos(\theta)\,\cos(\theta_r)\\
& - \mathrm{M_l}\,R\,\dot{\theta}^2\,\sin(\theta)\,\sin(\theta_f) - \mathrm{M_l}\,R\,\dot{\theta}^2\,\sin(\theta)\,\sin(\theta_r) - \mathrm{M_l}\,R\,\dot{\theta}_f^2\,\sin(\theta)\,\sin(\theta_f)\\
& - \mathrm{M_l}\,R\,\dot{\theta}_r^2\,\sin(\theta)\,\sin(\theta_r) + 2\,\mathrm{M_l}\,R\,\dot{\theta}\,\dot{\theta}_f\,\cos(\theta)\,\cos(\theta_f)\\
& + 2\,\mathrm{M_l}\,R\,\dot{\theta}\,\dot{\theta}_r\,\cos(\theta)\,\cos(\theta_r) - 2\,\mathrm{M_l}\,R\,\dot{\theta}\,\dot{\theta}_f\,\sin(\theta)\,\sin(\theta_f)\\
& - 2\,\mathrm{M_l}\,R\,\dot{\theta}\,\dot{\theta}_r\,\sin(\theta)\,\sin(\theta_r)
\end{aligned} \tag{125}$$

$$\begin{aligned}
0 =\ & T\,\cos(\theta) - \mathrm{M_b}\,\ddot{y} - 2\,g\,\mathrm{M_l} - 2\,\mathrm{M_l}\,\ddot{y} - \mathrm{M_b}\,g - \mathrm{L_f}\,\mathrm{M_l}\,\ddot{\theta}\,\cos(\theta)\\
& + \mathrm{L_r}\,\mathrm{M_l}\,\ddot{\theta}\,\cos(\theta) + \mathrm{L_f}\,\mathrm{M_l}\,\dot{\theta}^2\,\sin(\theta) - \mathrm{L_r}\,\mathrm{M_l}\,\dot{\theta}^2\,\sin(\theta)\\
& - \mathrm{M_l}\,R\,\ddot{\theta}\,\cos(\theta)\,\cos(\theta_f) - \mathrm{M_l}\,R\,\ddot{\theta}\,\cos(\theta)\,\cos(\theta_r) - \mathrm{M_l}\,R\,\ddot{\theta}_f\,\cos(\theta)\,\cos(\theta_f)\\
& - \mathrm{M_l}\,R\,\ddot{\theta}_r\,\cos(\theta)\,\cos(\theta_r) + \mathrm{M_l}\,R\,\ddot{\theta}\,\sin(\theta)\,\sin(\theta_f)\\
& + \mathrm{M_l}\,R\,\ddot{\theta}\,\sin(\theta)\,\sin(\theta_r) + \mathrm{M_l}\,R\,\ddot{\theta}_f\,\sin(\theta)\,\sin(\theta_f) + \mathrm{M_l}\,R\,\ddot{\theta}_r\,\sin(\theta)\,\sin(\theta_r)\\
& + \mathrm{M_l}\,R\,\dot{\theta}^2\,\cos(\theta)\,\sin(\theta_f) + \mathrm{M_l}\,R\,\dot{\theta}^2\,\cos(\theta_f)\,\sin(\theta) + \mathrm{M_l}\,R\,\dot{\theta}^2\,\cos(\theta)\,\sin(\theta_r)\\
& + \mathrm{M_l}\,R\,\dot{\theta}^2\,\cos(\theta_r)\,\sin(\theta) + \mathrm{M_l}\,R\,\dot{\theta}_f^2\,\cos(\theta)\,\sin(\theta_f) + \mathrm{M_l}\,R\,\dot{\theta}_f^2\,\cos(\theta_f)\,\sin(\theta)\\
& + \mathrm{M_l}\,R\,\dot{\theta}_r^2\,\cos(\theta)\,\sin(\theta_r) + \mathrm{M_l}\,R\,\dot{\theta}_r^2\,\cos(\theta_r)\,\sin(\theta)\\
& + 2\,\mathrm{M_l}\,R\,\dot{\theta}\,\dot{\theta}_f\,\cos(\theta)\,\sin(\theta_f) + 2\,\mathrm{M_l}\,R\,\dot{\theta}\,\dot{\theta}_f\,\cos(\theta_f)\,\sin(\theta)\\
& + 2\,\mathrm{M_l}\,R\,\dot{\theta}\,\dot{\theta}_r\,\cos(\theta)\,\sin(\theta_r) + 2\,\mathrm{M_l}\,R\,\dot{\theta}\,\dot{\theta}_r\,\cos(\theta_r)\,\sin(\theta)
\end{aligned} \tag{126}$$

$$
\begin{aligned}
0 = {} & \mathrm{T_f} + \mathrm{T_r} - \mathrm{I_b}\,\ddot{\theta} - {\mathrm{L_f}}^2\,\mathrm{M_l}\,\ddot{\theta}\cos(\theta)^2 - {\mathrm{L_r}}^2\,\mathrm{M_l}\,\ddot{\theta}\cos(\theta)^2 \\
& - {\mathrm{L_f}}^2\,\mathrm{M_l}\,\ddot{\theta}\sin(\theta)^2 - {\mathrm{L_r}}^2\,\mathrm{M_l}\,\ddot{\theta}\sin(\theta)^2 - \mathrm{L_f}\,g\,\mathrm{M_l}\,\cos(\theta) \\
& + \mathrm{L_r}\,g\,\mathrm{M_l}\,\cos(\theta) - \mathrm{L_f}\,\mathrm{M_l}\,\ddot{y}\,\cos(\theta) + \mathrm{L_r}\,\mathrm{M_l}\,\ddot{y}\,\cos(\theta) + \mathrm{L_f}\,\mathrm{M_l}\,\ddot{x}\,\sin(\theta) \\
& - \mathrm{L_r}\,\mathrm{M_l}\,\ddot{x}\,\sin(\theta) - \mathrm{L_f}\,\mathrm{M_l}\,R\,\ddot{\theta}\cos(\theta)^2\,\cos\left(\theta_f\right) - \mathrm{L_f}\,\mathrm{M_l}\,R\,\ddot{\theta}_f\cos(\theta)^2\,\cos\left(\theta_f\right) \\
& + \mathrm{L_r}\,\mathrm{M_l}\,R\,\ddot{\theta}\cos(\theta)^2\,\cos(\theta_r) + \mathrm{L_r}\,\mathrm{M_l}\,R\,\ddot{\theta}_r\cos(\theta)^2\,\cos(\theta_r) \\
& - \mathrm{L_f}\,\mathrm{M_l}\,R\,\ddot{\theta}\,\cos\left(\theta_f\right)\,\sin(\theta)^2 - \mathrm{L_f}\,\mathrm{M_l}\,R\,\ddot{\theta}_f\,\cos\left(\theta_f\right)\,\sin(\theta)^2 \\
& + \mathrm{L_r}\,\mathrm{M_l}\,R\,\ddot{\theta}\,\cos(\theta_r)\,\sin(\theta)^2 + \mathrm{L_r}\,\mathrm{M_l}\,R\,\ddot{\theta}_r\,\cos(\theta_r)\,\sin(\theta)^2 \\
& + \mathrm{L_f}\,\mathrm{M_l}\,R\,\dot{\theta}^2\cos(\theta)^2\,\sin\left(\theta_f\right) + \mathrm{L_f}\,\mathrm{M_l}\,R\,\dot{\theta}_f^2\cos(\theta)^2\,\sin\left(\theta_f\right) \\
& - \mathrm{L_r}\,\mathrm{M_l}\,R\,\dot{\theta}^2\cos(\theta)^2\,\sin(\theta_r) - \mathrm{L_r}\,\mathrm{M_l}\,R\,\dot{\theta}_r^2\cos(\theta)^2\,\sin(\theta_r) \\
& + \mathrm{L_f}\,\mathrm{M_l}\,R\,\dot{\theta}^2\sin(\theta)^2\,\sin\left(\theta_f\right) + \mathrm{L_f}\,\mathrm{M_l}\,R\,\dot{\theta}_f^2\sin(\theta)^2\,\sin\left(\theta_f\right) \\
& - \mathrm{L_r}\,\mathrm{M_l}\,R\,\dot{\theta}^2\sin(\theta)^2\,\sin(\theta_r) - \mathrm{L_r}\,\mathrm{M_l}\,R\,\dot{\theta}_r^2\sin(\theta)^2\,\sin(\theta_r) \\
& + 2\,\mathrm{L_f}\,\mathrm{M_l}\,R\,\dot{\theta}\,\dot{\theta}_f\cos(\theta)^2\,\sin\left(\theta_f\right) - 2\,\mathrm{L_r}\,\mathrm{M_l}\,R\,\dot{\theta}\,\dot{\theta}_r\cos(\theta)^2\,\sin(\theta_r) \\
& + 2\,\mathrm{L_f}\,\mathrm{M_l}\,R\,\dot{\theta}\,\dot{\theta}_f\sin(\theta)^2\,\sin\left(\theta_f\right) - 2\,\mathrm{L_r}\,\mathrm{M_l}\,R\,\dot{\theta}\,\dot{\theta}_r\sin(\theta)^2\,\sin(\theta_r)
\end{aligned}
\tag{127}
$$

$$
\begin{aligned}
0 = {} & g\,\mathrm{M_l}\,R\,\sin(\theta)\,\sin\left(\theta_f\right) - \mathrm{Il}\,\ddot{\theta} - \mathrm{Il}\,\ddot{\theta}_f - g\,\mathrm{M_l}\,R\,\cos(\theta)\,\cos\left(\theta_f\right) \\
& - \mathrm{M_l}\,R\,\ddot{y}\,\cos(\theta)\,\cos\left(\theta_f\right) - \mathrm{T_f} + \mathrm{M_l}\,R\,\ddot{x}\,\cos(\theta)\,\sin\left(\theta_f\right) + \mathrm{M_l}\,R\,\ddot{x}\,\cos\left(\theta_f\right)\,\sin(\theta) \\
& - \mathrm{M_l}\,R^2\,\ddot{\theta}\cos(\theta)^2\cos\left(\theta_f\right)^2 - \mathrm{M_l}\,R^2\,\ddot{\theta}_f\cos(\theta)^2\cos\left(\theta_f\right)^2 \\
& + \mathrm{M_l}\,R\,\ddot{y}\,\sin(\theta)\,\sin\left(\theta_f\right) - \mathrm{M_l}\,R^2\,\ddot{\theta}\cos(\theta)^2\sin\left(\theta_f\right)^2 - \mathrm{M_l}\,R^2\,\ddot{\theta}\cos\left(\theta_f\right)^2\sin(\theta)^2 \\
& - \mathrm{M_l}\,R^2\,\ddot{\theta}_f\cos(\theta)^2\sin\left(\theta_f\right)^2 - \mathrm{M_l}\,R^2\,\ddot{\theta}_f\cos\left(\theta_f\right)^2\sin(\theta)^2 - \mathrm{M_l}\,R^2\,\ddot{\theta}\sin(\theta)^2\sin\left(\theta_f\right)^2 \\
& - \mathrm{M_l}\,R^2\,\ddot{\theta}_f\sin(\theta)^2\sin\left(\theta_f\right)^2 - \mathrm{L_f}\,\mathrm{M_l}\,R\,\ddot{\theta}\cos(\theta)^2\,\cos\left(\theta_f\right) - \mathrm{L_f}\,\mathrm{M_l}\,R\,\ddot{\theta}\,\cos\left(\theta_f\right)\,\sin(\theta)^2 \\
& - \mathrm{L_f}\,\mathrm{M_l}\,R\,\dot{\theta}^2\cos(\theta)^2\,\sin\left(\theta_f\right) - \mathrm{L_f}\,\mathrm{M_l}\,R\,\dot{\theta}^2\sin(\theta)^2\,\sin\left(\theta_f\right)
\end{aligned}
\tag{128}
$$

$$
\begin{aligned}
0 = {} & g\,\mathrm{M_l}\,R\,\sin(\theta)\,\sin(\theta_r) - \mathrm{Il}\,\ddot{\theta} - \mathrm{Il}\,\ddot{\theta}_r - g\,\mathrm{M_l}\,R\,\cos(\theta)\,\cos(\theta_r) \\
& - \mathrm{M_l}\,R\,\ddot{y}\,\cos(\theta)\,\cos(\theta_r) - \mathrm{T_r} + \mathrm{M_l}\,R\,\ddot{x}\,\cos(\theta)\,\sin(\theta_r) + \mathrm{M_l}\,R\,\ddot{x}\,\cos(\theta_r)\,\sin(\theta) \\
& - \mathrm{M_l}\,R^2\,\ddot{\theta}\cos(\theta)^2\cos(\theta_r)^2 - \mathrm{M_l}\,R^2\,\ddot{\theta}_r\cos(\theta)^2\cos(\theta_r)^2 \\
& + \mathrm{M_l}\,R\,\ddot{y}\,\sin(\theta)\,\sin(\theta_r) - \mathrm{M_l}\,R^2\,\ddot{\theta}\cos(\theta)^2\sin(\theta_r)^2 \\
& - \mathrm{M_l}\,R^2\,\ddot{\theta}\cos(\theta_r)^2\sin(\theta)^2 - \mathrm{M_l}\,R^2\,\ddot{\theta}_r\cos(\theta)^2\sin(\theta_r)^2 \\
& - \mathrm{M_l}\,R^2\,\ddot{\theta}_r\cos(\theta_r)^2\sin(\theta)^2 - \mathrm{M_l}\,R^2\,\ddot{\theta}\sin(\theta)^2\sin(\theta_r)^2 \\
& - \mathrm{M_l}\,R^2\,\ddot{\theta}_r\sin(\theta)^2\sin(\theta_r)^2 + \mathrm{L_r}\,\mathrm{M_l}\,R\,\ddot{\theta}\cos(\theta)^2\,\cos(\theta_r) \\
& + \mathrm{L_r}\,\mathrm{M_l}\,R\,\ddot{\theta}\,\cos(\theta_r)\,\sin(\theta)^2 + \mathrm{L_r}\,\mathrm{M_l}\,R\,\dot{\theta}^2\cos(\theta)^2\,\sin(\theta_r) \\
& + \mathrm{L_r}\,\mathrm{M_l}\,R\,\dot{\theta}^2\sin(\theta)^2\,\sin(\theta_r)
\end{aligned} \tag{129}
$$

7.2. Appendix B

$$
\begin{aligned}
0 \;&= M_b g + M_b \ddot{y} \\
&+2gM_l + 2M_l\ddot{y} - T\cos(\theta) + L_f M_l \ddot{\theta}\cos(\theta) - L_r M_l \ddot{\theta}\cos(\theta) - L_f M_l \dot{\theta}^2 \sin(\theta) \\
&+L_r M_l \dot{\theta}^2 \sin(\theta) + M_l R\ddot{\theta}\cos(\theta)\cos\left(\theta_f\right) + M_l R\ddot{\theta}\cos(\theta)\cos\left(\theta_r\right) \\
&+M_l R\ddot{\theta}_f \cos(\theta)\cos\left(\theta_f\right) + M_l R\ddot{\theta}_R \cos(\theta)\cos\left(\theta_r\right) - M_l R\ddot{\theta}\sin(\theta)\sin\left(\theta_f\right) \\
&-M_l R\ddot{\theta}\sin(\theta)\sin\left(\theta_r\right) - M_l R\ddot{\theta}_f \sin(\theta)\sin\left(\theta_f\right) - M_l R\ddot{\theta}_R \sin(\theta)\sin\left(\theta_r\right) \\
&-M_l R\dot{\theta}^2 \cos(\theta)\sin\left(\theta_f\right) - M_l R\dot{\theta}^2 \cos\left(\theta_f\right)\sin(\theta) - M_l R\dot{\theta}^2 \cos(\theta)\sin\left(\theta_r\right) \\
&-M_l R\dot{\theta}^2 \cos\left(\theta_r\right)\sin(\theta) - M_l R\dot{\theta}_f^2 \cos(\theta)\sin\left(\theta_f\right) - M_l R\dot{\theta}_f^2 \cos\left(\theta_f\right)\sin(\theta) \\
&-M_l R\dot{\theta}_R^2 \cos(\theta)\sin\left(\theta_r\right) - M_l R\dot{\theta}_R^2 \cos\left(\theta_r\right)\sin(\theta) - 2M_l R\dot{\theta}\dot{\theta}_f \cos(\theta)\sin\left(\theta_f\right) \\
&-2M_l R\dot{\theta}\dot{\theta}_f \cos\left(\theta_f\right)\sin(\theta) - 2M_l R\dot{\theta}\dot{\theta}_R \cos(\theta)\sin\left(\theta_r\right) - 2M_l R\dot{\theta}_{\dot{\theta}}\dot{\theta}_R \cos\left(\theta_r\right)\sin(\theta)
\end{aligned}
\tag{130}
$$

$$
\begin{aligned}
0 = {} & M_b\ddot{x} + 2M_l\ddot{x} + T\sin(\theta) \\
& - L_f M_l \ddot{\theta}\sin(\theta) + L_r M_l \ddot{\theta}\sin(\theta) - L_f M_l \dot{\theta}^2 \cos(\theta) + L_r M_l \dot{\theta}^2 \cos(\theta) \\
& - M_l R\ddot{\theta}\cos(\theta)\sin\left(\theta_f\right) - M_l R\ddot{\theta}\cos\left(\theta_f\right)\sin(\theta) - M_l R\ddot{\theta}\cos(\theta)\sin\left(\theta_r\right) \\
& - M_l R\ddot{\theta}\cos\left(\theta_r\right)\sin(\theta) - M_l R\ddot{\theta}_f \cos(\theta)\sin\left(\theta_f\right) - M_l R\ddot{\theta}_f \cos\left(\theta_f\right)\sin(\theta) \\
& - M_l R\ddot{\theta}_R \cos(\theta)\sin\left(\theta_r\right) - M_l R\ddot{\theta}_R \cos\left(\theta_r\right)\sin(\theta) - M_l R\dot{\theta}^2 \cos(\theta)\cos\left(\theta_f\right) \\
& - M_l R\dot{\theta}^2 \cos(\theta)\cos\left(\theta_r\right) - M_l R\dot{\theta}_f^2 \cos(\theta)\cos\left(\theta_f\right) - M_l R\dot{\theta}_R^2 \cos(\theta)\cos\left(\theta_r\right) \\
& + M_l R\dot{\theta}^2 \sin(\theta)\sin\left(\theta_f\right) + M_l R\dot{\theta}^2 \sin(\theta)\sin\left(\theta_r\right) + M_l R\dot{\theta}_f^2 \sin(\theta)\sin\left(\theta_f\right) \\
& + M_l R\dot{\theta}_R^2 \sin(\theta)\sin\left(\theta_r\right) - 2M_l R\dot{\theta}\dot{\theta}_f \cos(\theta)\cos\left(\theta_f\right) - 2M_l R\dot{\theta}\dot{\theta}_R \cos(\theta)\cos\left(\theta_r\right) \\
& + 2M_l R\dot{\theta}\dot{\theta}_f \sin(\theta)\sin\left(\theta_f\right) + 2M_l R\dot{\theta}\dot{\theta}_R \sin(\theta)\sin\left(\theta_r\right)
\end{aligned}
\tag{131}
$$

$$
\begin{aligned}
0 &= I_b\ddot{\theta} + 2I_l\ddot{\theta} + I_l\ddot{\theta}_f + I_l\ddot{\theta}_R + L_f^2 M_l\ddot{\theta}\cos^2(\theta) + L_r^2 M_l\ddot{\theta}\cos^2(\theta) + L_f^2 M_l\ddot{\theta}\sin^2(\theta) \\
&+ L_r^2 M_l\ddot{\theta}\sin^2(\theta) + L_f g M_l\cos(\theta) - L_r g M_l\cos(\theta) + L_f M_l\ddot{y}\cos(\theta) \\
&- L_r M_l\ddot{y}\cos(\theta) - L_f M_l\ddot{x}\sin(\theta) + L_r M_l\ddot{x}\sin(\theta) \\
&+ gM_lR\cos(\theta)\cos\left(\theta_f\right) + gM_lR\cos(\theta)\cos\left(\theta_r\right) + M_lR\ddot{y}\cos(\theta)\cos\left(\theta_f\right) \\
&+ M_lR\ddot{y}\cos(\theta)\cos\left(\theta_r\right) - gM_lR\sin(\theta)\sin\left(\theta_f\right) - gM_lR\sin(\theta)\sin\left(\theta_r\right) \\
&- M_lR\ddot{x}\cos(\theta)\sin\left(\theta_f\right) - M_lR\ddot{x}\cos\left(\theta_f\right)\sin(\theta) - M_lR\ddot{x}\cos(\theta)\sin\left(\theta_r\right) \\
&- M_lR\ddot{x}\cos\left(\theta_r\right)\sin(\theta) + M_lR^2\ddot{\theta}\cos^2(\theta)\cos^2\left(\theta_f\right) + M_lR^2\ddot{\theta}\cos^2(\theta)\cos^2\left(\theta_r\right) \\
&+ M_lR^2\ddot{\theta}_f\cos^2(\theta)\cos^2\left(\theta_f\right) + M_lR^2\ddot{\theta}_R\cos^2(\theta)\cos^2\left(\theta_r\right) - M_lR\ddot{y}\sin(\theta)\sin\left(\theta_f\right) \\
&- M_lR\ddot{y}\sin(\theta)\sin\left(\theta_r\right) + M_lR^2\ddot{\theta}\cos^2(\theta)\sin^2\left(\theta_f\right) + M_lR^2\ddot{\theta}\cos^2\left(\theta_f\right)\sin^2(\theta) \\
&+ M_lR^2\ddot{\theta}\cos^2(\theta)\sin^2\left(\theta_r\right) + M_lR^2\ddot{\theta}\cos^2\left(\theta_r\right)\sin^2(\theta) + M_lR^2\ddot{\theta}_f\cos^2(\theta)\sin^2\left(\theta_f\right) \\
&+ M_lR^2\ddot{\theta}_f\cos^2\left(\theta_f\right)\sin^2(\theta) + M_lR^2\ddot{\theta}_R\cos^2(\theta)\sin^2\left(\theta_r\right) + M_lR^2\ddot{\theta}_R\cos^2\left(\theta_r\right)\sin^2(\theta) \\
&+ M_lR^2\ddot{\theta}\sin^2(\theta)\sin^2\left(\theta_f\right) + M_lR^2\ddot{\theta}\sin^2(\theta)\sin^2\left(\theta_r\right) + M_lR^2\ddot{\theta}_f\sin^2(\theta)\sin^2\left(\theta_f\right) \\
&+ M_lR^2\ddot{\theta}_R\sin^2(\theta)\sin^2\left(\theta_r\right) + 2L_fM_lR\ddot{\theta}\cos^2(\theta)\cos\left(\theta_f\right) + L_fM_lR\ddot{\theta}_f\cos^2(\theta)\cos\left(\theta_f\right) \\
&- 2L_rM_lR\ddot{\theta}\cos^2(\theta)\cos\left(\theta_r\right) - L_rM_lR\ddot{\theta}_R\cos^2(\theta)\cos\left(\theta_r\right) + 2L_fM_lR\ddot{\theta}\cos\left(\theta_f\right)\sin^2(\theta) \\
&+ L_fM_lR\ddot{\theta}_f\cos\left(\theta_f\right)\sin^2(\theta) - 2L_rM_lR\ddot{\theta}\cos\left(\theta_r\right)\sin^2(\theta) - L_rM_lR\ddot{\theta}_R\cos\left(\theta_r\right)\sin^2(\theta) \\
&- L_fM_lR\dot{\theta}_f^2\cos^2(\theta)\sin\left(\theta_f\right) + L_rM_lR\dot{\theta}_R^2\cos^2(\theta)\sin\left(\theta_r\right) - L_fM_lR\dot{\theta}_f^2\sin^2(\theta)\sin\left(\theta_f\right) \\
&+ L_rM_lR\dot{\theta}_R^2\sin^2(\theta)\sin\left(\theta_r\right) - 2L_fM_lR\dot{\theta}\dot{\theta}_f\cos^2(\theta)\sin\left(\theta_f\right) \\
&+ 2L_rM_lR\dot{\theta}\dot{\theta}_R\cos^2(\theta)\sin\left(\theta_r\right) - 2L_fM_lR\dot{\theta}\dot{\theta}_f\sin^2(\theta)\sin\left(\theta_f\right) \\
&+ 2L_rM_lR\dot{\theta}\dot{\theta}_R\sin^2(\theta)\sin\left(\theta_r\right)
\end{aligned}
\tag{132}
$$

$$
\begin{aligned}
0 &= T_f + I_l\ddot{\theta} + I_l\ddot{\theta}_f \\
&+ gM_lR\cos(\theta)\cos\left(\theta_f\right) + M_lR\ddot{y}\cos(\theta)\cos\left(\theta_f\right) - gM_lR\sin(\theta)\sin\left(\theta_f\right) \\
&- M_lR\ddot{x}\cos(\theta)\sin\left(\theta_f\right) - M_lR\ddot{x}\cos\left(\theta_f\right)\sin(\theta) + M_lR^2\ddot{\theta}\cos^2(\theta)\cos^2\left(\theta_f\right) \\
&+ M_lR^2\ddot{\theta}_f\cos^2(\theta)\cos^2\left(\theta_f\right) - M_lR\ddot{y}\sin(\theta)\sin\left(\theta_f\right) + M_lR^2\ddot{\theta}\cos^2(\theta)\sin^2\left(\theta_f\right) \\
&+ M_lR^2\ddot{\theta}\cos^2\left(\theta_f\right)\sin^2(\theta) + M_lR^2\ddot{\theta}_f\cos^2(\theta)\sin^2\left(\theta_f\right) + M_lR^2\ddot{\theta}_f\cos^2\left(\theta_f\right)\sin^2(\theta) \\
&+ M_lR^2\ddot{\theta}\sin^2(\theta)\sin^2\left(\theta_f\right) + M_lR^2\ddot{\theta}_f\sin^2(\theta)\sin^2\left(\theta_f\right) + L_fM_lR\ddot{\theta}\cos^2(\theta)\cos\left(\theta_f\right) \\
&+ L_fM_lR\ddot{\theta}\cos\left(\theta_f\right)\sin^2(\theta) + L_fM_lR\dot{\theta}^2\cos^2(\theta)\sin\left(\theta_f\right) + L_fM_lR\dot{\theta}^2\sin^2(\theta)\sin\left(\theta_f\right)
\end{aligned} \tag{133}
$$

$$
\begin{aligned}
0 &= T_r + I_l\ddot{\theta} + I_l\ddot{\theta}_R \\
&+ gM_lR\cos(\theta)\cos\left(\theta_r\right) + M_lR\ddot{y}\cos(\theta)\cos\left(\theta_r\right) - gM_lR\sin(\theta)\sin\left(\theta_r\right) \\
&- M_lR\ddot{x}\cos(\theta)\sin\left(\theta_r\right) - M_lR\ddot{x}\cos\left(\theta_r\right)\sin(\theta) + M_lR^2\ddot{\theta}\cos^2(\theta)\cos^2\left(\theta_r\right) \\
&+ M_lR^2\ddot{\theta}_R\cos^2(\theta)\cos^2\left(\theta_r\right) - M_lR\ddot{y}\sin(\theta)\sin\left(\theta_r\right) + M_lR^2\ddot{\theta}\cos^2(\theta)\sin^2\left(\theta_r\right) \\
&+ M_lR^2\ddot{\theta}\cos^2\left(\theta_r\right)\sin^2(\theta) + M_lR^2\ddot{\theta}_R\cos^2(\theta)\sin^2\left(\theta_r\right) + M_lR^2\ddot{\theta}_R\cos^2\left(\theta_r\right)\sin^2(\theta) \\
&+ M_lR^2\ddot{\theta}\sin^2(\theta)\sin^2\left(\theta_r\right) + M_lR^2\ddot{\theta}_R\sin^2(\theta)\sin^2\left(\theta_r\right) - L_rM_lR\ddot{\theta}\cos^2(\theta)\cos\left(\theta_r\right) \\
&- L_rM_lR\ddot{\theta}\cos\left(\theta_r\right)\sin^2(\theta) - L_rM_lR\dot{\theta}^2\cos^2(\theta)\sin\left(\theta_r\right) - L_rM_lR\dot{\theta}^2\sin^2(\theta)\sin\left(\theta_r\right)
\end{aligned} \tag{134}
$$

7.3. Appendix C

The first five columns of the controllability matrix:

$$\begin{pmatrix} 0 & 0 & 0 & 0 & 3.93 \\ 0 & 0 & 0 & 0.307 & 0 \\ 0 & 0 & 0 & 0 & 51.8 \\ 0 & 0 & 0 & 0 & -4120.0 \\ 0 & 0 & 0 & 0 & -101.0 \\ 0 & 3.93 & 3.93 & 0 & 0 \\ 0.307 & 0 & 0 & 0 & 0 \\ 0 & 51.8 & 51.8 & 0 & 0 \\ 0 & -4120.0 & -101.0 & 0 & 0 \\ 0 & -101.0 & -4120.0 & 0 & 0 \end{pmatrix} \tag{135}$$

Sixth to tenth columns of the controllability matrix:

$$\begin{pmatrix} 3.93 & 0 & 0 & 0 & 0 \\ 0 & 0 & 0 & 0 & 0 \\ 51.8 & 0 & 0 & 0 & 0 \\ -101.0 & 0 & 0 & 0 & 0 \\ -4120.0 & 0 & 0 & 0 & 0 \\ 0 & 0 & -1010.0 & -1010.0 & 0 \\ 0 & 0 & 0 & 0 & 0 \\ 0 & 0 & 0 & 0 & 0 \\ 0 & 0 & 5.1e{+}5 & 1.87e{+}4 & 0 \\ 0 & 0 & 1.87e{+}4 & 5.1e{+}5 & 0 \end{pmatrix} \tag{136}$$

Eleventh to fifteenth columns of the controllability matrix:

$$\begin{pmatrix} -1010.0 & -1010.0 & 0 & 0 & 0 \\ 0 & 0 & 0 & 0 & 0 \\ 0 & 0 & 0 & 0 & 0 \\ 5.1\text{e+}5 & 1.87\text{e+}4 & 0 & 0 & 0 \\ 1.87\text{e+}4 & 5.1\text{e+}5 & 0 & 0 & 0 \\ 0 & 0 & 0 & 6.35\text{e+}4 & 6.35\text{e+}4 \\ 0 & 0 & 0 & 0 & 0 \\ 0 & 0 & 0 & 0 & 0 \\ 0 & 0 & 0 & -6.33\text{e+}7 & -3.08\text{e+}6 \\ 0 & 0 & 0 & -3.08\text{e+}6 & -6.33\text{e+}7 \end{pmatrix} \tag{137}$$

Sixteenth to twentieth columns of the controllability matrix:

$$\begin{pmatrix} 0 & 6.35\text{e+}4 & 6.35\text{e+}4 & 0 & 0 \\ 0 & 0 & 0 & 0 & 0 \\ 0 & 0 & 0 & 0 & 0 \\ 0 & -6.33\text{e+}7 & -3.08\text{e+}6 & 0 & 0 \\ 0 & -3.08\text{e+}6 & -6.33\text{e+}7 & 0 & 0 \\ 0 & 0 & 0 & 0 & -7.96\text{e+}6 \\ 0 & 0 & 0 & 0 & 0 \\ 0 & 0 & 0 & 0 & 0 \\ 0 & 0 & 0 & 0 & 7.85\text{e+}9 \\ 0 & 0 & 0 & 0 & 4.77\text{e+}8 \end{pmatrix} \tag{138}$$

Twenty-first to twenty-fifth columns of the controllability matrix:

$$\begin{pmatrix} 0 & 0 & -7.96e{+}6 & -7.96e{+}6 & 0 \\ 0 & 0 & 0 & 0 & 0 \\ 0 & 0 & 0 & 0 & 0 \\ 0 & 0 & 7.85e{+}9 & 4.77e{+}8 & 0 \\ 0 & 0 & 4.77e{+}8 & 7.85e{+}9 & 0 \\ -7.96e{+}6 & 0 & 0 & 0 & 0 \\ 0 & 0 & 0 & 0 & 0 \\ 0 & 0 & 0 & 0 & 0 \\ 4.77e{+}8 & 0 & 0 & 0 & 0 \\ 7.85e{+}9 & 0 & 0 & 0 & 0 \end{pmatrix} \tag{139}$$

Twenty-sixth to thirtieth columns of the controllability matrix:

$$\begin{pmatrix} 0 & 0 & 0 & 9.99e{+}8 & 9.99e{+}8 \\ 0 & 0 & 0 & 0 & 0 \\ 0 & 0 & 0 & 0 & 0 \\ 0 & 0 & 0 & -9.75e{+}11 & -7.09e{+}10 \\ 0 & 0 & 0 & -7.09e{+}10 & -9.75e{+}11 \\ 9.99e{+}8 & 9.99e{+}8 & 0 & 0 & 0 \\ 0 & 0 & 0 & 0 & 0 \\ 0 & 0 & 0 & 0 & 0 \\ -9.75e{+}11 & -7.09e{+}10 & 0 & 0 & 0 \\ -7.09e{+}10 & -9.75e{+}11 & 0 & 0 & 0 \end{pmatrix} \tag{140}$$

7.4. Appendix D

From x reference input to outputs in the first column and y reference input to outputs in the second column:

$$\begin{pmatrix} -\frac{4.45\,s^6}{s^8+248.0\,s^6+1.54\text{e+}4\,s^4} & \frac{7.11\text{e-}14\,s^6}{s^8+248.0\,s^6+1.54\text{e+}4\,s^4} \\ \frac{3.51\text{e-}8}{s^2} & \frac{128.0}{s^2} \\ -\frac{58.6}{s^2} & \frac{9.38\text{e-}13}{s^2} \\ 0 & 0 \\ 0 & 0 \\ -\frac{4.45\,s^6}{s^7+248.0\,s^5+1.54\text{e+}4\,s^3} & \frac{7.12\text{e-}14\,s^6}{s^7+248.0\,s^5+1.54\text{e+}4\,s^3} \\ \frac{3.51\text{e-}8}{s} & \frac{128.0}{s} \\ -\frac{58.6}{s} & \frac{9.38\text{e-}13}{s} \\ 0 & 0 \\ 0 & 0 \end{pmatrix} \tag{141}$$

From θ reference input to outputs in the first column and θ_f reference input to outputs in the second column:

$$\begin{pmatrix} \frac{18.8\,s^6}{s^8+248.0\,s^6+1.54\text{e+}4\,s^4} & -\frac{0.57\,s^6}{s^8+248.0\,s^6+1.54\text{e+}4\,s^4} \\ -\frac{1.33\text{e-}7}{s^2} & -\frac{44.2}{s^2} \\ \frac{248.0}{s^2} & -\frac{7.5}{s^2} \\ 0 & 0 \\ 0 & 0 \\ \frac{18.8\,s^6}{s^7+248.0\,s^5+1.54\text{e+}4\,s^3} & -\frac{0.57\,s^6}{s^7+248.0\,s^5+1.54\text{e+}4\,s^3} \\ -\frac{1.33\text{e-}7}{s} & -\frac{44.2}{s} \\ \frac{248.0}{s} & -\frac{7.5}{s} \\ 0 & 0 \\ 0 & 0 \end{pmatrix} \tag{142}$$

From θ_r reference input to outputs in the first column and $\dot{x}$ reference input to outputs in the second column:

$$\begin{pmatrix} -\frac{0.57\,s^6}{s^8+248.0\,s^6+1.54\text{e+4}\,s^4} & -\frac{3.7\,s^6}{s^8+248.0\,s^6+1.54\text{e+4}\,s^4} \\ \frac{44.2}{s^2} & \frac{2.71\text{e-8}}{s^2} \\ -\frac{7.5}{s^2} & -\frac{48.8}{s^2} \\ 0 & 0 \\ 0 & 0 \\ -\frac{0.57\,s^6}{s^7+248.0\,s^5+1.54\text{e+4}\,s^3} & -\frac{3.7\,s^6}{s^7+248.0\,s^5+1.54\text{e+4}\,s^3} \\ \frac{44.2}{s} & \frac{2.71\text{e-8}}{s} \\ -\frac{7.5}{s} & -\frac{48.8}{s} \\ 0 & 0 \\ 0 & 0 \end{pmatrix} \tag{143}$$

From $\dot{y}$ reference input to outputs in the first column and $\dot{\theta}$ reference input to outputs in the second column:

$$\begin{pmatrix} \frac{4.45\text{e-15}\,s^6}{s^8+248.0\,s^6+1.54\text{e+4}\,s^4} & \frac{4.69\,s^6}{s^8+248.0\,s^6+1.54\text{e+4}\,s^4} \\ \frac{24.3}{s^2} & -\frac{2.92\text{e-8}}{s^2} \\ \frac{5.86\text{e-14}}{s^2} & \frac{61.8}{s^2} \\ 0 & 0 \\ 0 & 0 \\ \frac{4.45\text{e-15}\,s^6}{s^7+248.0\,s^5+1.54\text{e+4}\,s^3} & \frac{4.69\,s^6}{s^7+248.0\,s^5+1.54\text{e+4}\,s^3} \\ \frac{24.3}{s} & -\frac{2.92\text{e-8}}{s} \\ \frac{5.86\text{e-14}}{s} & \frac{61.8}{s} \\ 0 & 0 \\ 0 & 0 \end{pmatrix} \tag{144}$$

From $\dot{\theta}_f$ reference input to outputs in the first column and $\dot{\theta}_r$ reference input to outputs in the second column:

$$\begin{pmatrix} \frac{0.00565\,s^6}{s^8+248.0\,s^6+1.54\text{e+4}\,s^4} & \frac{0.00565\,s^6}{s^8+248.0\,s^6+1.54\text{e+4}\,s^4} \\ -\frac{3.53}{s^2} & \frac{3.53}{s^2} \\ \frac{0.0744}{s^2} & \frac{0.0744}{s^2} \\ 0 & 0 \\ 0 & 0 \\ \frac{0.00565\,s^6}{s^7+248.0\,s^5+1.54\text{e+4}\,s^3} & \frac{0.00565\,s^6}{s^7+248.0\,s^5+1.54\text{e+4}\,s^3} \\ -\frac{3.53}{s} & \frac{3.53}{s} \\ \frac{0.0744}{s} & \frac{0.0744}{s} \\ 0 & 0 \\ 0 & 0 \end{pmatrix} \tag{145}$$